CRANFIELD UNIVERSITY

Fabio Veronesi

3D Advance mapping of soil properties

School of Applied Sciences

Ph.D.
Academic Year: 2009 - 2012

Supervisors: T. Mayr and R. Corstanje

07/2012

CRANFIELD UNIVERSITY

School of Applied Sciences

Ph.D.

Academic Year 2009 - 2012

Fabio Veronesi

3D Advance mapping of soil properties

Supervisors: T. Mayr and R. Corstanje

07/2012

This thesis is submitted in partial fulfilment of the requirements for the degree of Ph.D.

ABSTRACT

Soil is extremely important for providing food, biomass and raw materials, water and nutrient storage; supporting biodiversity and providing foundations for man-made structures. However, its health is threatened by human activities, which can greatly affect the potential of soils to fulfil their functions and, consequently, result in environmental, economic and social damage.

These issues require the characterisation of the impact and spatial extent of the problems. This can be achieved through the creation of detailed and comprehensive soil maps that describe both the spatial and vertical variability of key soil properties. Detailed three-dimensional (3D) digital soil maps can be readily used and embedded into environmental models.

Three-dimensional soil mapping is not a new concept. However, only with the recent development of more powerful computers has it become feasible to undertake such data processing. Common techniques to estimate soil properties in the three-dimensional space include geostatistical interpolation, or a combination of depth functions and geostatistics. However, these two methods are both partially flawed. Geostatistical interpolation and kriging in particular, estimate soil properties in unsampled locations using a weighted average of the nearby observations. In order to produce the best possible estimate, this form of interpolation minimises the variance of each weighted average, thus decreasing the standard deviation of the estimates, compared to the soil observations. This appears as a smoothing effect on the data and, as a consequence, kriging interpolation is not reliable when the dataset is not sampled with a sampling designs optimised for geostatistics.

Depth function approaches, as they are generally applied in literature, implement a spline regression of the soil profile data that aims to better describe the changes of the soil properties with depth. Subsequently, the spline is resampled at determined depths and, for each of these depths, a bi-dimensional (2D) geostatistical interpolation is performed. Consequently, the 3D soil model is a combination of a series of bi-dimensional slices. This approach can effectively decrease or eliminate any smoothing issues, but the way in which the

model is created, by combining several 2D horizontal slices, can potentially lead to erroneous estimations. The fact that the geostatistical interpolation is performed in 2D implies that an unsampled location is estimated only by considering values at the same depth, thus excluding the vertical variability from the mapping, and potentially undermining the accuracy of the method.

For these reasons, the literature review identified a clear need for developing, a new method for accurately estimating soil properties in 3D – the target of this research,

The method studied in this thesis explores the concept of soil specific depth functions, which are simple mathematical equations, chosen for their ability to describe the general profile pattern of a soil dataset. This way, fitting the depth function to a particular sample becomes a diagnostic tool. If the pattern shown in a particular soil profile is dissimilar to the average pattern described by the depth function, it means that in that region there are localised changes in the soil profiles, and these can be identified from the goodness of fit of the function. This way, areas where soil properties have a homogeneous profile pattern can be easily identified and the depth function can be changed accordingly.

The application of this new mapping technique is based on the geostatistical interpolation of the depth function coefficients across the study area. Subsequently, the equation is solved for each interpolated location to create a 3D lattice of soil properties estimations. For this way of mapping, this new methodology was denoted as top-down mapping method.

The methodology was assessed through three case studies, where the top-down mapping method was developed, tested, and validated. Three datasets of diverse soil properties and at different spatial extents were selected. The results were validated primarily using cross-validation and, when possible, by comparing the estimates with independently sampled datasets (independent validation). In addition, the results were compared with estimates obtained using established literature methods, such as 3D kriging interpolation and the spline approach, in order to define some basic rule of application.

The results indicate that the top-down mapping method can be used in circumstances where the soil profiles present a pattern that can be described by

a function with maximum three coefficients. If this condition is met, as it was with key soil properties during the research, the top-down mapping method can be used for obtaining reliable estimates at different spatial extents.

Keywords: *digital soil mapping, geostatistics, kriging, depth function, soil compaction, soil texture, soil carbon, soil bulk density, soil carbon stock.*

ACKNOWLEDGEMENTS

This studentship was funded by the iSOIL project. iSOIL- "Interactions between soil related sciences - Linking geophysics, soil science and digital soil mapping" is a Collaborative Project (Grant Agreement number 211386) co-funded by the Research DG of the European Commission within the RTD activities of the FP7 Thematic Priority Environment.

A special thank you to my two supervisors for their help during the course of my project, and for tolerating me and my Italian English for these three years.
I am also grateful to all the iSoil partners for providing data and support.

Last but not least, very very special thanks to my girlfriend Deborah for her courage and strength in accepting our British adventure; and to Stefano, because even if he is a pain in the neck, our discussions helped me a lot during the research work.

LIST OF FIGURES

LIST OF TABLES

LIST OF EQUATIONS

TABLE OF CONTENTS

ABBREVIATIONS

BD	Bulk Density (from Unger et al., 1998)
BGS	British Geological Survey
C	Carbon
CEH	Centre of Ecology & Hydrology
CULS	Czech University of Life Sciences
DSM	Digital Soil Mapping
EM	Electro Magnetic
GUI	Graphical User Interface
IPCC	Intergovernmental Panel on Climate Change
N	Nitrogen
NSI	National Soil Inventory
NSRI	National Soils Resources Institute
PR	Penetration resistance
R^2	Pearson R squared
REML	Residual Maximum Likelihood
RMSD	Root mean squared deviation
S	Sulphur

St.Dev	Standard Deviation

CHAPTER 1 - Introduction

Soil is extremely important for nutrient cycle, water relations, biodiversity and habitat, filtering and buffering, physical stability and support. These five general categories of soil functions illustrate the importance of soil in providing food, biomass and raw materials, water and nutrients storage, supporting biodiversity and providing foundations for man-made structures.

Many human activities can be detrimental to soil. These include accelerated soil erosion, decline in soil organic matter, soil contamination and compaction, decline in biodiversity and soil salinisation. All these changes can greatly undermine the potential of soils to fulfil their functions, and this can consequently cause not only environmental detriment, but also economic and social damages.

The first step to assess and solve these problems is to explore better ways to characterise the amount and spatial extent of key soil properties in the landscape. This implies the creation of detailed soil maps that assess the spatial variation of soil properties with depth. These can be used to increase the accuracy of existing environmental models. This requires the creation of data representing a three-dimensional (3D) model of the soil.

The creation of detailed 3D soil maps is not an easy task, as soil is a very heterogeneous entity. Its composition is the product of millennia of physical, chemical weathering and biological activity while its vertical and horizontal variation is derived by a complex pattern of soil processes. These can form soil horizons which are relatively homogeneous layers whose physical, chemical and biological characteristics are different from layers above and below them. This implies that with depth, soil properties can change substantially.

Soil scientists have been aware of the importance of depth in understanding soil processes since the 1940's with the work of Jenny (1941). He understood that soil was the results of complex interactions between rocks and climate, and that the key to represent its complexity was to take into account the variation of the whole profile.

Traditional soil maps, and subsequent digital versions of these maps, do not implicitly transmit this complexity. These maps are based on taxonomic soil units (i.e. soil series), which extend through areas where a soil displays similar pedogenetic, chemical and physical properties. In these maps, depth is well considered and described, however in these taxonomic units soil properties present a range of values and it is difficult to assign a single numerical number to every point in the landscape. For this reason, a single location within a soil series can be defined by having soil properties values that varies within a defined range, but it is impossible to assign a number to each property.

The advent of quantitative soil mapping has dramatically increased the capacity to represent soil variation, both in the horizontal and the vertical space. For example, real concentrations or percentages of a soil property of interest can be represented, and not a range of possible values from representative soils. This type of mapping is very important because quantitative soil estimates can be readily embedded in other environmental models, such as erosion, flood risk and climate change models, processes which are dependent on the changes in the soil profile and therefore operate in 3D.

In addition the soil map greatly affects the resolution that environmental models can achieve. For example, JULES (Cox et al., 1999; Essery et al. 2001) is based on a simple three layer soil model and this constrains its use to resolutions equal or above 1 km^2. This is certainly a limitation of the model, but it is caused by a lack of spatially-precise and quantitative estimates that can be obtained only from detailed 3D soil maps. For this reason, there is a need for a more sophisticated approach that is able to produce high resolution 3D soil maps, which can then be used to increase the resolution of existing models. However, producing a 3D map should not be the only objective, because estimating soil properties can be easily done with commercially available software, such as the Spatial Analyst in the ArcGIS software (© ESRI), which is extremely easy to use even by inexperienced users. However, without a deep understanding of soil processes, having a detailed set of predictions does not help in understanding, for instance, the reasons why a model works well in one area but fails in another. For this reason, there is a need not only of producing

detailed quantitative soil maps, but also in providing tools to easily identify areas where the uncertainty of the soil model is below the level at which the map can be considered accurate.

1.1 iSoil Project

This PhD was funded and is an integrating part of the iSoil project, which ended in 2011. ISoil was a Collaborative Project (Grant Agreement number 211386) co-funded by the European Commission DG Research of the within the EU's FP7 Thematic Priority Environment. The main purpose of this project was to link geophysics, soil science and digital soil mapping to improve interactions between soil related sciences.

To achieve this goal, an essential prerequisite, alongside sustainable land use, water management and environmental management, is the availability of detailed soil property maps. The project identified a clear need, in the European context, to improve the methodologies used in digital soil mapping (DSM). In particular, one of the main tasks of the iSoil project was the development of cost- and time-efficient new methodologies for mapping soil, which can be reasonably applied over large areas. Starting from the realisation that sampled-based soil mapping can be time-consuming and cost-intensive, the project aimed to develop or improve non-destructing, minimally-invasive and relatively inexpensive techniques for exploring the soil spatial variability, in particular geophysical techniques. Among these techniques, electromagnetic induction and gamma ray spectrometry were primarily used for collecting soil data at high spatial resolution. These techniques were adopted by iSoil because their use is common practice among soil practitioners for collecting inexpensive data about the spatial pattern of key soil properties. For this reason, alongside the study of a new method for mapping soil properties in 3D, this thesis also presents an analysis of the use of these covariates for mapping soil in 3D. Chapter 4 shows how these data were used as covariates for soil mapping at the field scale, as they are commonly used in literature. However, because their use for 3D soil

mapping was never properly explored, Chapter 5 aims to understand their use and possible limitations in the context of 3D DSM.

1.2 Thesis structure

The thesis is written in an article format. This means that each chapter is presented with a separate introduction and literature review, adjusted for the main topic under discussion. Moreover, sections on results, discussion and conclusion are also presented for each chapter. In these sections only the results of each specific topic will be analysed and discussed.

In order to increase the readability of the thesis, an overall introductory chapter is also presented. However, in order to minimise repetitions the overall introduction is focused only on the presentation of the main problems identified from the literature. These problems with literature methods were the starting point of the research and the key to understand the reason why this research was undertaken. On the other hand, the literature review in Chapter 1 is not presented as an exhaustive discussion about all the topics treated in the thesis, as each topic is introduced where required.

Chapter 2 presents a brief introduction of the geostatistical techniques used during the research. From Chapter 3 to Chapter 6, a series of case studies are presented. These studies were used for developing, testing and validating the 3D mapping method with different datasets and spatial extent. In detail, Chapter 3 presents a case study were a 3D mapping experiment was undertaken using a dataset of field scale penetrometer resistance readings. During this case study a new method for 3D DSM was developed for use at the field scale, and validated with cross-validation which compared its results with 3D kriging. In Chapter 4, the developed method was tested alongside other 3D mapping methods, in order to obtain more information regarding the applicability of each mapping approach. At this stage, the soil property estimation was performed in the way suggested in the iSoil project, by using algorithms that can exploit covariates for their relation with the soil properties under study in order to increase the accuracy of the estimates. Due to the results obtained in Chapter

4, Chapter 5 focused on the use of covariates, with particular attention to the geophysical data, in the context of 3D DSM. The use of geophysical data is a crucial aspect of the iSoil project and testing their accuracy when mapping subsoil was part of this research.

Chapter 6 presents a mapping experiment in which the developed method was tested at large spatial extent, in order to test the iSoil project requirement for a method for mapping, with an acceptable accuracy, large areas using limited analytical data.

Chapter 7 is intended as a general discussion. The objective of this chapter is to summarise, discuss and place all the results and topics introduced during the three stages of the research into a general scientific context.

Finally, a concluding chapter is presented outlining some general issues regarding the topics analysed in the PhD.

During the course of the research, a Graphical User Interface (GUI) was developed in the Python scripting language for a 2D and 3D soil mapping application. This software is presented as an appendix to the thesis.

1.3 Literature review

In recent years, with advancements in computing technology and algorithms, embedding the third dimension in modelling has become not only possible but also affordable and relatively quick. With the advancements of the entertainment industry, 3D viewing systems are becoming widespread and this can provide scientists with a new set of instruments to explore the concept of 3D modelling.

The origin of 3D as a novel way to visualise the world can be traced back to 1964 with the work of the American computer art director William Fetter. Mr. Fetter, while working at Boeing, created the first 3D human representation using computer graphics (Wu, 2012). From that point 3D visualisation and rendering were rapidly implemented in other software, such as CADs (in 1968, by Donald Welbourn) and GIS (in 1975, by Randolph Franklin). This has created a whole new generation of scientific work.

For example, 3D imaging techniques have been developed for modelling internal body structures in order to indirectly assess patient condition. Techniques such as the computed tomography (CT), ultrasound (US), positron emission tomography (PET), and magnetic resonance imaging (MRI) have been developed with the purpose of creating a 3D realistic model of the patient body and help surgeons during their work (Friedlinger et al., 1995; Fenster et al., 2002; Hikishima et al., 2008).

Another example is the digital face reconstruction tool that is widely used for security purposes (i.e. face recognition); gaming and entertainment (i.e. movie character generation and person specific game); and for surgical simulations (Jiang et al., 2005; Lee et al., 2011; Liu et al., 2012).

More familiar examples are found in geography, geology and geophysics where 3D modelling has been widely used for terrain visualization (Bourke, 1993; Döllner et al., 2000; Zhang, 2003; Jenny et al., 2011), analytical hillshading (Jenny, 2001, 2007; Leonowicz et al., 2010, 2010b), three-dimensional representations of the underground for mining exploration (Xue et al., 2004; Jian and Fanhua, 2009; Darabi et al., 2010; Yang et al., 2011; Wang et al., 2012), hydrological modelling (Dagallier et al., 2000; Bonomi et al., 2002; Bonomi et al., 2007; Butscher and Huggenberger, 2007; Bonomi, 2009; Pairaud et al., 2011), soil root analysis (Wagner et al., 2011; Wu et al., 2007; Bingham and Wu, 2011).

1.3.1 3D in soil science

Three-dimensional quantitative modelling is relatively new in soil science. While the third dimension was already embedded in soil series maps, the advent of quantitative mapping has improved the potential to model soil complexity in 3D using advanced algorithms and geostatistical techniques.

Generally, two possible methods are available in literature for undertaking a 3D mapping exercise: geostatistics or a combination of depth functions and geostatistical interpolation.

The *first* method is based uniquely on three-dimensional geostatistical interpolation. There are many examples in literature where geostatistics has been used for producing soil property volumetric estimates, such as the studies by Castrignanò et al. (2002) and Carrara et al. (2007), who mapped cone penetration resistance in a relatively small volume of soil affected by heavy machineries transit. Other examples include the work of Bonomi et al. (2002, 2007 and 2009), who relied on inverse distance interpolation to estimate the surface of aquifers starting from geology cores and cone penetrometer tests.

With geostatistics, the property of interest is predicted in any given unsampled location from a weighted average of the nearby observations. With this method, all the soil values in the 3D space are considered for computing the variogram, assigning weights and computing the weighted averages. For this reason both the horizontal as well as the vertical variability of the soil properties are taken into account. However, this method presents some limitations that can restrict its usage: in particular the fact that soil estimates present a standard deviation (which is a standard measure for the spread of the data) that is much lower than the standard deviation of the sampled dataset. This phenomenon is referred to as a "smoothing effect" (Deutsch and Journel, 1998); it can be reduced by using dense datasets sampled with a design specific for geostatistics, but it cannot be avoided, being a fundamental characteristic of the algorithm (see section 2.5). The smoothing effect does have an advantage as it can decrease the effect of outliers in the data (Odeh, 1994), by excluding the tails of the distribution. However, it can also undermine the accuracy of the mapping, as it substantially cuts the spatial variability that can be described by the map.

Moreover, geostatistics is very time demanding, and the computational time increases exponentially with the increment of the prediction points (Kerry and Hawick, 1998). For 3D mapping this can be a problem, such as when mapping ten depth intervals equates at estimating ten times the points of the surface map with the same extent.

The *second* method is the depth function approach, which has two specific variations. The first method assumes that the soil properties vary continuously along the depth profile and therefore the horizon sampling is not accurate in

describing their changes. Many authors, since the middle of the 20th century, have tried to solve this problem by increasing the vertical resolution of the samples. The earliest attempt involved drawing free hand curves between data points (see Jenny, 1941) assuming that the bulk value represents the soil property in the mid-point of the horizon. More complex methods involve linear and polynomial regression (Campbell et al., 1970; Colwell, 1970), fitting of exponential decay functions (Brewer, 1968; Russell and Moore, 1968; Moore et al., 1972) or fitting a spline through soil data (Erh, 1972; Ponce-Hernandez et al., 1986; Bishop et al., 1999; McBratney et al., 2000). The purpose is always to increase the vertical resolution of the horizons data and to supply data at points which may have not been sampled. The subsequent mapping is done at set depths using standard 2D interpolation methods (e.g. geostatistics or inverse distance weighting) based on data extrapolated from the function curve, at those depths (Minasny et al., 2006; Malone et al., 2009). Because the regression and the 2D interpolation are distinct phases, with no connection, soil properties are estimated using only values at the same depth. Therefore, the vertical variability of the soil property is assumed independent of the horizontal variation. This can potentially decrease the mapping accuracy.

The second variation was recently developed by Kempen et al. (2011) to deal with areas where the soil contains sharp discontinuities. These can be caused by human influence, contrasting parent materials or weathering; in either case the assumption of continuous variation along the profile is not valid. In this method, the variation of the property of interest is estimated by creating “soil type-specific” depth functions, using the horizons data (thickness, depth and soil property value) as coefficients, and then interpolating them with geostatistics, in order to create the 3D map. The results indicate that this method requires far too many coefficients and the authors recognise that this can limit its application in “data-poor environments”.

1.4 Research question

The literature review has identified a clear need in soil science for a new method for digital soil mapping in 3D. A method that can be used to produce high resolution and accurate soil properties estimates, solving the issues identified in the available algorithms (e.g. smoothing effect; lack of connection between vertical and horizontal variation; need for detailed soil datasets). Moreover, because soil maps nowadays are tools for obtaining continuous estimates of soil properties to use in environmental modelling, there is a need for a method able to be used as a diagnostic instrument so that, if the model is unable to obtain reliable outputs for a particular area, the soil map can give indications about the possible causes.
In summary, this PhD project has the objective of developing and testing a new method for 3D digital soil mapping with the aforementioned characteristics and of critically reviewing it, alongside existing literature methods for 3D mapping. From these conclusions and from the requirements of the iSoil project, a hypothesis, two aims and three objectives were set.

Hypothesis

High resolution 3D mapping can be accurately achieved, with a method able to estimate soil properties even with relatively poor data support, thus minimising the cost of the survey, and which can reasonably be applied over large areas.

Aims

Develop a novel method, based on simple soil specific depth functions, for three-dimensional digital soil mapping.

Test the method with different datasets and spatial extents, and compare it with methods available in literature to assess its overall accuracy.

Objectives

1) The first objective involves the development of a new method for mapping soil properties in 3D. This method needs to accurately assess the vertical variability of the property of interest in relation to the horizontal variation. It needs also to be flexible enough to be used in a quicker and easier way compared to the commonly used 3D interpolation techniques. Moreover, it has to be accurate even where the dataset available for the study is relatively small, in order to reduce the cost of the survey and be able to work with legacy soil information. The new method needs to be tested in order to understand how it represents the soil property variation in 3D. With a set of descriptive statistics indexes and uncertainty estimation, it is important to assess its overall accuracy in relation to literature methods.

2) The second objective is based on the assumption, from the iSoil project, that environmental covariates, especially geophysical data, can be implemented in the mapping algorithm in order to increase its efficiency. This type of data was one of the key components, in the iSoil project, for developing new techniques for time- and cost-effective soil mapping. Although not directly a measure of soil properties, these data are the result of biogeochemical and physical processes and by studying their spatial variability through geostatistics, these data can potentially increase the accuracy of the digital soil maps, while relying on reduced soil sample datasets.

3) Finally, the third objective is to apply the new method increasing the extent of the study area, in order to assess if can acceptably be used for large areas. At field scale the soil samples are often numerous and well distributed across the area of interest. When the analysis is performed in larger areas however, the density of samples is generally much sparser. At a landscape scale, the practitioner relies on high resolution covariates for estimating the soil properties where the sample coverage is limited.

However, the types of covariates are very different compared to those used for field scale analysis. In fact, the usual covariates at this scale are non-geophysical: DEM derivatives, such as slope, aspect, curvature etc.; land use maps; geological maps; soil classes or soil associations maps. These data are relatively cheap to collect and normally they are sufficient for soil mapping at this scale. Their use for 3D DSM however, needs to be tested.

These objectives define a clear direction to follow in order to complete the research required for reviewing existing approaches and to define a new method for 3D soil mapping. The project was therefore divided into three stages.

The *first stage*, described in Chapter 3, was focused on the development of an improved 3D soil mapping method. This method was then tested and validated, by comparing it with a benchmark literature method known as 3D ordinary kriging. A decision was made to use only soil observations for the development of the method, excluding the use of covariates because the main purpose of this study was to test the overall accuracy of the new methodology and excluding potential influences from external factors.

In the *second stage*, attention was focused on the use of covariates for 3D soil mapping. Three methods for 3D digital soil mapping, two from literature and the one developed in the first stage, were tested for their ability to predict soil properties in the 3D space using covariates to improve the accuracy of the map. The main focus of this stage was to create a mapping experiment in which the three methods could be compared in order to determine their relative strengths and the weaknesses. The experiment simulated a texture dataset with average horizon data. Subsequently, each method was used independently to estimate soil textures, and cross-validated.

In concluding this experiment, it was realised that each method, even though very different in the execution from the others, presented a common result: a vertical decrement in the prediction accuracy. Consequently, another test was developed to assess the accuracy of the environmental and geophysical

covariates in predicting various soil properties along the depth profile. For this purpose several combinations of covariates were used and a simple 1-out cross-validation was carried out for each depth layer sampled.

At this point the attention shifted from the development and testing of the mapping method to its possible applications (*third stage*). One of the main aims of the soil science community is to produce reliable estimates of soil parameters to modellers in order to predict future changes in the soil system. These models are normally used at relatively low spatial resolution, for instance JULES cannot predict below a 1 Km^2 cell, for predicting key soil properties over large areas. For these reasons, the developed method was tested in the third stage by making predictions over a much larger extent than the previous two case studies. The validation was undertaken using cross-validation and the results were compared with other validated literature studies. Moreover, an independently sampled dataset was used in order to perform an independent validation. Finally, a method was proposed for calculating the map uncertainty that can also be used for other depth function approaches.

CHAPTER 2 - Theoretical background

2.1 Introduction

The research described in this thesis involved several geostatistical techniques. This chapter provide the reader with a brief theoretical background regarding these techniques.

2.2 Geostatistics

In the early days of quantitative geography, scientists became aware that they could not continuously measure all landscape attributes. They had to work with fragmentary information and use it carefully in order to predict attributes in unknown locations. Geographers realised that landscape attributes were dependent on their location and that two points close to each other were more likely to be similar than points further apart. These concepts were explored in numerous papers and scientific works but their solution was not recognised until the 1960's when D.G. Krige, a South African engineer, observed that his estimates of ore grades could be improved if he took into account the characteristics of neighbouring blocks. His pioneering work was mathematically formalised by the French mathematician G. Matheron in his doctoral thesis (Matheron, 1965), when he created the theory of regionalised variables.
According to this theory, all the geographical attributes observed in point locations are a single realisation of a regionalised process that can be expressed by the following equation:

$$Z(\mathbf{x}) = \sum a_k f_k(\mathbf{x}) + \varepsilon(\mathbf{x}) \qquad (2.1)$$

where x denotes the spatial coordinates in the three-dimensional space of the sampled location; f_k, with k = (0, 1, …), are functions of the spatial location; a_k are unknown coefficients, and $\varepsilon(\mathbf{x})$ is a spatially dependent random component.

The first term of the right hand side of the equation represents a deterministic component which can be modelled as a trend (from: Oliver et al., 1989). Early scientific works have discovered empirically that in most studies the random component was the largest and that the impact of the trend was negligible (from: Oliver et al., 1989).
For practical purposes, it is often assumed that the variation can be represented by the second term of the equation and that the first term can be replaced by a constant:

$$Z(\mathbf{x}) = \mu_v + \varepsilon(\mathbf{x}) \tag{2.2}$$

Where μ_v is the constant mean and $\varepsilon(\mathbf{x})$ is the spatially dependent random component. The latter has zero mean,

$$\mathbf{E}[\varepsilon(\mathbf{x})] = 0 \tag{2.3}$$

and a variance defined by:

$$\mathbf{var}[\varepsilon(\mathbf{x}) - \varepsilon(\mathbf{x}+\mathbf{h})] = \mathbf{E}[\{\varepsilon(\mathbf{x}) - \varepsilon(\mathbf{x}+\mathbf{h})\}^2] = 2\gamma(\mathbf{h}) \tag{2.4}$$

where **h** is a vector that separates the two locations **x** and **x**+**h**.
This means that the variance of the random component depends only on the direction and distance between two points, and not by their actual position. Matheron realised that with a constant mean, Eq. 2.4 was equivalent to:

$$\mathbf{var}[z(\mathbf{x}) - z(\mathbf{x}+\mathbf{h})] = \mathbf{E}[\{z(\mathbf{x}) - z(\mathbf{x}+\mathbf{h})\}^2] = 2\gamma(\mathbf{h}) \tag{2.5}$$

This is known as *intrinsic stationarity hypothesis*, by which the random component has zero mean and a variance that depends only by the quantity $\gamma(\mathbf{x})$, known as semi-variance.

2.3 Variogram

The semi-variance is expressed as half the expected squared difference between two locations separated by the vector **h**:

$$\gamma(\mathbf{h}) = \frac{1}{2}\,\mathbf{E}[\{z(\mathbf{x}) - z(\mathbf{x}+\mathbf{h})\}^2] \qquad (2.6)$$

and it is described by the variogram cloud in which the semi-variance values are calculated for each couplet of locations. In order to compute the variogram, the values of semi-variances are averaged by lag distances. When the intrinsic hypothesis holds, the variogram contains all the information about the spatial correlation. For this reason, constructing the variogram and fitting the variogram model are two crucial step of the geostatistical analysis (Webster and Oliver, 2007; Cressie, 2008).

In this research, the fitting of the variogram model was done using the REML method, proposed by Patterson and Thomson (1971). This method gives a more robust estimation of the variogram parameters and can be used in cases when the sampling scheme was not adapted for geostatistics such as grid sampling (Lark and Cullis, 2004), or when the number of sampled points is below 100 but higher than 50 (Kerry and Oliver, 2007).

There are three parameters of the variogram that need to be estimated and that are used to assign weights during the kriging interpolation. These parameters are shown in Fig. 2.1.

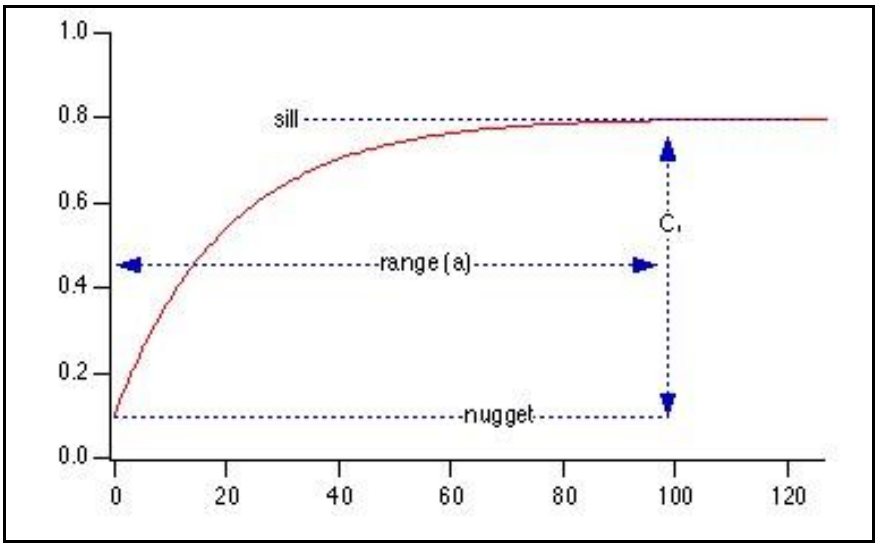

Fig. 2.1: variogram model and graphical description of the three variogram parameters.

In this figure, the variogram is bounded by a sill, which is the maximum possible variance in the data; the distance at which the variogram reaches the sill, interpretable as the maximum distance at which two points are correlated and co-vary, is the range. The nugget represents the variability at distances smaller than the typical samples spacing, including measurements errors.

2.4 Ordinary kriging

One of the most important uses of the regionalised variable theory is the local estimation of geographical attributes in the spatial domain, is a process known as kriging from the name of the South African engineer D.G. Krige who first applied it. This technique is very popular in numerous scientific fields because its estimates are unbiased and have a minimum variance. Furthermore, this interpolation method can estimate the error associated with each prediction and it is exact, meaning that in a sampled point the estimate value is equal to the observed one.

Ordinary kriging is one of the simplest forms of geostatistical interpolation and it must be used under the intrinsic hypothesis, Eq. 2.5 (Webster and Oliver,

2007). It is able to determine a continuous set of estimations, starting from a discrete set of samples by using their spatial auto-correlation model. This interpolation method can predict values of a variable of interest in any unsampled location using a weighted average of the nearby observations, with the following equation:

$$\hat{Z}(\mathbf{x_0}) = \sum_{i=1}^{n} \mathbf{w}_i [z(\mathbf{x}]_i) \qquad (2.7)$$

where $\hat{Z}(\mathbf{x_0})$ is the unsampled point to be predicted; w_i are the weights, assigned from the variogram analysis, and $\mathbf{x}_i$ are the samples values. To ensure the estimates are unbiased, the weights sum is made to 1,

$$\sum_{i=1}^{n} \mathbf{w}_i = \mathbf{1} \qquad (2.8)$$

and the expected error is zero:

$$\mathbf{E}[\hat{Z}(\mathbf{x_0}) - Z(\mathbf{x_0})] = \mathbf{0} \qquad (2.9)$$

The estimation variance is:

$$\mathbf{var}[\hat{Z}(\mathbf{x_0})] = \mathbf{E}\left[\{\hat{Z}(\mathbf{x_0}) - Z(\mathbf{x_0})\}^2\right] = \mathbf{2}\sum_{i=1}^{n} \mathbf{w}_i \varphi(\mathbf{x}_i, \mathbf{x_0}) - \sum_{i=1}^{n}\sum_{j=1}^{n} \mathbf{w}_i \mathbf{w}_j \varphi(\mathbf{x}_i, \mathbf{x}_j) \qquad (2.10)$$

where $\varphi(\mathbf{x}_i,\mathbf{x}_j)$ is the semi-variance between the data point $\mathbf{x}_i$ and $\mathbf{x}_j$, and $\varphi(\mathbf{x}_i,\mathbf{x}_0)$ is the semi-variance between the i^{th} data point and the unknown point $\mathbf{x}_0$ (from: Webster and Oliver, 2007).

2.5 Conditional simulation

With kriging, the best estimation is achieved by minimising the variance of each weighted average, hence minimising the following,

$$\sigma_k^2 = \mathbf{E}\left[z(\mathbf{x_0}) - \widehat{Z}(\mathbf{x_0})\right] \quad (2.11)$$

where $\mathbf{x}_0$ is the true value at the location, and $\widehat{Z}(\mathbf{x_0})$ is the estimation. With this method the variance of the estimated data is less than the variance of the data. For this reason, kriging can produce the best estimate for a single location or an area, but it does not reproduce the variance of the dataset well, i.e. it has a *smoothing* effect (from: Webster and Oliver, 2007).

In cases where the objective is to keep the variance to a value similar to the one observed in the data, kriging cannot be used. In these cases it is necessary to adopt another technique: such as conditional simulation.

With simulation, it is possible to create a series of equi-probable realisations of the regionalised variable in the space, honouring both the distribution and the variogram model of the variable. For each sampled point the simulation reproduces the observed value, which is why it is denoted as conditional.

2.6 Universal kriging

The theory of ordinary kriging is based on the assumption of intrinsic stationarity. Under this assumption the deterministic term in Eq. 2.1 can be replaced by a constant. Even though in most studies the intrinsic hypothesis holds, there are cases in which assuming a constant mean across the study area is not appropriate, particularly at large extents. In these instances practitioners have to model the deterministic term of Eq. 2.1, and only afterward they are able to model the spatially dependent random term. The functions to model the trend are usually simple polynomials of order 1 and 2 (Webster and Oliver, 2007).

After this preliminary analysis of the trend, the variogram is computed using the residuals between the observations and the values predicted by the trend analysis. Matheron (1969) described this technique as "*le krigeage universel*", though its applicability is not universal (Webster and Burgess, 1980) and for this reason it is often called "kriging with an external drift".

This technique can be used for univariate distributions, by modelling the trend in the variables and then solving the kriging system. However, in most cases universal kriging is adopted when limited landscape observations are coupled with high resolution environmental covariates (e.g. DEM), which are much simpler and relatively cheaper to collect. Under these circumstances, the trend is modelled by a linear or a polynomial regression between the observed values and the covariates; the residuals are then used to model the variogram. From this is possible to obtain weights for solving the kriging algorithm.

CHAPTER 3 - Mapping of soil compaction in 3D with depth functions

DEVELOPMENT OF THE 3D MAPPING METHOD

Abstract

Soil compaction is a form of physical degradation, which causes soil densification and distortion that can lead to changes in the three-dimensional soil structure variability. To test the effectiveness of depth functions for mapping soil compaction in three-dimensions, a field-scale dataset of penetration resistance at constant depth intervals was used to develop a novel approach.

This method, referred to as top-down mapping, is based on a multiple-step approach. It starts with a framework for selecting the depth function that best describes the soil specific variation by depth and continues with an interpolation of the coefficients of the function across the field. Finally, for each interpolated point, the equation is solved in order to estimate soil compaction in the 3D space.

The top-down mapping method was applied on the penetration resistance (PR) dataset (n = 57), collected at the CULS (Czech University of Life Sciences) farm in Lany. In order to test its accuracy in predicting cone-index variation in the 3D space, the mapping method was also compared with the 3D ordinary kriging, using descriptive statistics and cross-validation (performed by excluding a percentage of soil profiles).

The results indicate that the top-down mapping method reproduces the variance of the observed dataset better than 3D kriging, and, consequently, its estimates are more accurate than when using more generally accepted 3D geostatistical procedures. The cross-validation results reveal that ordinary kriging can obtain values of root mean squared deviation (RMSD) that range from 0.5, to 0.57, depending on the percentage of profiles excluded for validation. By contrast, the

top-down mapping method gives RMSD values that range from 0.47 to 0.53, thus, outperforming ordinary kriging.

3.1 Introduction

Soil compaction is a form of physical degradation that causes soil densification and distortion, decreasing soil porosity and permeability. This obstructs air, water, nutrient movement and root penetration. In arable soils compaction is often caused by repeated ploughing and the passage of heavy harvesting machinery. It can occur at the surface or in subsurface horizons. Ploughing can rectify topsoil compaction but once subsoil compaction occurs it is difficult and expensive to alleviate. The effect of compaction may also accumulate over time, creating a compacted soil layer that is almost impermeable and highly resistant to root penetration (Jones and Montanarella, 2001), known as a plough pan. Compaction changes the three-dimensional soil structure variability, and these modifications can be high even in relatively homogeneous soils (Carrara et al., 2007). For these reasons, there is a need for a rapid and accurate method for mapping soil compaction and the associated changes in three-dimensional soil structure.

3.1.1 Measuring soil compaction

Penetration resistance (PR) is an inexpensive way to monitor and assess soil compaction. The resistance measured by a penetrometer reflects the pressure encountered by roots (Carrara et al., 2007). However, penetrometer measurements have a major disadvantage: the accuracy of the data depends by the ability of the operator to push the rod at a constant speed, and this is almost impossible. For this reason a certain level of uncertainty is always attached to the values measured by a penetrometer. This error can increase where the compaction increases, but it is almost impossible to measure. Even though this uncertainty cannot be assessed, it must be taken into account

during the mapping. If it is not sufficiently considered, the resulting soil map can be biased.

Moreover, compaction can occur at any point throughout the profile, and this can be highly variable both by depth and across the field. It is not feasible to measure penetration resistance at high resolution, and usually not cost effective even to do so at sufficient locations to fully capture the vertical and horizontal variability on soil compaction.

3.1.2 New mapping method

In the past, these problems have been solved by interpolating PR data with 3D geostatistical algorithms (Castrignanò et al., 2002). However, as described in section 1.2.1, 3D geostatistics is difficult to use if the dataset was not sampled with appropriate designs. Moreover, a 3D model can be very difficult to present and interpret, having to rely on volumetric rendering or slicing. This can limit the effectiveness of the soil 3D map, as the interpretation of the soil pattern from a 3D volumetric model can be very complex.

In order to deal with penetrometer point uncertainties, and overcome the difficulty in interpreting 3D models, a new method for 3D soil mapping was developed. It is based on a framework for selecting the most accurate soil specific depth function; the one that can parsimoniously and effectively describe the average pattern of the soil property variation with depth, decreasing the impact of the measured point uncertainties.

By fitting this soil specific function to the soil profiles, and looking at its goodness of fit, it is possible to determine if a particular soil profile deviates significantly from the general behaviour in the field. If a particular goodness of fit value is low, this means there are localised changes in soil compaction pattern that can be easily identified and considered with more attention. This way it is possible to obtain a preliminary assessment of soil compaction before the creation of the 3D model, easing the interpretation of the final map. After this step geostatistics are used to interpolate the coefficients of the function in order to create a more detailed map. This method relies on two-dimensional mapping

to create a 3D lattice, for this reason in the thesis it is referred to as top-down mapping.

The main purpose of this chapter was to develop the method and test its performances without any influence from external factors; for this reason it was decided to exclude the use of covariates. The top-down mapping was also compared with the more generally accepted 3D ordinary kriging, already used in literature for 3D compaction mapping (Castrignanò et al., 2002), in order to illustrate the advantages of using a 3D soil mapping method based upon depth functions.

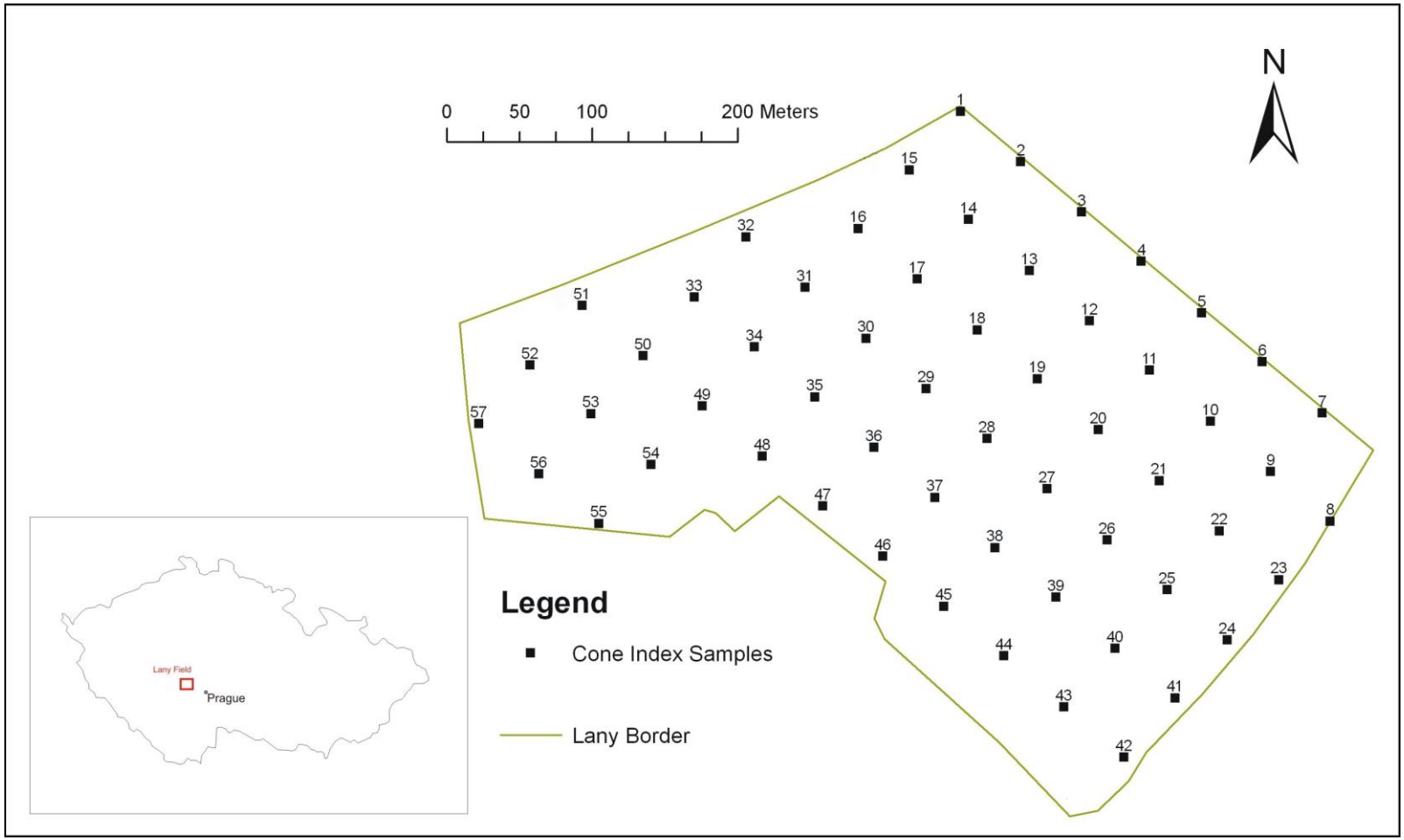

Fig. 3.1: Location of the study area. The CULS Lany farm is in the Stredocesky Region, near the city of Ruda, about 40 km W of Prague.

3.2 Materials and methods

3.2.1 Study site and sampling methods

The study site was a plot on the CULS (Czech University of Life Sciences) Farm at Lany (21 ha) located in the Czech Republic (central Bohemia), near the city of Ruda (50.14N, 13.86E), 40 km west of Prague (Fig. 3.1). The field was in arable use and managed by conventional ploughing techniques. The soil type, according to the WRB classification (World reference base for soil resources, 2006), is a Haplic Cambisol and according to the geological map at scale of 1:50,000, the Lany Farm is located on an alluvial terrace with a rocky to gravelly calcareous texture, which lies directly over a formation composed primarily of basaltic breccias, conglomerates and sandstones (Czech Geological Survey, 2004).

The Lany dataset consists of cone-index data measured at 57 locations with a static penetrometer PM 10, designed and constructed in CULS (cone edge has vertex angle of 30° and basis area of 3.23 cm^2). The instrument measured cone-index in intervals of 0.04 m to a depth of -0.52 m. Every sample is located at an average distance of 55 m on a regular grid. The data were collected in the spring of 2005, at field capacity, in two days with homogeneous weather condition.

Some corrections were applied to the dataset, disregarding the first measure from 0 to -0.04 m depth, because the instrument is known to generate unreliable surface readings. One observation at depth -0.44 m was also identified as an outlier. Table 3.1 presents the basic summary statistics of the dataset. In order to underline the major characteristics of the dataset, in addition to normal summary statistics, the octile skew (Brys et al., 2004) is presented. This index takes into account the symmetry of the first and the seventh octile on the median (Lark and Bishop, 2007), thus providing a more robust way to assess the skewness of the distribution.

Table 3.1: Descriptive statistics of the cone-index dataset (n = 57).

	Cone-index data
	(MPa)
Mean	1.95
St.Dev	0.73
Median	1.88
Minimum value	0.82
Maximum value	4.20
Skewness	0.49
Kurtosis	-0.65
Octile skew	0.55
Variance	0.54

Fig. 3.2a shows a box-plot of the distribution of cone-index values at each measured layer. From this plot is evident that on average this dataset presents a pattern characterized by two distinct layers. The first starts at -0.08 m and ends at -0.28 m depth, with cone-index values varying from 0.7 MPa to a maximum of 17 MPa; the second layer has values varying from 15 to 35 MPa, starting at -0.28 m to the maximum sampling depth.

This average pattern is not applicable to every sample. Fig. 3.2b shows two very different soil profiles from sample number 25 and 54. Sample 25 has a pattern very similar to the average; while sample 54 has a very different shape, with a constant increase in the cone-index value throughout the whole investigated profile.

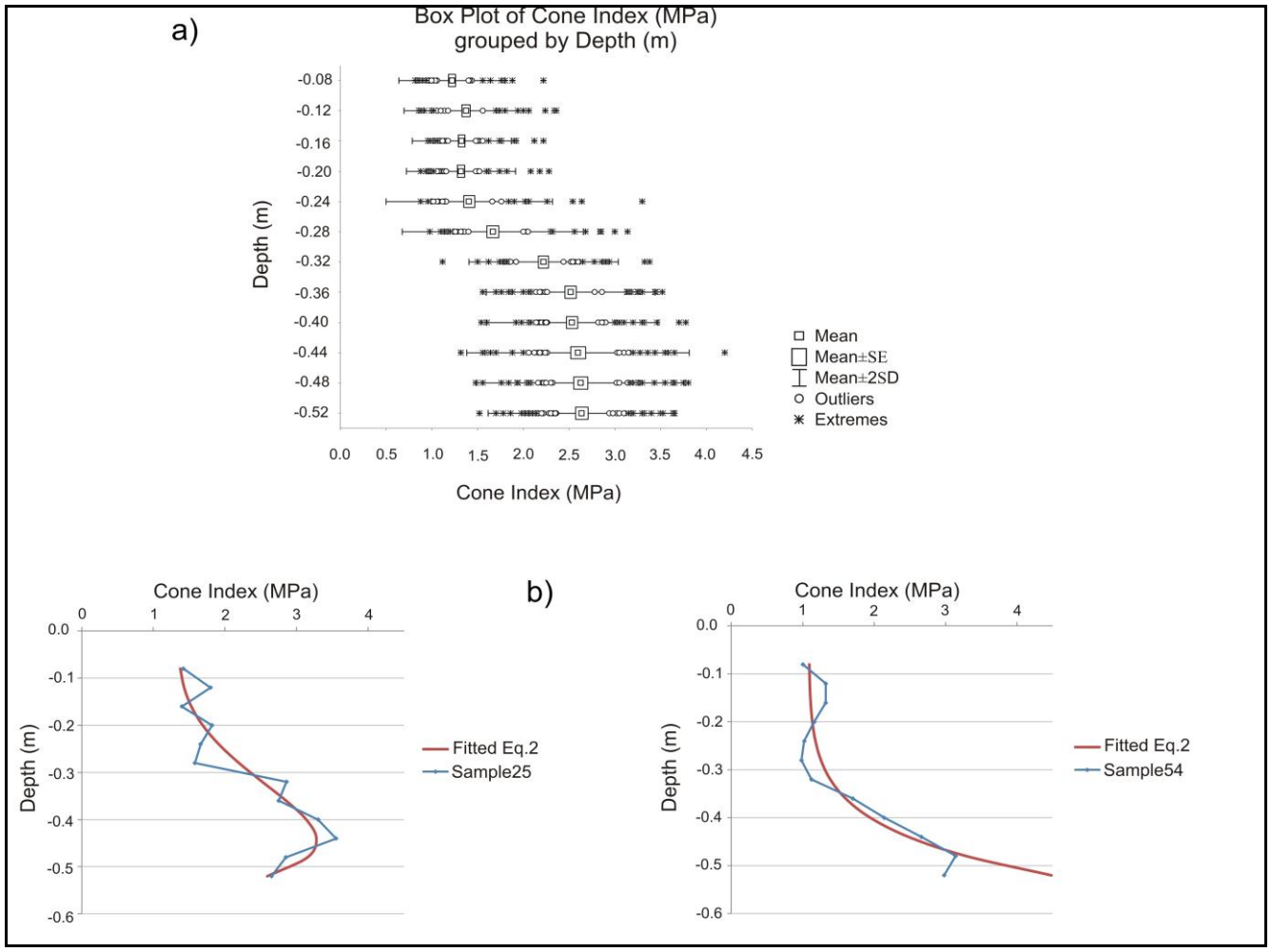

Fig. 3.2: Plot cone-index/depth for the entire Lany dataset. The first plot (a) illustrates the general pattern of the dataset. The second part (b) shows the two possible shapes of the curve generated by Eq. 3.1

3.2.2 Mapping method

This mapping method is based on a four-step approach:

- The *first* step involves the selection of the best soil specific depth function to describe the PR dataset (Fig. 3.2a).
- In the *second* phase, this depth function is fitted to each soil profile, calculating the function coefficients for each sampled location.
- The *third* step relies on geostatistical interpolation of the function coefficients on a bi-dimensional grid.
- Finally, in the *fourth* step the depth function is solved for each interpolated point in order to create a 3D digital soil map.

3.2.3 Framework for selecting the best depth function

The selection of the depth function is the single most important aspect in the application of the top-down mapping method. This method is based on the concept of soil specific depth functions. These are simple mathematical equations that cannot be applied automatically to every soil dataset, but they need to be selected for their ability to describe the general behaviour of the soil properties of interest, with depth, over the study area.
With mapping methods based on complex depth functions, such as splines, their application does not require any knowledge of the behaviour of the soil properties with depth. These functions are so complex that it is assumed they can fit perfectly to every soil dataset. However, because soil profiles are based on depth averages and the mathematical equations are fitted to these points, having a good R^2 (coefficient of multiple correlation, is a measure of how well the values predicted by the depth function correspond to the horizons values), does not necessarily means that the shape of the curve describe the soil profile accurately. There are many curves that can fit to the same set of points, but

only one can best describe the shape of the profiles in the study area (i.e. the soil specific depth function).

With this mapping method, the selection of the depth function is an integrating part of the process. A specific framework was developed for helping with the identification of the best depth function. In this framework, groups of common functions are tested for their general ability to describe the soil property variation by depth. These generic groups contained for instance, exponential functions, sets of polynomials and others. These functions are fitted to the horizons data and the goodness of fit is computed. Subsequently, the shape of the curve that presents the best values of R^2 is analysed by comparing it with the soil profiles values, in order to obtain on single group of function. At this point, the best performing group of equations is screened to obtain the best soil specific depth function. The fitting proceed by repeatedly changing the exponents of each variable in order to find the single equation, from the group, which shape best describes the general depth pattern and fits the data with an acceptable level of accuracy.

This procedure can ease the process of the depth function selection, but it cannot be used in an automatic way. This mapping method is highly dependent upon the pedological knowledge of the area under study and the knowledge of the processes that defined the depth pattern observed in the samples. For this reason, the depth function selection requires a detailed analysis of the soil dataset and the soil property under study.

3.2.4 Depth function for best describing the cone-index profiles

In this case study, prior to the application of the framework, an analysis of the depth variation of the cone-index data and their spatial and vertical variation was performed. This analysis highlighted that PR in this area presented the general depth pattern presented in Fig. 3.2a. Moreover, from the soil property analysis was concluded that PR datasets present uncertainties related to each sampled points, as presented in section 3.1.

This supported the conclusion that for describing PR in Lany, a depth function with the following characteristics was required:

- Its shape needs to fit the general pattern. Thus, its needs a change of inclination at around -0.30 m, where the shift between the two layers was identified.
- Its needs to be relatively simple in order to avoid fitting the measured points, which values are affected by a certain level of uncertainty, too closely.

After this preliminary analysis, the framework was applied to the cone-index data. From the goodness of fit analysis, polynomials were found to be the group of equations that are better suited for describing the pattern in Fig. 3.2a.

The results of the preliminary analysis suggested that the complexity of the depth function needed to be kept to a minimum in order to reduce the influence of the point uncertainties. For this reason, 2nd order polynomials were selected from the framework, with values of R^2 of 0.79 and root mean squared deviation (RMSD, is an index that computes the squared root of the average sum of the squared residuals, from Schunn and Wallach, 2005) of 0.26.

After this step, the exponents of the 2nd order polynomial were changed repeatedly in order to minimize the sum of the squared residuals and finding the best 2nd order polynomial for this dataset.

The equation chosen as soil specific depth function is the following:

$$y_{(i,j)} = \beta_1 \cdot x_{(i,j)}^{6} + \beta_2 \cdot x_{(i,j)}^{3} + \beta_3 \qquad (3.1)$$

For every point of depth $x_{(i,j)}$, the value of the soil compaction, $y_{(i,j)}$, can be calculated with a polynomial in which β_1, β_2 and β_3 are the coefficients of the equation, fitted with a least squares estimation.

In order to examine in details the behaviour of the soil property and the error associated to the regression, a spatial study of the goodness of fit indexes and the residuals of the polynomial regression is presented.

3.2.4.1 Geostatistical interpolation

In this study, the top-down mapping relies on the fitting of a polynomial depth function to the cone-index data, coupled with an interpolation of the coefficients of the polynomial. Ordinary kriging interpolation was used with the variogram model fitted using a residual maximum likelihood estimator (REML, Patterson and Thomson, 1971).

In order to demonstrate the accuracy of the developed method, it was compared with the established 3D ordinary kriging, which was already used by Castrignanò et al. (2002) for mapping cone-index data.

3.2.5 Validation

The validation process involved a random exclusion of a percentage of soil profiles (10, 20, 30, 40 and 50% of the population). Subsequently, the cone-index values in the excluded profiles were re-predicted using the top-down mapping method, and then the observed and predicted values were compared using common statistical indexes (i.e. RMSD). The random subsampling was repeated 500 times in order to have a statistically significant population of results.

3.2.6 Software

The geostatistical analyses were undertaken with the statistical programming language *R* (*R* Development Core Team, 2009) and the package **gstat** (Pebesma, 1992; 2004). The three-dimensional visualization of the soil map was created using Golden Software *Voxler* (Golden Software, 2008).

3.3 Results and discussion

3.3.1 Polynomial depth function

A method, denoted top-down mapping, was developed for describing the horizontal and vertical variation of PR, based on 3D mapping with simple depth functions. This method is based on the assumption that penetrometer data are characterized by uncertainties at each measured point, caused by variations in the use of instrument (the penetrometer should be pushed into the soil at a constant speed in order to obtain reliable data, and this is almost impossible in reality).

For this reason the hypothesis is that a simple depth function can optimally describe the general shape of the PR profiles, by filtering out these point uncertainties that would cause error propagation with more complex functions. The top-down mapping is therefore based on a framework developed for determining the best site specific depth function, from which the polynomial in Eq. 3.1 was selected.

This function can accurately fit to the average pattern (Fig. 3.2a), because its shape is adapted to the two-layer pattern with the topsoil relatively loose, below which the subsoil is generally more compacted. This is demonstrated by the goodness of fit analysis, presented in Fig. 3.3 in form of an observed versus predicted scatterplot. The result shows high accuracy in predicting cone-index along the profile, with a mean R^2 value of 0.84, and a value of RMSD of 0.22. However, the average pattern described in Fig. 3.2a is the combination between areas where the PR increases uniformly along the profiles (Fig. 3.2b, sample 54) and areas in which there is a rapid increase in PR between -0.24 m and 0.32 m (Fig. 3.2b, sample 25), which can be fully explained only if a plough pan is taken into account.

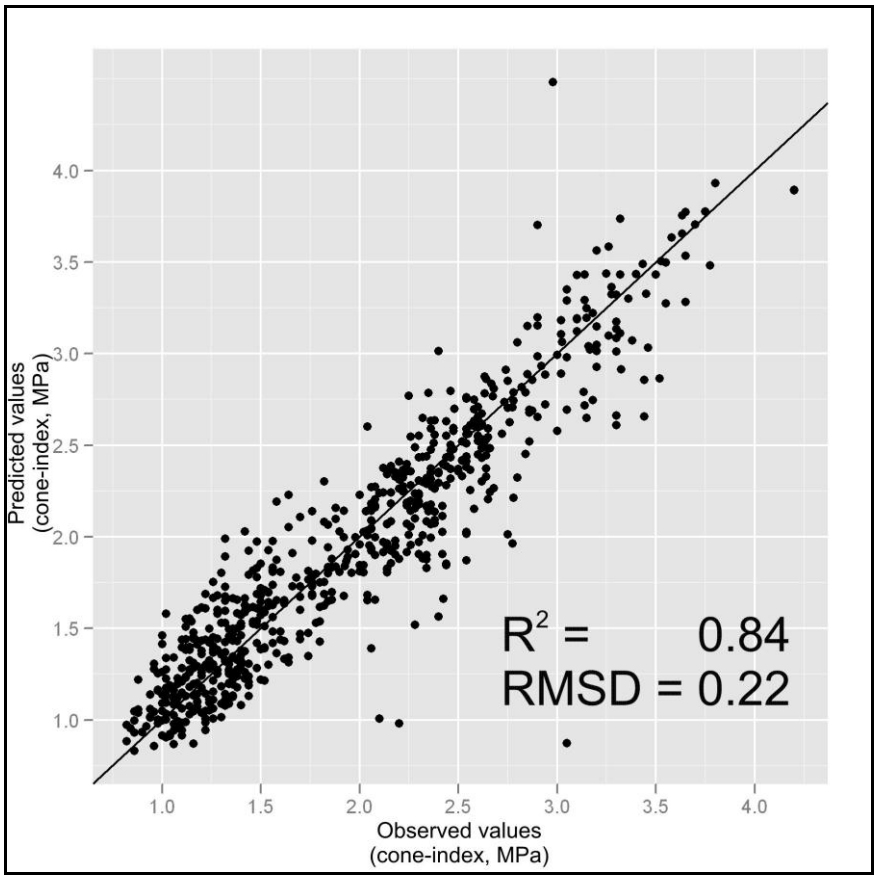

Fig. 3.3: Scatterplot of observed/predicted values. On the X axis the profile values excluded during the cross-validation are represented; on the Y axis are represented the values predicted by the proposed mapping method. The selected depth function is able to predict the cone-index data with a high level of accuracy.

3.3.2 Soil specific depth functions as diagnostic tools

A soil specific depth function can be used effectively as a diagnostic tool. It is selected for its accuracy in fitting the average depth pattern, which is typical of the majority of the soil profiles, as demonstrated by the high value of R^2. However, not every sample presents the same pattern and in some cases the goodness of fit values are relatively low. This indicates a change in the pattern of soil resistance, which can be easily spotted.

In order to explore this concept, two interpolated maps of the Lany field were created showing the distribution of R^2 and RMSD values throughout the field (Fig. 3.4a). The largest proportion (>70%) of the samples presents good fit statistics, having a mean R^2 of 0.88 and a mean RMSD value of 0.20. However, there are areas of the field where the fitting of the polynomial is not as accurate, coloured in grey in Fig. 3.4a. This means that the soil profiles in these areas present a different form compared to the average pattern described by the depth function.

There are two reasons for this: *firstly,* in some cases the plough pan causes a peak in the cone-index value that is far higher than the average, causing the polynomial to fail in describing it with the usual accuracy. The *second* reason is related to a general increase in the data error in certain samples, probably caused by a change of speed in pushing the penetrometer into the soil. Where this is too severe, the polynomial fails to describe the local soil compaction pattern. However, in this dataset the values of goodness of fit are below an acceptable level (R^2<0.5) for only a single profile. For this reason, the profile was considered to be an outlier and Eq. 3.1 was considered valid for the entire field.

In order to better discriminate between these two possible causes it was necessary to further explore the results of the fitting, by looking at the residuals along the profile. The residuals values at three depth layers were computed (-0.12, -0.32 and -0.44 m; Fig. 3.4c). By looking at these data, it is evident that the top layer (between -0.08 and -0.28 m) is the most homogeneous, with low values indicating a general good performance of the polynomial in describing the topsoil PR. Conversely, the subsoil presents local high absolute residuals which signify areas with cone-index values much different from the depth average.

In the -0.32 m layer, the residuals values are mostly positive, meaning an above average compaction, consistent with the presence of a plough pan. By contrast, the residuals in the deeper layer (below -0.32 m) are mostly negative indicating a below average compaction that can be due to a general decrease in soil compaction probably caused by a recovery of soil structure. There are also

three areas of positive residuals, which are probably due to an increase in the data error in the lower part of these profiles.

In summary, with this uncertainty analysis it was possible to determine the amount and the spatial distribution of areas affected by subsoil compaction, before undertaking the full geostatistical analysis. It is also possible to identify profiles, or areas, where the depth function fit the data below the level of accuracy that can be considered acceptable. At field scale, and in areas with homogeneous soil features, if only a limited number of profiles present R2 values below 0.5, the probable cause is the presence of outliers. In such datasets, the depth function can be considered valid for the entire study area, as it was in this study.

Conversely, in areas that present heterogeneous soil features the analysis of the goodness of fit maps can give an indication of these changes. In these areas, such maps can be used to discriminate plots with homogeneous depth behaviours that can be mapped individually, using the method more appropriate for each soil type. This requires using either a different depth function or using a completely different but more suitable mapping method.

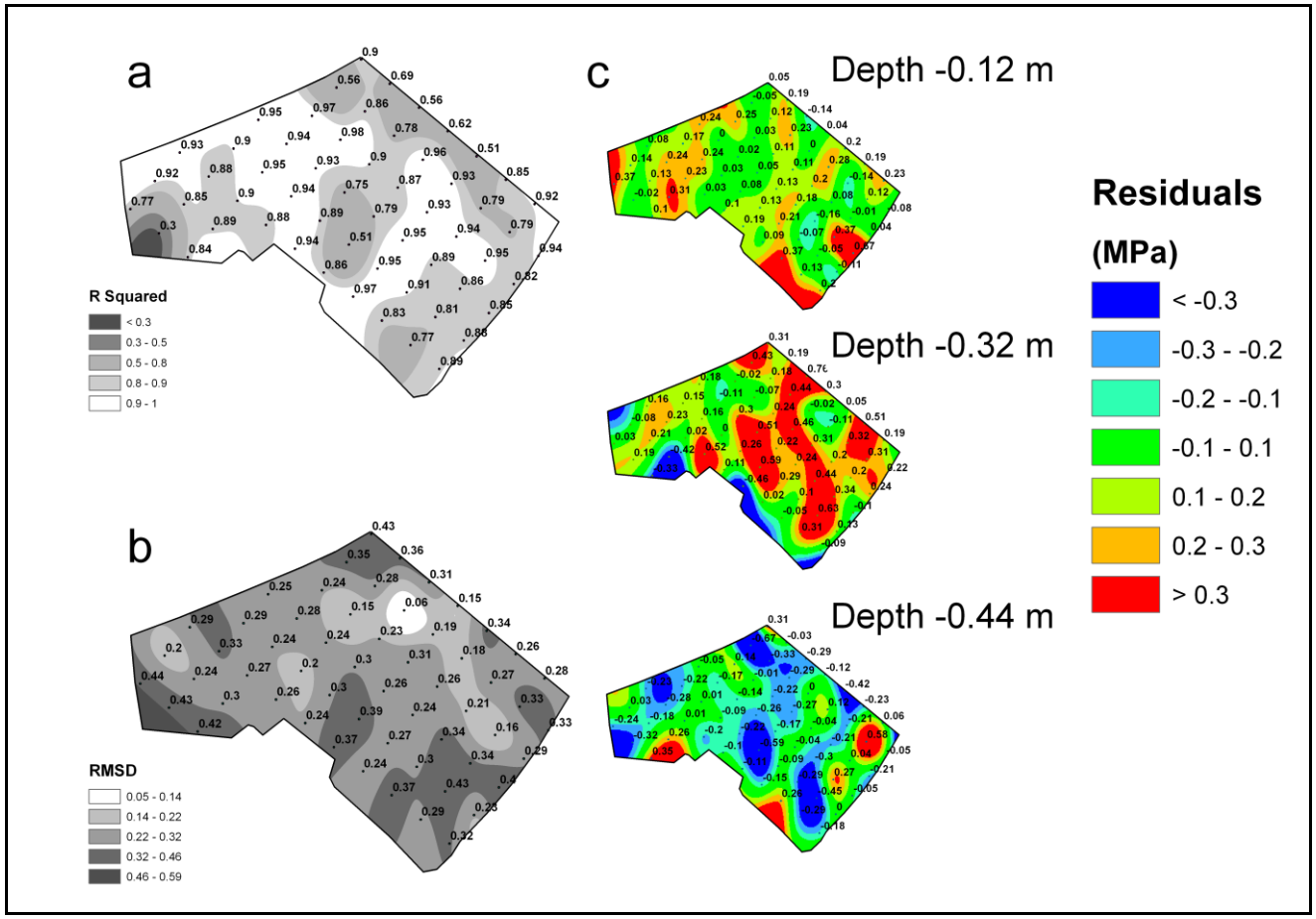

Fig. 3.4: a, b) Interpolated maps of two goodness of fit indexes: R^2 and RMSD. c) Map of the residuals of the Eq. 3.1.

3.3.3 Comparison with 3D ordinary kriging

The subsequent phase of the study aimed to demonstrate the accuracy of the top-down method by comparing it with a technique that was widely used in literature for PR mapping, in this case 3D kriging (Castrignanò et al., 2002). Two 3D maps of the field were created using both methods and descriptive statistics and cross-validation were used to determine the most accurate.

The process started by computing the standard deviation of the original population, which is 0.73, and comparing it with the standard deviations of the two predicted datasets, which are 0.63 for the top-down mapping method (a reduction of 14%) and 0.57 for the 3D kriging prediction (a reduction of 22%). This suggests that the top-down mapping described the distribution of the predicted population to a level comparable with the original dataset, avoiding the smoothing typical of kriging (Deutsch and Journel, 1998). Therefore, its predictions can potentially be more accurate.

In order to demonstrate the prediction accuracy of the method, a cross-validation experiment was set up by randomly excluding a percentage of profiles from the original dataset and then re-predicting their cone-index values. The results are presented in Fig. 3.5 and Table 3.2, and indicate a higher accuracy of the top-down mapping method with values of RMSD always lower than 3D ordinary kriging, even when the exclusion percentage reaches 50%. The top-down mapping method can therefore be sufficiently accurate even where the sample size is small.

In summary, the top-down mapping method can achieve a higher mapping accuracy because it can effectively reduce the smoothing associated with 3D geostatistical interpolation. It is also generally less complex to apply because it relies on bi-dimensional interpolation which is more commonly used that its 3D counterpart.

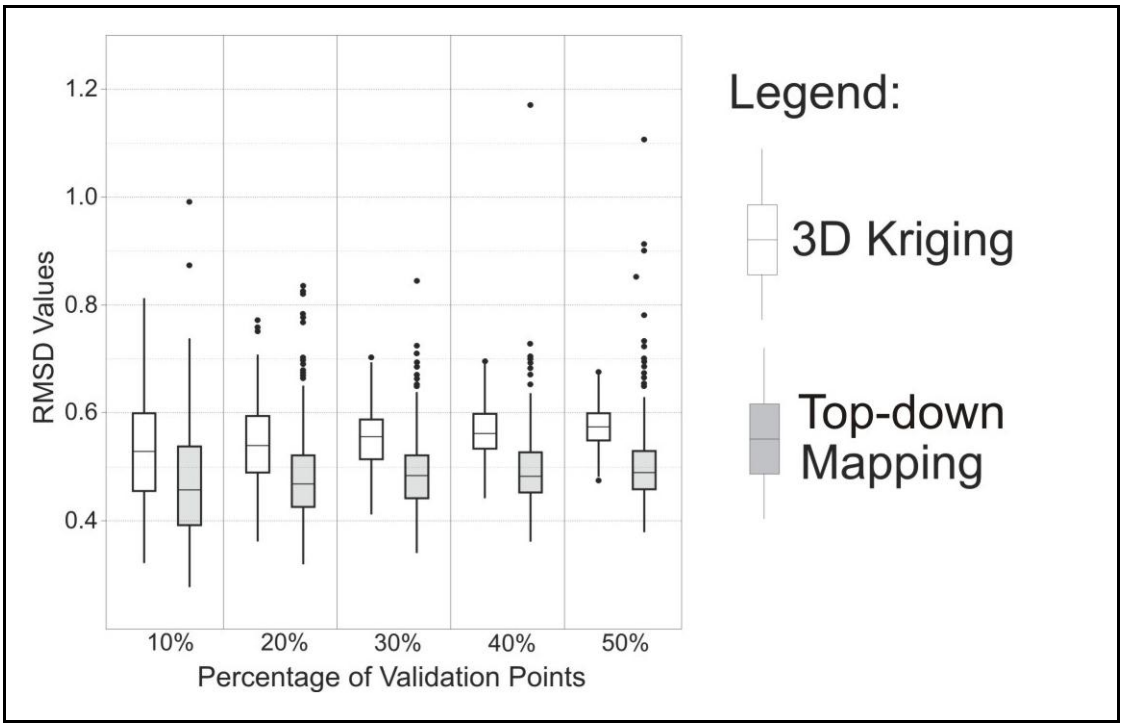

Fig. 3.5: Box plot of the cross-validation results, divided for exclusion percentages.

Table 3.2: Numerical cross-validation results.

	3D Ordinary Kriging					**Top-down Mapping**				
Exclusion	*10*	*20*	*30*	*40*	*50*	*10*	*20*	*30*	*40*	*50*
Mean	0.54	0.54	0.55	0.56	0.57	0.47	0.48	0.49	0.52	0.53
Median	0.53	0.54	0.56	0.56	0.57	0.46	0.47	0.48	0.48	0.49
St.Dev.	0.10	0.07	0.05	0.05	0.04	0.10	0.09	0.07	0.32	0.45
Minimum	0.32	0.36	0.41	0.44	0.47	0.28	0.32	0.34	0.36	0.38
Maximum	0.81	0.77	0.70	0.70	0.68	0.99	0.84	0.84	6.18	9.14

3.3.4 Visualization

From these conclusions, a 3D map of Lany field was generated, solving the Eq. 3.1 for a grid of 6,700 points (1 m of horizontal resolution, 1 cm of vertical resolution). Visualizing a 3D soil model in a way that it is visually accessible is a challenging task. With the visualization techniques normally applied, soil 3D map are generally difficult to interpret. This was demonstrated by applying three different techniques for presenting the soil map, showing their advantages and disadvantages.

The *first* method uses horizontal slices (Fig. 3.6). The advantage of this technique is that is widely used and the two maps can be easily compared. The disadvantages are that the slice selection is not objective and depends on the map author, and that it is difficult to determine the lateral or vertical extent of compaction areas from these maps, especially when their shapes are elongated as in this case study.

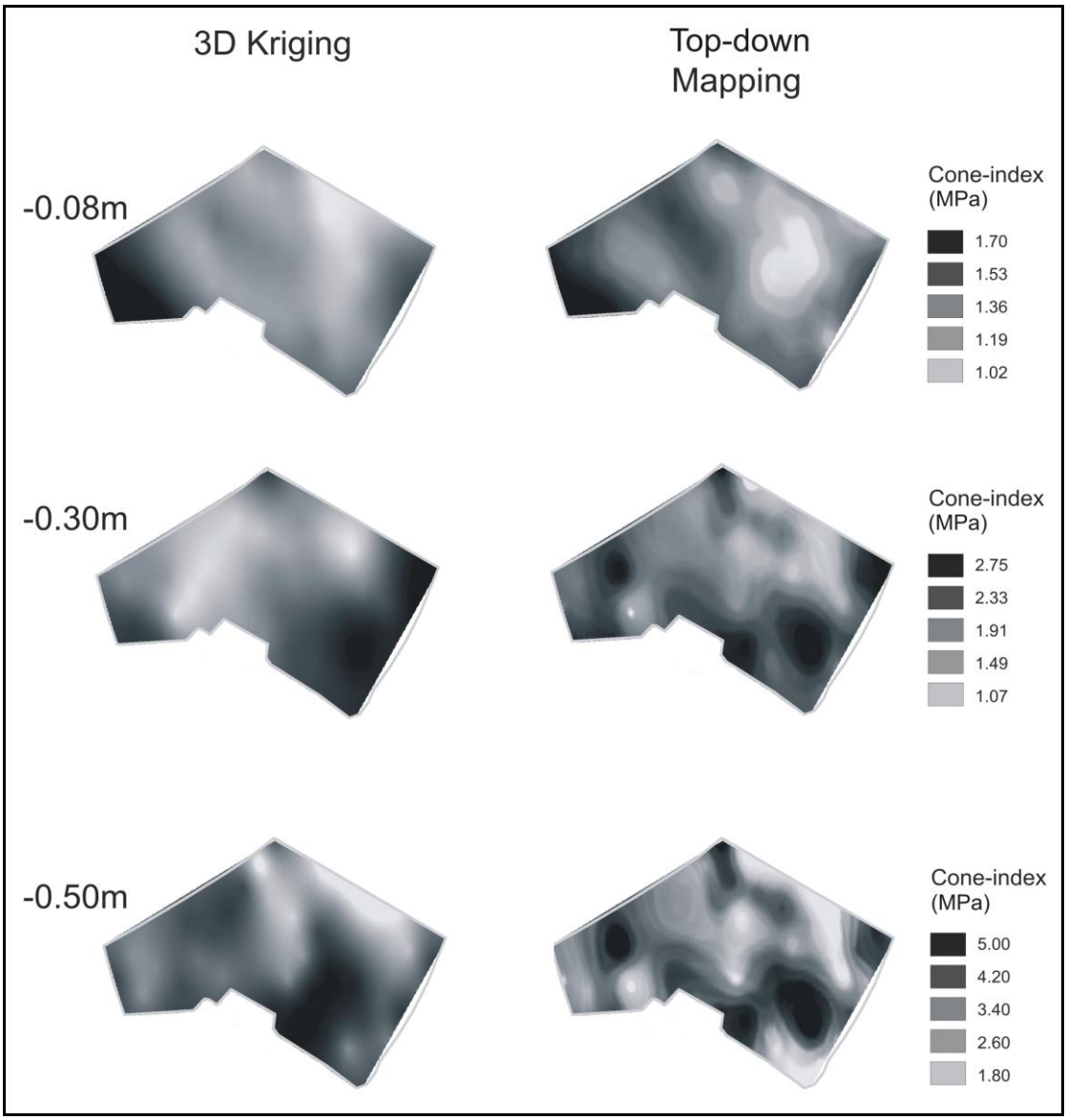

Fig. 3.6: Sliced maps of Lany field, created using the two tested algorithms.

The *second* method is based on 3D visualization (Fig. 3.7). This technique uses vertical slices and contours, which define lines of equal compaction on the horizontal plane. The advantage of this technique is that it effectively shows areas of higher compaction, which are highlighted by darker colours and by a denser set of contours. The main disadvantage is that it is very difficult to interpret because the user needs to understand the orientation of the 3D image, an issue that is difficult even for people experienced in viewing 3D models.

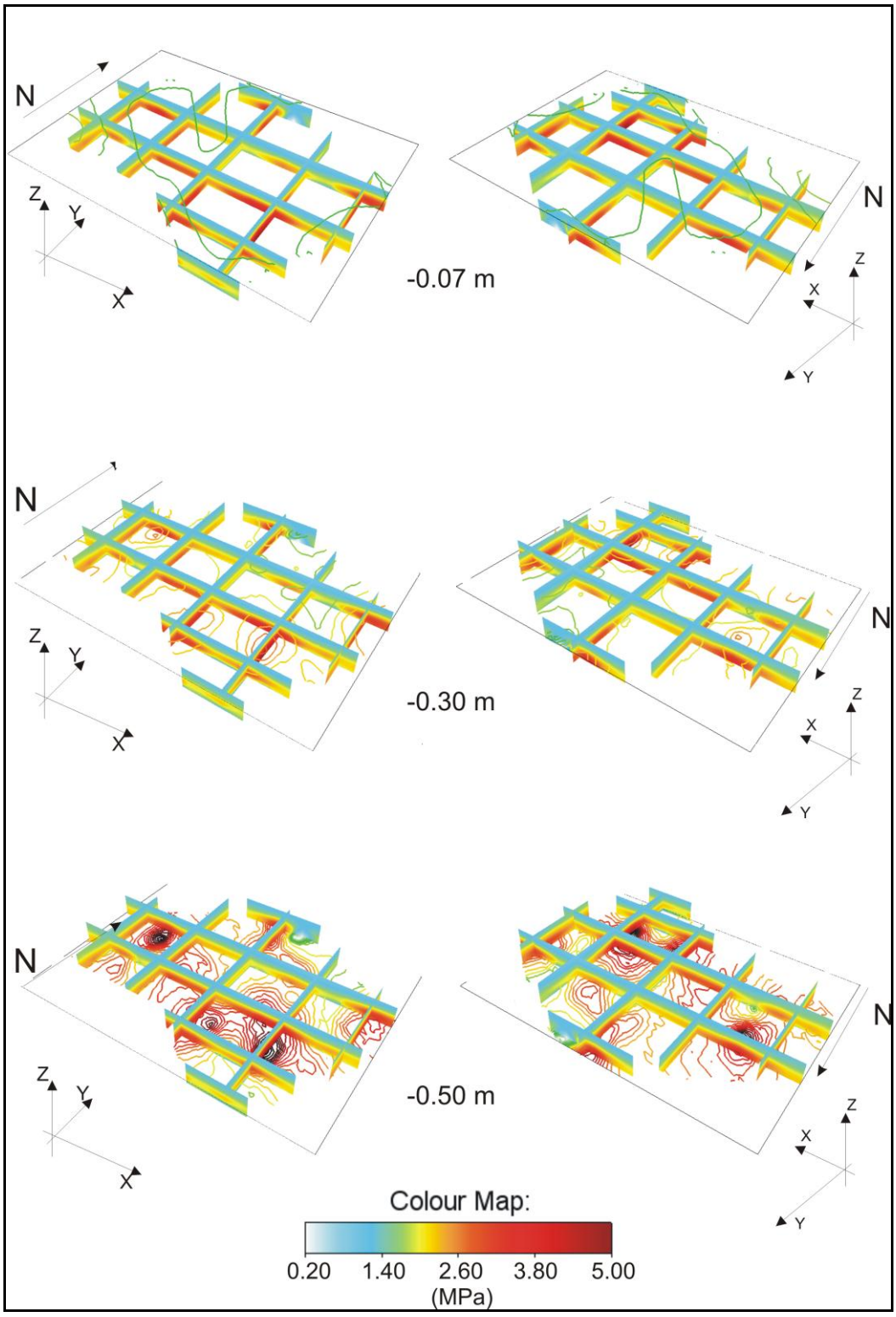

Fig. 3.7: Three-dimensional visualization of the soil map created using the top-down mapping method.

Finally, the *third* visualization technique requires the map to be subdivided in slices along the three geometrical axis. This way the slices for each axis can be grouped into a video animation that produces a “fly-through” experience. This gives the user a more accessible and simpler way to visualize the 3D model. However, such visualization techniques require a large effort in both producing the slices (in this case, for a relatively small area, 48 images were necessary for each axis to produce the video) and creating the animations.

The advantage of the top-down mapping method is the possibility to have goodness of fit and residual maps (Fig. 3.4). These maps can give an accessible way to understand the compaction pattern of the study area, even before the final map is visualized. If, in certain areas, the compaction pattern is complex, the visualization can focus on these areas, producing more slices in order to describe in details the soil changes. This way one the most interpretable technique, which is probably the use of 2D horizontal or vertical slices, can be used. However, the slices are not selected subjectively but based on areas in the field that present important depth changes.

3.3.5 3D animation

To visualize the soil compaction pattern in the Lany field, a set of 3D animations were created. The Eq. 3.1 was solved for a regular grid of 6,700 points starting from the predicted coefficients. The vertical resolution of the 3D grid is 1 cm, the horizontal resolution is 1 m. A volumetric rendering with a natural neighbour interpolator was performed on the 3D grid, and the resultant volume was sliced along X, Y, and Z. The result is a collection of slices every metre for X, and Y directions and a slice every centimetre along Z.

All these images are presented in three animations, one for each direction, in which the viewer can navigate through the soil and appreciate the compaction pattern. In these animations the blue and light blue colours characterize low compaction values. The rapid change due to the plough pan is highlighted by a green colour. The presence of the plough layer is particularly evident in sections along X and Y; the top soil layer presents a general blue colour and a constant

width. Below 35 cm, depth of the plough layer, the complexity become easily appreciable because of the presence of high compaction lenses, which colour ranges from orange to red.
These animations are available on line at:
http://dx.doi.org/10.1016/j.still.2012.05.009

3.3.6 Soil interpretation

Soil compaction is a property that depends on several factors: water content, soil texture, soil organic matter content and land management (Busscher et al., 1997; Soane and van Ouwerkerk, 1995; Medvedev and Cybulko, 1995; Hamza and Anderson, 2005). At the CULS Lany farm, variations in the cone-index values, especially in the topsoil, is predominantly caused by land management practices. The field is covered by arable crops and is managed by conventional ploughing technology. The predominance of the land management above other factors is illustrated by the relatively constant value of compaction in the topsoil. At around 30 cm there is the transition between the managed topsoil and the natural subsoil, and this is observed by a general increased in the compaction values. However, this increase in soil compaction does not coincide everywhere with the presence of a plough pan. In certain areas the increase is smoother. Assuming a uniform load for the whole area, this pattern could be driven by localised changes in soil texture. However, penetration resistance is an indirect measure and its pattern can be influenced by other factors, which are difficult to discriminate.
Below 35 cm the soil pattern became more complex with areas of high compaction and areas with low cone-index values distributed without any recognizable pattern. In general, directly below the plough layer, there is a decreasing tendency in the compaction values but there are areas in which high values of cone-index are maintained to the maximum survey depth. Although the homogeneity of the top soil is certainly due to land management, the factors that may cause the observed pattern in the subsurface are less easily

identifiable. Compaction may be derived from several factors and there are not enough textural and moisture data to fully clarify which one is the major cause of the depth distribution of the cone-index data below the plough layer.

3.4 Conclusions

In this chapter a novel method was developed for mapping soil compaction in 3D. This technique is based on simple soil specific depth functions to describe the general variation with depth of PR, thus decreasing the impact of the point uncertainties related to penetrometer measures. This method can also be used as a diagnostic tool in order to easily identify soil profiles in which there are deviations from the average pattern. This way the compaction pattern can be much better assessed.

This novel method was tested and compared with 3D ordinary kriging at the field scale, using descriptive statistics and cross-validation. The results indicate that the developed method can increase the amount of variance described in the mapping, reproducing the distribution of PR more closely to the original dataset, when compared with 3D kriging. As a consequence, this method can predict PR in the 3D space more accurately than 3D kriging, even with a smaller dataset.

This study presents an example of soil mapping with a limited dataset and its successful application to 3D mapping. Although this study was restricted to a single field with particular soil properties, this approach could be applied to a larger area, if soil specific depth functions can be identified. Moreover, if it is possible to identify a general pattern and determine a simple depth function, then it is also possible to map the field with less analytical data.

CHAPTER 4 – Mapping soil texture in 3D

COMPARISON BETWEEN THREE METHODS OF 3D SOIL MAPPING

Abstract

Soil texture is important as it affects several key soil functions. However, the classic approach of mapping soil features in space, building polygons of taxonomic units, does not offer a sufficient level of spatial variability within each polygon that is necessary when soil maps are needed as primary sources for environmental modelling. For this reason three geostatistical methods for 3D quantitative mapping of soil texture were tested: the top-down mapping method, developed in the first stage of the PhD; 3D universal kriging; and the equal area spline approach. In order to properly compare these methods, which are different in their approach, an experiment was set up in which a new dataset was simulated on a regular grid, and then a series of validations were performed.

The results show that each method is able to describe the variation by depth of the three textural percentages, but during the cross-validation procedure, the universal kriging emerged as best predictor, with RMSD values consistently lower than the other methods. The smoothing effect described in the previous chapter that undermined the reliability of kriging for 3D soil mapping is still present, and causes a decrement of around 20% of the estimated variance. However, in this case 3D kriging was the best predictor, probably because the complex pattern in the soil texture profiles decreases the accuracy of the depth function approaches.

Conversely, depth function methods are better at replicating the distribution of the textural percentages observed in the simulated dataset, but predict texture less accurately. In particular, the top-down mapping method fails to accurately predict soil texture due to the complexity of the textural profiles and it is not

possible to describe them with a simple equation. Interpolating too many coefficients probably causes a decrement in the estimation accuracy that undermines the feasibility of the method with properties that present a complex depth pattern.

4.1 Introduction

Soil texture is defined as the relative proportion of sand, silt and clay in a mass of soil. It is an extremely important soil property because it affects various soil functions such as drainage, water holding capacity, aeration, susceptibility to erosion, organic matter content, cation exchange capacity, pH buffering capacity, and soil tilth (Berry et al., 2007; Brown, 2003).

Soil texture is one of the key features used to divide soil profiles into horizons, which are layers of soil, approximately parallel to the surface, having distinct characteristics produced by soil-forming processes that distinguish them from layers above and beneath.

4.1.1 Mapping soil texture

A soil survey consists in taking soil samples at specific locations in the landscape. Each sample can be located on a regular grid or, more often, its location is determined by the experience of the surveyor and the relation between geomorphology, geology and vegetation with the soil distribution. The soil is then analysed and classified into soil groups using, for example, the WRB system (World Reference Base for Soil Resources, 2006). Each of these groups is defined according to diagnostic characteristics and properties of the soil body. The soil map is created by matching the changes in geomorphology, geology and vegetation to the changes in soil by creating polygons of homogeneous soil type. The problem is that these maps do not sufficiently account for the spatial variability of the soil properties (Triantafilis et al., 2002).

The advent of quantitative soil mapping has dramatically increased the capacity to represent soil variation, both in the horizontal as well as in the vertical space.

From a soil classes map, each location was characterized by having texture ranging within a set of values dependent by the soil type. With 3D DSM is possible to obtain, for each location and depth, a set of unique estimates that can be readily embedded in environmental models, such as erosion, flood risk and hydrological; processes which operate in the three-dimensional domain.
Limited research focuses on 3D soil quantitative mapping, with particular focus on mapping organic carbon (Minasny et al., 2006; Malone et al., 2009; Kempen et al., 2011; Meersmans et al., 2009; Mishra et al., 2009). It is mandatory to start reviewing these methods in predicting other soil properties because the future of digital soil mapping will be based on continuous 3D soil models. This has been confirmed by the specifications for the Global Soil Map project (GlobalSoilMap.net, 2011), which will look at volumetric soil units predicting several soil properties and their variation with depth. For these reasons, it is important to review common methods for 3D soil mapping, alongside the top-down mapping method developed in this PhD, in order to define their level of accuracy and the amount of variation that each method can describe. The final aim is to give some guidance for their use in future projects.

4.1.2 Quantitative mapping techniques

In this study two commonly used 3D mapping methods, and the top-down mapping, were reviewed at the field scale. The objective was to compare the results of each method and assess their accuracy, both in term of cross-validation results but also in term of their ability to fully replicate the soil property observed variation.
Probably the most common technique is based on spline depth functions, denoted as equal area spline. It was developed by Bishop et al. (1999) and assumes that soil properties vary continuously with depth. Therefore, the average horizon data do not fully represent the real changes of physical properties in the soil profile. This method relies on mathematical regression to calculate the property of interest continuously along the depth profile, increasing the vertical data resolution, combined with subsequent geostatistical

interpolation for creating the 3D lattice. This method was chosen because it was used, by Bishop et al. (1999), to describe soil texture profile data, and it was already used successfully for digital soil mapping (Minasny et al., 2006; Malone et al., 2009).

Another common technique for 3D mapping involves the use of three-dimensional geostatistical interpolation (Castrignanò et al., 2002; You and Lee, 2006; Thierry et al., 2009). In this case the interpolation is performed directly on soil data, and the values are predicted as weighted averages of the nearby observations, using the spatial auto-correlation of the soil property to assign the weights.

4.2 Environmental covariates

The term “environmental covariates” is used to describe all the data that can be collected with minimal or no direct contact with soil. It comprehends the remote sensed datasets, such as DEM and its derivatives, and the proximal soil sensed data, such as geophysical data. Environmental covariates can provide non-destructing, minimally-invasive and relatively inexpensive ways to describe the soil spatial variability and therefore improve the mapping accuracy on a reduced physical set of observations.

Remote sensed data, such as DEM and DEM derivatives, can be obtained by digitising a topographic map but more often are derived by measurements taken by satellites or laser scan. These data are extremely useful for digital soil mapping because the spatial variation of soil in the landscape is partly driven by geomorphological changes and these data can provide a numerical representation of these changes.

Proximal soil sensed data in the iSoil project are represented by geophysical covariates, such as electro-magnetic (EM) and gamma-ray measurements. EM data measure the soil electrical conductivity, which is a physical property that indicates the ability of a material to conduct an electric current. Clay content presents a high electrical conductivity and therefore is highly correlated with EM

data. Sand and silt are less conductive and therefore more difficult to correlate with EM.

Gamma-ray data measured the amount of gamma radiation emitted by the soil volume investigated. The radiation is emitted by particular radionuclei such as Thorium, Uranium, Caesium and Potassium, which concentration can then be measured. These concentrations can be used to fingerprint particular textures (Egmond et al., 2010; van Wijngaarden et al., 2002).

As part of the iSoil project, which aims at exploring the use of these data in DSM, this PhD explores the use of environmental covariates in 3D mapping. This is achieved, in this Chapter, by using these data as they are generally used in DSM: as source of ancillary information regarding the soil spatial variability (i.e. as covariates).

4.3 Materials and methods

4.3.1 Study area

The study site is the CULS (Czech University of Life Sciences) Farm at Lany.

The Lany texture dataset consist of 30 soil profiles, sampled at three depth intervals (0-10 cm; 10-30 cm; 30-70 cm). The samples were collected following a sampling scheme designed by Tubingen University, using Latin Hypercube (Carré et al., 2007), which is optimized for mapping with covariates. Fig. 4.2 presents the texture plot at each investigated layer. From this image is evident that the soil is generally loamy with an increase in clay content, and a shift to clay loam, with depth.

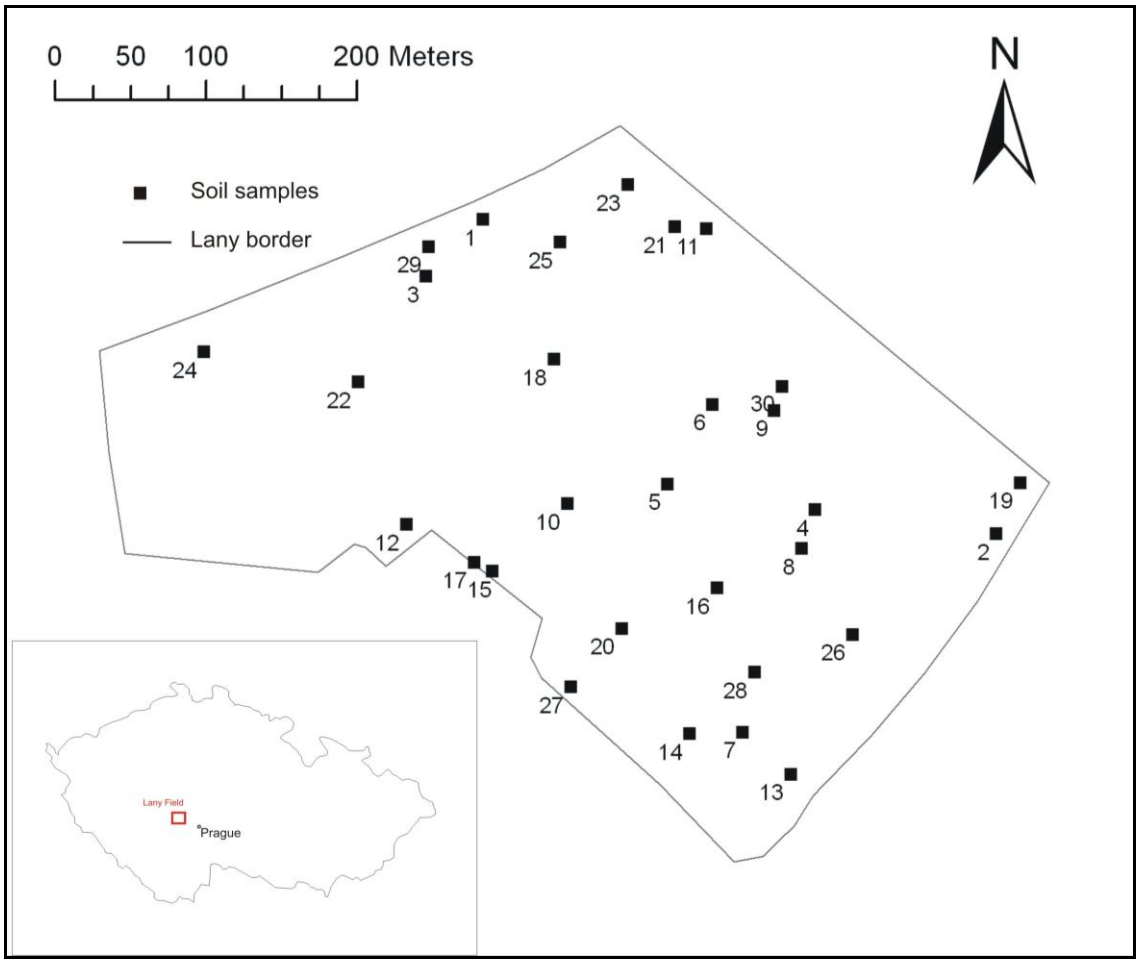

Fig. 4.1: Lany field map with texture samples.

4.3.2 Covariates

Several continuous covariates, both geophysical and non-geophysical, are available for the Lany site. The geophysical covariates are electromagnetic and gamma-ray data. Electromagnetic surveys were undertaken with two instruments: EM38 and EM31 from Geonics (McNeill, 1980) by the Helmholtz Centre for Environmental Research. The gamma ray data were collected by the Soil Company using their own spectrometer known as the Mole (Egmond et al., 2010). For this site a 10 m DEM is also available, created by the CULS. From this slope, aspect and curvature were derived.

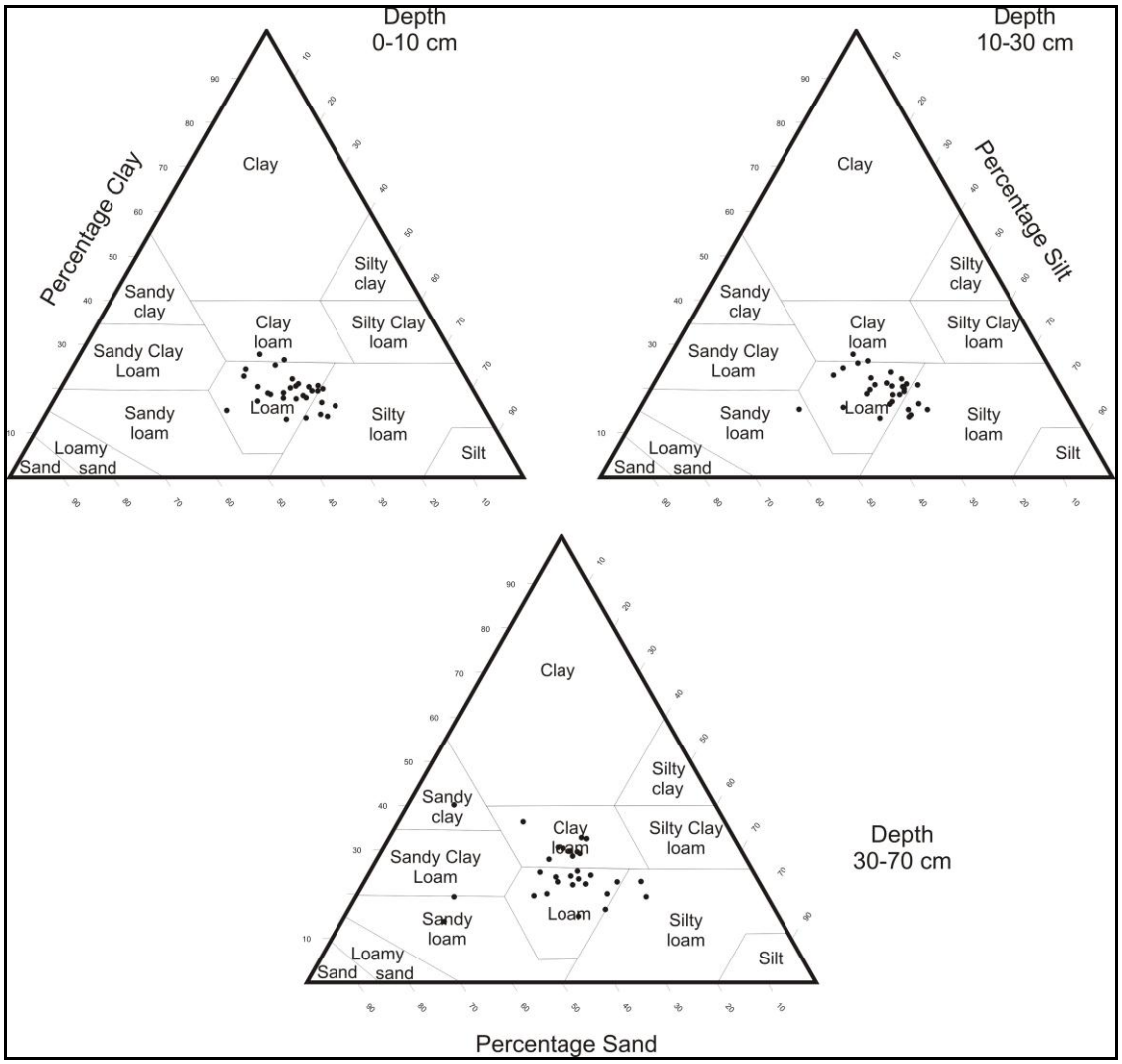

Fig. 4.2: Texture plots with percentages of sand, silt and clay in the three depth layers considered in the profiles.

4.3.3 Conditional simulation

In order to properly compare the three selected mapping methods, and give statistical significance to the validation procedure, it was necessary to simulate a new dataset, starting from the texture observations. For this reason a stochastic conditional Gaussian simulation (Davis, 1987; Myers, 1989; Gomez-Hernandez and Journel, 1993; Pebesma, 2004) was used to generate random realizations of the soil properties, selecting the most appropriate based on its similarity in terms of distribution with the original dataset. A new dataset of soil

observations was then extracted from the simulation results, on a regular grid of 40x40 m and a vertical resolution of 10 cm. Subsequently, because the aim of the study was to compare different soil mapping methods and considering that the most soil data are sampled by horizons, the simulated profiles were averaged into the following pseudo-horizons: from 0 to 10 cm, from 10 to 20 cm, from 20 to 40 cm and from 40 to 70 cm.

4.3.4 Mapping Methods

4.3.4.1 Equal area spline mapping

This method consists in fitting a quadratic spline to the horizon averages in order to increase the vertical resolution of the soil profiles. This function is potentially extremely effective in describing the soil profile because it is mathematically bounded to respect the horizon averages (Bishop et al., 1999).
The soil mapping is undertaken by interpolating the spline parameters, which are the values that the function predicts at defined depth intervals, across the field using geostatistical interpolation. In this experiment a universal kriging algorithm was applied. Fig. 4.3 presents a visual example on how this method works.

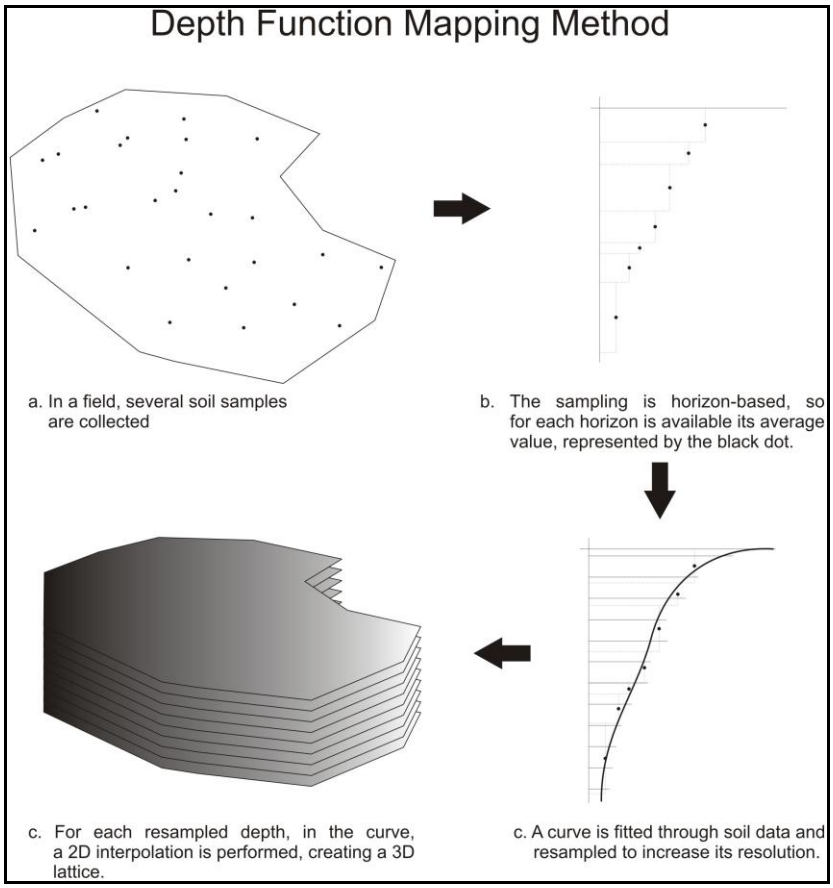

Fig. 4.3: Synthetic scheme of the equal area spline mapping method.

4.3.4.2 3D Universal kriging

Kriging interpolation in 3D is based on the same assumptions described in section 2.4. The main difference is that it computes the variogram in the three-dimensional space by calculating the semi-variance on pairs of observations and it depends on the distance, direction and dip of the vector **h** (lag distance). The 3D variogram is used to assign the weights and calculate the values in unsampled locations, as a weighted average of the nearby observations.

For this study universal kriging was used due to its ability to predict soil variables based upon the spatial variability of environmental covariates.

4.3.4.3 Top-down mapping

This method was developed and tested in the first stage of the project, and it is based on the framework for selecting the best soil specific depth function, described in section 3.2.3.

The preliminary analysis of the dataset concluded that in the study area, soil texture profiles do not present a depth pattern that can generalised. For this reason the depth function needs to be relatively complex in order for its shape to be flexible enough to fit all the profiles. As a consequence, the best soil specific depth function was found in a 3rd order polynomial with the following equation:

$$y_{(i,j)} = \beta_1 \cdot x^3_{(i,j)} + \beta_2 \cdot x^2_{(i,j)} + \beta_3 \cdot x_{(i,j)} + \beta_4 \quad (4.1)$$

For every point of depth $x_{(i,j)}$, the value of the soil compaction, $y_{(i,j)}$, can be calculated with a polynomial in which β_1, β_2, β_3 and β_4 are the coefficients of the equation, fitted with a least squares estimation.

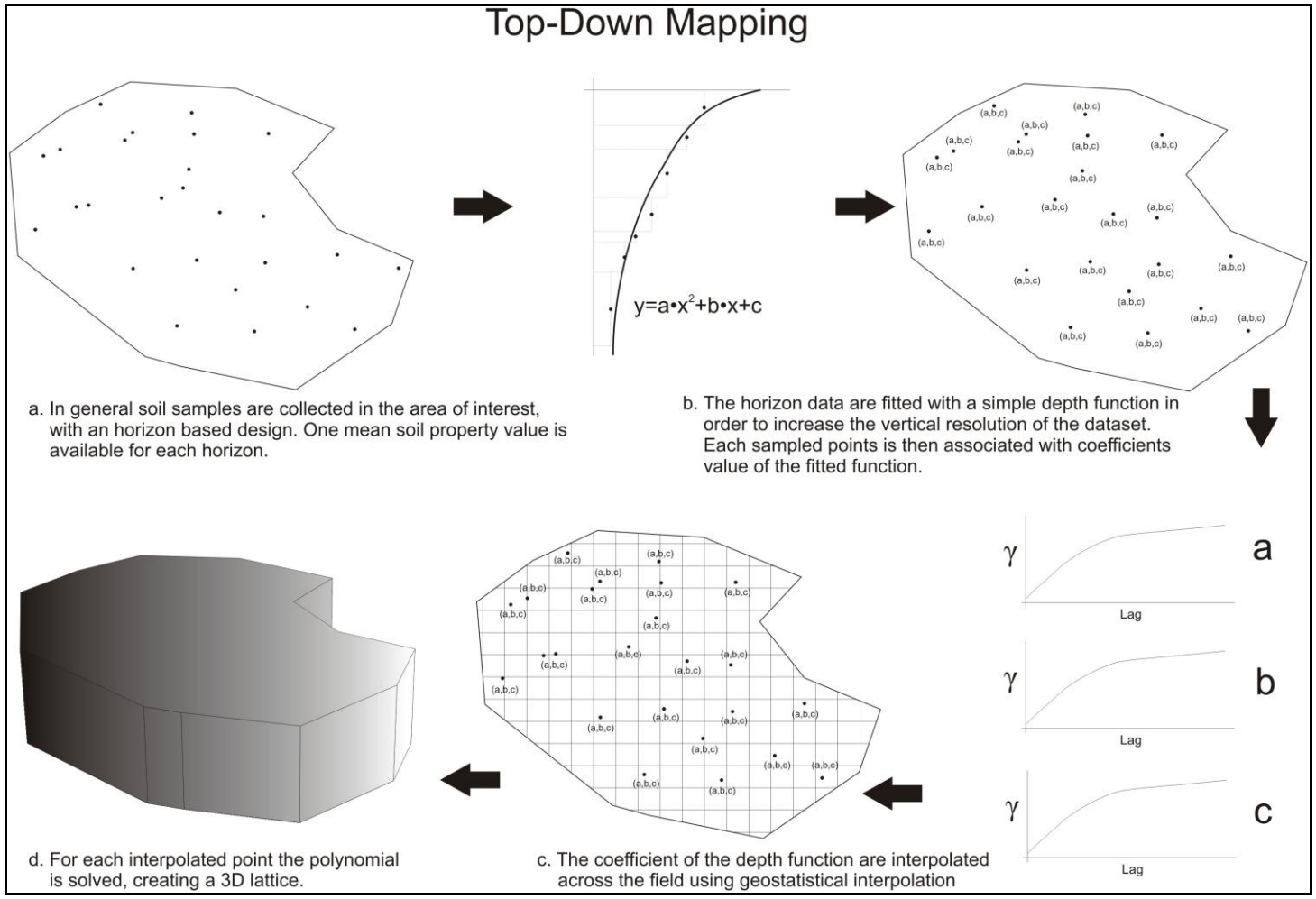

Fig. 4.4: Synthetic scheme of the top-down mapping method.

4.3.5 Validation

In this experiment, three validation methods were used.

The *First* (validation A) tests the ability to describe the variation of the soil properties with depth. This validation was undertaken by using the pseudo-horizons data to estimates the other simulated data along the profile, which were excluded during the averaging of the pseudo-horizons.

The *Second* (validation B) is a cross-validation approach where a percentage of soil pseudo-horizons profiles (10, 20, 30, 40, 50%) were excluded and re-predicted. The process was repeated 500 times in order to obtain a statistically significant set of results. For each validation, the observed and predicted values were compared using the root mean squared deviation index (RMSD; Schunn and Wallach, 2005). This method, by excluding a varying percentage of profiles, tests the predictive accuracy of each method with changes in the data support. From this validation is possible to determine the changes in accuracy of the method when the amount of soil observation is gradually reduced.

The *Third* (validation C) validation has the same approach of the cross-validation (validation B). However, in the previous validation, the predictions were performed starting from pseudo-horizons data and re-predicting pseudo-horizons data. In this validation the starting points are again pseudo-horizons data but the entire simulated dataset is used for comparing observations and predictions.

4.3.6 Software

For conditional simulation and kriging, the *R* statistical programming language (*R* Development Core Team, 2009) was used, with the package **gstat** (Pebesma, 1992; 2004).

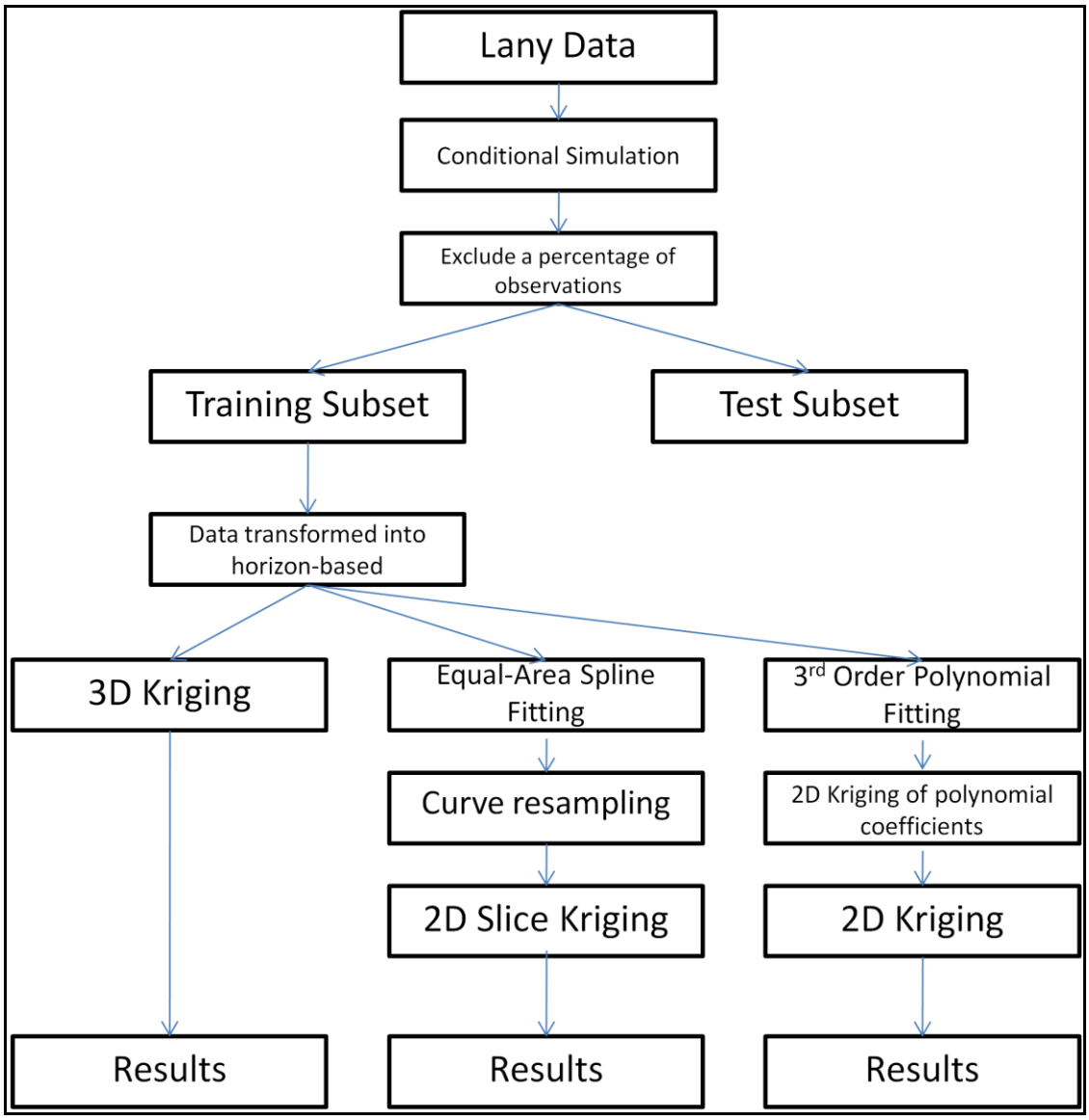

Fig. 4.5: Working flow diagram of the study.

4.4 Results and discussion

The objective of this study was to evaluate different methods of 3D mapping in order to assess their predictive accuracy. A simulated dataset, with soil texture (percentage of sand, silt and clay) and a large set of covariates (geophysical and non-geophysical), was used as inputs for comparing three methods: the equal area spline approach, 3D universal kriging algorithm and the top-down mapping method (developed in the first stage). In order to avoid differences in the results due to different combination of covariates, all the available covariates were used with each method. Universal kriging was employed as a standard interpolation method in such a way that the conditional simulation equally affects each mapping method. Consequently, the differences in the results are caused only by differences in the methodology.

These methods were compared in terms of prediction accuracy with changes in data support, using three validations that were designed to test their accuracy in the description of both the vertical and the horizontal variability of soil texture. Fig. 4.5 presents a detailed flow diagram that describes all the steps taken for this experiment.

4.4.1 Profile description (validation A)

The initial goal is to analyse which method was optimal for re-creating the observed soil profile by using the pseudo-horizons data to estimate all the other simulated values. The results, presented in Fig. 4.6, indicate a generally good performance for each method in describing the overall variability of soil texture by depth. The RMSD values vary from a minimum of 1.61 when 3D universal kriging is applied in predicting clay content, to a maximum of 2.58 from the top-down mapping in predicting silt content variation with depth.

The results appear to suggest that clay content is easier to estimate and 3D universal kriging performs slightly better than the other two depth function approaches. The latter is unusual because the depth function approach was

developed in order to increase the vertical resolution of soil profile data, assuming that a regression is needed prior to the interpolation for better results. These results seem to challenge this view by suggesting that a 3D interpolation, in some cases, is sufficient to both describe the vertical and the horizontal variability of the soil property of interest.

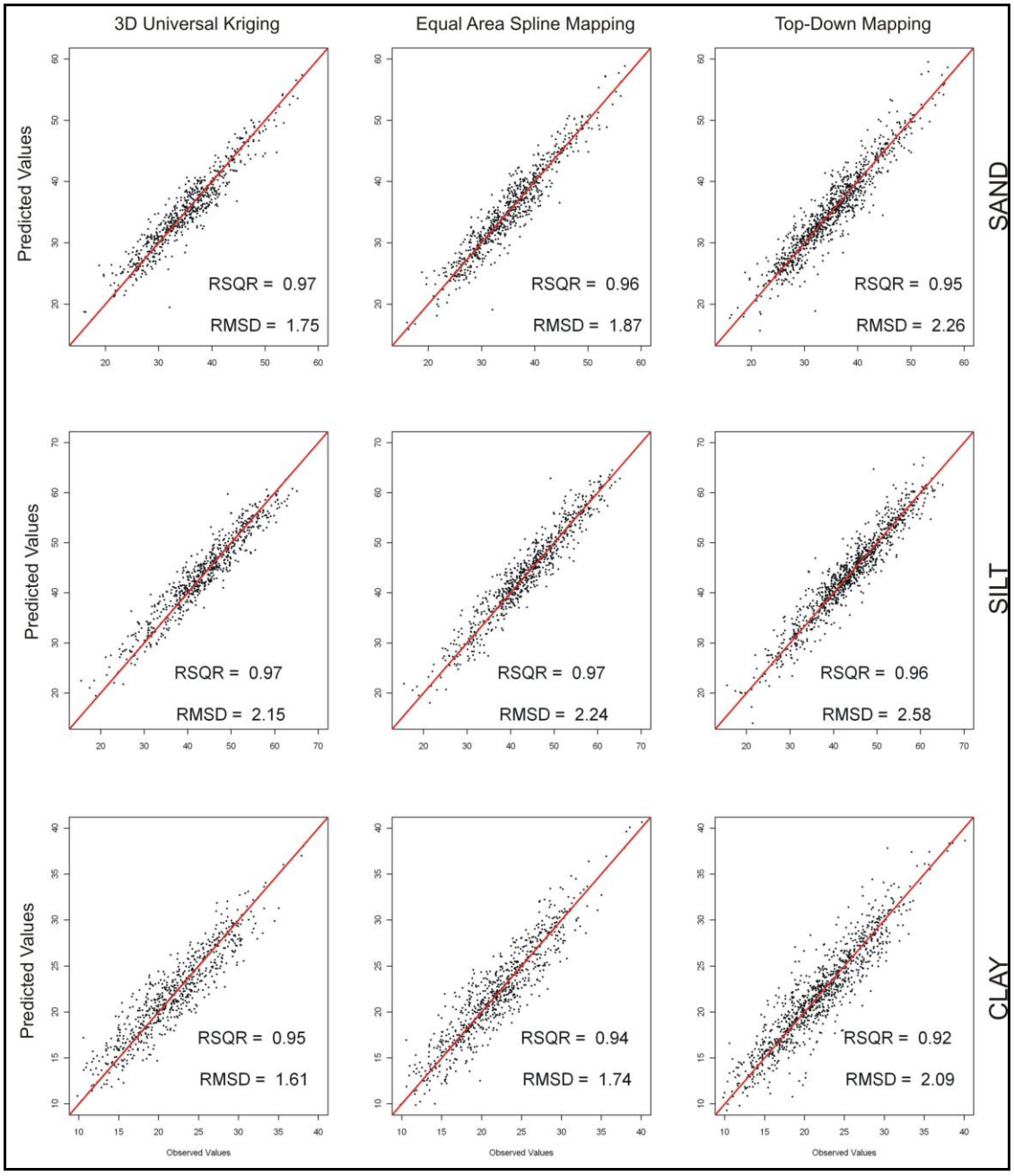

Fig. 4.6: Scatterplot of predicted/observed values for the prediction along the profile. In this case the three estimation methods were used, starting from the pseudo-horizons dataset, to predict all the other values in the soil profiles.

4.4.2 Cross-validation (validation B)

In order to test these preliminary results, it was necessary to start the cross-validation phase in which a varying percentage of soil profiles were excluded and their texture values re-predicted using the three methods. The results, showed in Table 4.1, confirm the outcome of the previous analysis.

Table 4.1: Cross-validation results. Equal area spline approach (EAS); 3D universal kriging (3DUK); Top-down mapping (TDM).

Validation Percentage	**10%**			**30%**					
	EAS	3DUK	TDM	EAS	3DUK	TDM	EAS	3DUK	TDM
Sand	5.45	5.21	6.14	5.76	5.51	6.58	6.26	5.82	8.00
Silt	6.57	6.14	7.54	6.98	6.67	9.79	7.70	7.49	10.84
Clay	5.08	5.04	7.30	5.15	5.11	14.11	5.24	5.17	385.78

Validation Percentage	**20%**			**40%**		
Sand	5.52	5.28	6.39	6.05	5.71	7.21
Silt	6.84	6.51	9.19	7.21	6.88	11.70
Clay	5.11	5.07	9.10	5.17	5.14	10.57

Clay content predictions were most accurate, even though not all methods can predict clay better than the other two properties. Universal kriging and the equal area spline approach are more accurate in predicting clay content compared with silt and sand. A minimum RMSD value of 5.04 was obtained for kriging and 5.08 for equal area spline resulted from an exclusion of 10% of the soil profiles. By contrast, the top-down mapping resulted to be less accurate in estimating

clay content (7.30 RMSD value with 10% profiles exclusion) compared to sand (6.14 RMSD value with 10% profiles exclusion).

These results can be explained by the fact that the geophysical covariates that were used are, in general, highly correlated with clay content (Egmond et al., 2010; Triantafilis and Lesch, 2005; Schnyder et al., 2006; Bierwirth and Brodie, 2008), in particular EM data and Thorium concentration.

Regarding the estimation accuracy of each method, the results show that 3D universal kriging is the best performer, with RMSD values always lower than the other two methods, confirming the results of the prediction along the depth profile. In summary it appears that three-dimensional interpolation is the most accurate method for 3D soil texture mapping, followed by the equal area spline approach which presents very similar results, and by the top-down mapping that fails in accurately estimating soil texture.

The results (Table 4.2) of the distribution analysis indicate that the smoothing effect typical of geostatistical interpolation is not particularly evident, as suggested by the fact that almost 80% of the variation of each soil property is represented in the estimations with 3D universal kriging. This indicates that the smoothing effect can probably be reduced, by adopting sampling design optimized for geostatistical interpolation.

Table 4.2: Standard deviations of the observed and predicted datasets.

St.Dev	Sand	Silt	Clay
3D Universal kriging	6.09	7.77	4.84
Equal area spline approach	6.75	8.42	5.47
Polynomial mapping	10.41	12.17	8.77
Original	6.86	8.45	5.33

The equal area spline approach can describe the standard deviation of the observed dataset much better, but it predicts slightly less accurately than 3D kriging.

Another difference between equal area spline approach and 3D universal kriging is that the first relies on two-dimensional mapping of the depth values calculated with the spline. In doing so the horizontal variation of the soil property is not considered in the mapping, because the variogram is computed by using only values at the same depth. This can be a minor problem when mapping small areas, but can become a source of errors as soon as the extent of the study is increased. In this scenario this technique can potentially under- or over-estimate the shape and size of local changes in the soil body (e.g. lenses of higher sand content).

Moreover, the main advantage of 3D geostatistics is the availability of an estimation of uncertainty, which is not available for the regression part of depth function approach. This is a very important aspect because with 3D geostatistical interpolation, scientists can instantly have an understanding of the error associated with the estimation. With the equal area spline approach, the only way to roughly assess the uncertainty of the estimations is using an additional empirical assessment, as suggested by Malone et al. (2011).

Regarding the top-down mapping method, it fails to accurately describe the spatial variation of the textural properties. Demonstrating why this happens is difficult, but there are probably two causes. The first is the use of covariates, but this does not explain why this method is the worst among others that share the

same set of covariates and the same geostatistical interpolation. The other reason is the use of a different and more complex depth function, a three-coefficient polynomial. Because this method is based on the interpolation of the coefficients of the polynomial and some coefficients presents a very poor spatial auto-correlation (see Fig. 4.7), having more than three coefficients can increase the error propagation between the predicted coefficients and the soil properties estimations, to a level that badly affect the mapping results.

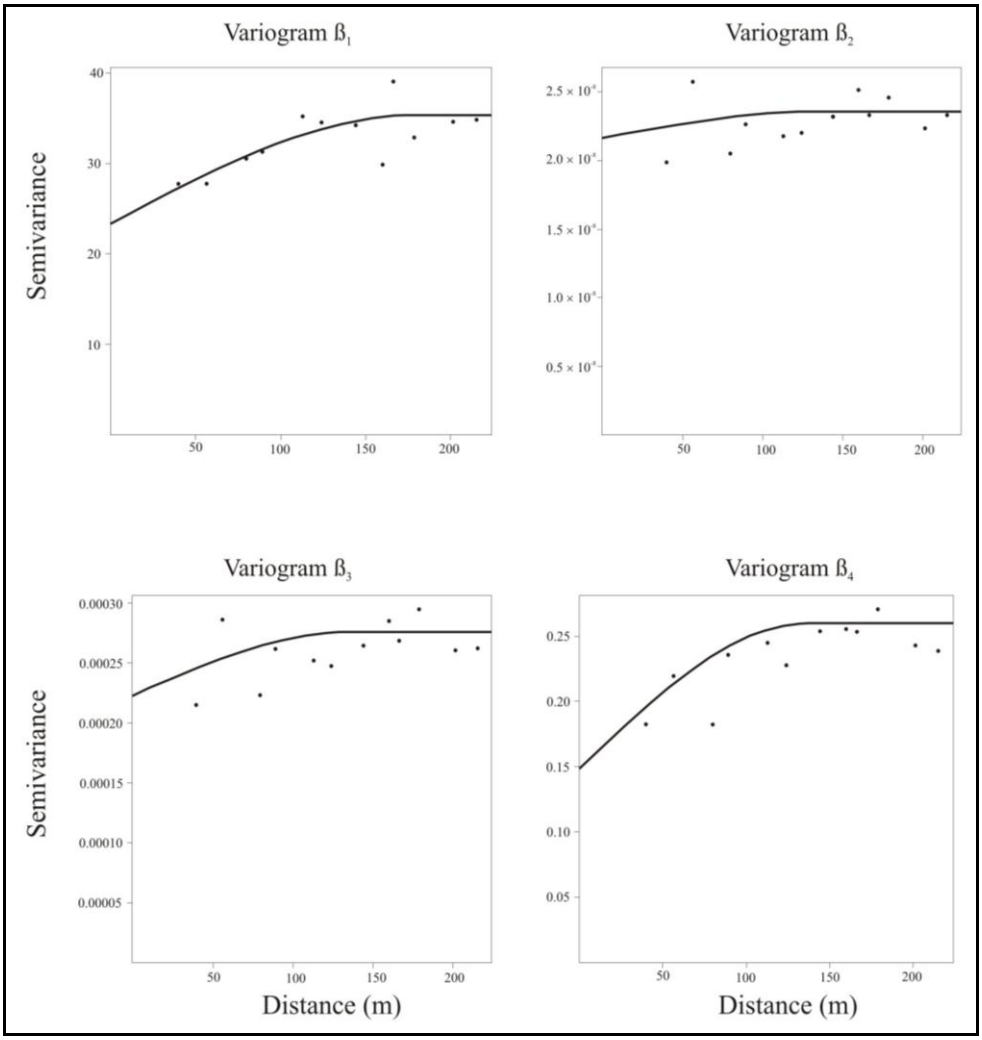

Fig. 4.7: Variograms of the four coefficients of the third order polynomial used as depth function.

4.4.3 Prediction along the profile (validation C)

For the final step of the validation process the details of the cross-validation were analysed in terms of predictions along the soil profiles. The cross-validation process was repeated, with the aim of not re-predicting the pseudo-horizons averages but of re-predicting the entire profile, comparing the estimates with all the simulated values. The results are shown in Fig. 4.8 and indicate a general decrease in the accuracy of the prediction along the profile, observed with each method and obviously less evident in the 3D universal kriging.

The reasons for this vertical decrement, which was observed by other authors in their 3D soil mapping tests (Malone et al., 2009; Kempen et al., 2011), are necessarily complex. For 3D geostatistics the most probable cause is the large difference between the horizontal and the vertical resolution that is translated in a variogram in which the vertical component stands at the very beginning of the plot and cannot be properly described by the variogram model. This can severely affect the accuracy of the variogram in assessing the spatial auto-correlation of the dataset, and especially the changes along the profile.

This problem should be avoidable by using a depth function approach in which the vertical variation is taken into account during the regression, and the interpolation is done in two dimensions. However, this is not the case and therefore the cause probably lies elsewhere, such as relevance of the geophysical covariates and their subsoil prediction accuracy.

For instance, a drop in the correlation between gamma-ray measures and soil properties in the subsoil is expected because 90% the gamma radiation comes from the first 30 cm of soil (Taylor et al., 2002) and the entire spectrum cover the first 30-45 cm of ground (Bierwirth and Brodie, 2008). Secondly, for the electromagnetic techniques, even if the depth of investigation is in general in the order of less than a metre to several metres, the final electrical conductivity value is a depth average and it is mostly affected by the first 50 cm of soil (McNeill, 1980).

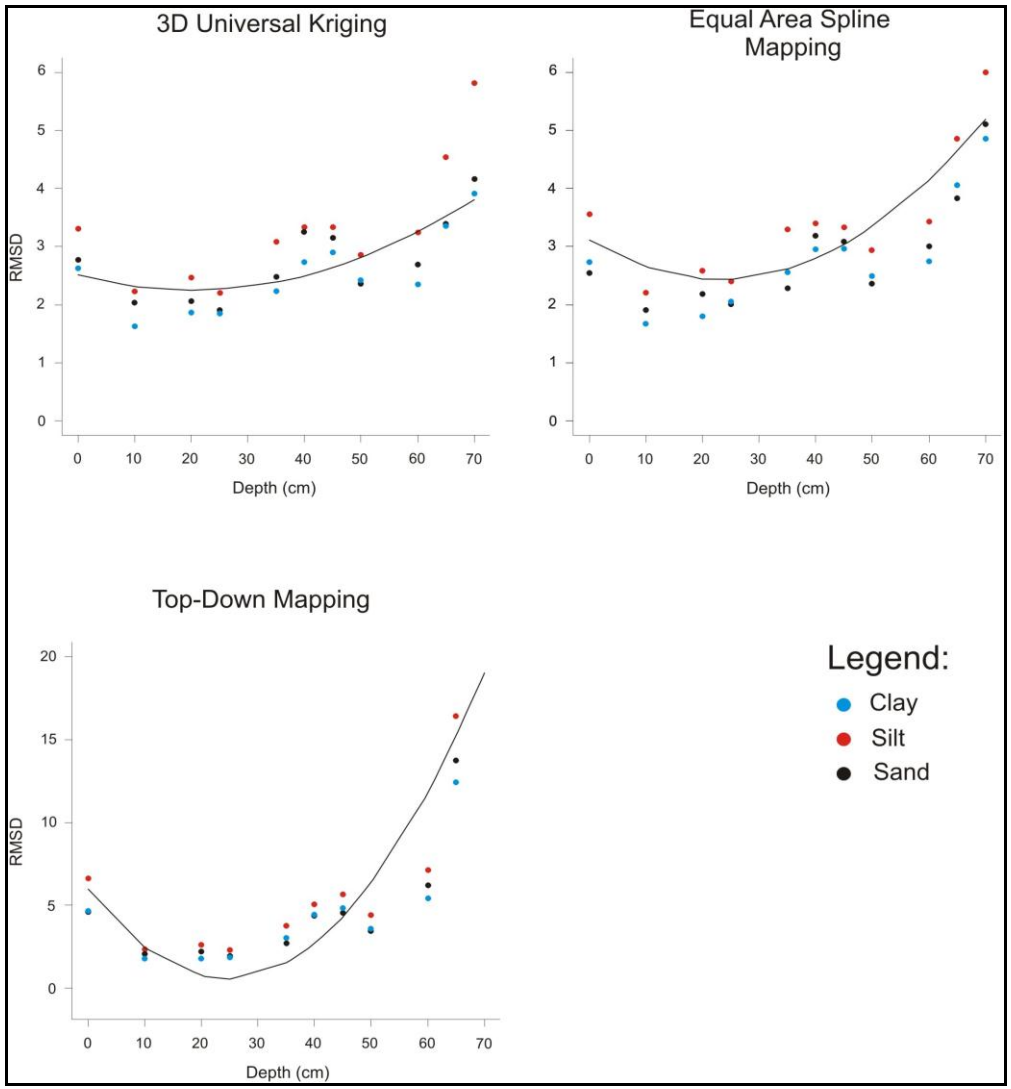

Fig. 4.8: Cross-validation accuracy in term of RMSD of each mapping method along the soil profile. The general results indicate a vertical decrement which can be observed in this image.

However, this study takes into account only predictions of soil texture, maybe for other soil properties the results would be different and the vertical decrement not present. For this reason, in the next Chapter, the use of geophysical covariates will be further investigated by predicting with the same geostatistical interpolation all the soil properties available in the Lany site with different combination of covariates.

4.5 Conclusions

In conclusion, this review compared three methods of 3D soil texture mapping, at the field scale. From the results presented in this Chapter, it is possible to draw some general conclusions regarding the advantages and disadvantages that practitioners need to address in order to successfully apply them:

- **3D UNIVERSAL KRIGING**: Even though the results obtained by universal kriging were the most accurate the method presents several disadvantages that could decrease its feasibility for 3D soil mapping. First, the smoothing effect can drastically reduce the variance that can be reproduced by the algorithm. This can be a problem especially where the soil was not sampled with designs specific for geostatistics. In this case, the smoothing effect was reduced by using a dense set of observations. Conversely, the reduction of the standard deviation of the predicted dataset can be an advantage in certain areas, as the smoothing can effectively reduce the influence of outliers during the prediction.
- **EQUAL AREA SPLINE APPROACH**: This method performs very similarly to the previous, with relatively good cross-validation results and with a distribution of the predicted values closer to the observed one (reducing the overall smoothing). It is not the best predictor, probably because the complexity of the soil pattern affects its accuracy. This is a major finding that can undermine the use of this method in areas or with soil properties which present similar depth patterns.

  The main disadvantage is the lack of a readily available uncertainties estimation which, as mentioned, needs to be addressed using an

empirical approach (Malone et al., 2011). Another possible disadvantage is related to the use of two-dimensional interpolation of the depth values calculated with the spline, which assumes that the horizontal variation of the soil property is independent of the vertical variation. This can become a concern when mapping large extents as it can potentially under- or over-estimate the shape and size of local changes in the soil body (e.g. lenses of higher sand content).

- **TOP-DOWN MAPPING**: This study demonstrates the major limitation of this mapping method. In this case study, the soil texture data did not exhibit an average depth pattern than can be described by a simple equation. With these data it was necessary to rely on a more complex function which can adapt its shape to these particular data (i.e. a third-order polynomial). This polynomial is able to describe the variation by depth of soil textures but fails during the interpolation phase. This suggests that a four-coefficient polynomial cannot be used for mapping, because there is a potential propagation of the error between each predicted coefficients and the final estimations. This case study demonstrated that the key for this method to work is the depth function, and in particular the number of coefficients that should be kept to a minimum (maximum three). If from the framework, described in section 3.2.3, the only function with a good R^2 has more than three coefficients, this method cannot be used.

CHAPTER 5 - Proximal soil sensing in 3D digital soil mapping

USE OF COVARIATES IN PREDICTING SUBSOIL CHANGES

Abstract

Proximal soil sensing includes all the techniques for indirectly collecting soil information. In the context of the iSoil project these techniques were a key component for improving, accelerating and objectifying the collection of soil data. These techniques were explored in the project, with the purpose of developing non-destructive and minimally-invasive approaches.

Of particular interest, within iSoil, were the advancements in recent years of geophysical techniques, which aim to provide data about the spatial variability of several soil properties. The other advantage of using geophysics is the ability to provide a cost- and time-efficient approach to increase the amount of information that can be used for DSM without the need for additional physical sampling.

These data can be used in DSM by correlating their spatial pattern with the soil observation, as showed and tested in Chapter 4. This can potentially increase the accuracy of the map, because the spatial pattern of geophysical data is driven by their correlation with a set of physical soil properties. Moreover, geophysical data are generally depth averages. This means that their spatial pattern is dependent not only from changes in the topsoil but also from changes in subsoil layers. This signifies that geophysical data can potentially be a very good source of secondary information for 3D DSM.

Chapter 4 described a vertical decrement in the prediction accuracy of predictive mapping, and an influence from the geophysical covariates was hypothesised. For this reason, this chapter quantitatively explores the use of

geophysical covariates for 3D digital soil mapping. The entire Lany dataset was used and the following soil properties were predicted: texture (percentage of sand, silt and clay), organic carbon, S, N and pH.

In order to test the accuracy of each geophysical covariate or groups of covariates, a cross-validation experiment was set up on the three sampled depth intervals (0-10 cm, 10-30 cm, and 30-70 cm). For each layer, universal kriging and 1-out cross-validation were used to compare every possible combination of covariates. The results indicate that on average there is a decrement in the accuracy of the prediction of 44% between topsoil and subsoil, meaning that probably the correlation between soil properties and geophysical data decreases with depth. In general, for soil properties that vary little along the profile, each covariate can achieve relatively high accuracy during the prediction. On the other hand, for properties with higher variances, such as soil texture, the choice of the best covariate is very important and a correlation analysis is therefore required.

5.1 Introduction

Proximal soil sensing includes all those techniques of collecting ancillary soil information, by instruments that operate near or in contact with the soil surface. Its development coincides with the realisation that in order to expose or study soil features the only direct way was by digging numerous, expensive and time consuming pits. For this reason soil scientists started developing new techniques to gather soil information and avoid the need to excavate pits. Historically, these include the measurements of tillage strength with a strain gauge trained by horses in 1925 by Bernard Keen and William Hanes in Rothamsted. From these pioneering works, proximal soil sensing has become a well developed science. It is primarily intended for measuring soil geophysical parameters, such as electrical conductivity and radionuclide concentration.

5.1.1 Geophysical data

These techniques were developed to measure particular physical properties that are generally well correlated with several soil properties.

For example, electrical conductivity, which can be measured with electromagnetic instruments, is function of: salinity, clay content, moisture content, bulk density, organic matter and mineralogy (Rhoades et al., 1976; Triantafilis and Lesch, 2005; Corwin, 2003). Comparably, the radionuclei concentration, assessed by measuring the gamma emitted radiation, was found to be correlated with soil texture and mineralogy, clay content, moisture content and grain size, and was used to assess soil pollution (Egmond et al., 2010).

This makes geophysical covariates useful indicators of the spatial variability of key soil properties, and their use is well documented in literature (few examples are: Israil and Pachauri, 2003; Rampant and Abuzar, 2004; Samouëlian et al., 2005; Triantafilis and Lesch, 2005). However, their dependence upon several soil properties means that the spatial pattern they show is the results of a combination of factors, which are difficult to discriminate.

Moreover, all geophysical data are influenced by the soil volume under investigation. For example, electromagnetic (EM) instruments work by generating an EM field that penetrates the soil body. This produces a secondary magnetic field in the soil that can be measured allowing a value of electrical conductivity (ECa) to be calculated. This value is referred to as apparent because it is dependent upon the depth of investigation of the instrument, which depends on the separation between the two coils that the instrument uses for producing the primary EM field.

Regarding gamma-ray spectrometry, this technique passively measures the amount of gamma radiation the soil produces. In each surveyed location the measured value depends, for the major part, on the radiation emitted by the first 30 cm of soil (Taylor et al., 2002).

All these characteristics make geophysical data good sources of secondary information for DSM but this also implies that geophysical data cannot be as the only source of information in soil mapping. They need to be implemented in a wider soil model in which soil chemical and physical attributes are taken into

account. However, since geophysical data are depth averages, they can become very interesting in the context of 3D digital soil mapping, as they can potentially provide useful insights not only about the soil surface, but also about the subsurface spatial variation.

In the iSoil project these data were explored for their promise of providing a cost- and time-efficient way of gathering soil information that can be used to increase the accuracy of soil maps by reducing the demand for analytical support.

In general, DSM relies almost blindly on covariates assuming that because their spatial pattern is the result of interactions between key soil properties in the soil, their use increases the accuracy of the map. A part of this PhD tests this assumption for 3D DSM (see Chapter 4).

In this Chapter, the use of covariates is further explored with an experiment aimed at testing the accuracy of single geophysical data in mapping soil profile changes.

5.2 Materials and methods

5.2.1 Study area

For this experiment, the Lany dataset, described in section 4.2.1, was used. In the previous experiment only soil texture was predicted. In this study, all the available soil properties were estimated (i.e. clay, sand and silt percentage; soil organic carbon; pH; sulphur and nitrogen concentrations). Table 5.1 presents the summary statistics of each soil property.

Table 5.1: Descriptive statistics of the investigated soil properties.

Property	Unit	Min.	1st Qu.	Median	Mean	3rd Qu.	Max.	St.Dev.
Sand	*%*	23.25	31.80	34.53	36.02	38.95	66.13	6.86
Silt	*%*	9.00	37.92	43.63	42.87	49.03	56.82	8.47
Clay	*%*	12.78	17.54	20.24	21.11	23.89	39.91	5.34
SOC	*Total Count*	0.26	0.64	1.30	1.16	1.52	2.37	0.55
S	*Total Count*	0.02	0.03	0.04	0.04	0.05	0.08	0.01
N	*Total Count*	0.03	0.07	0.13	0.11	0.15	0.22	0.05
pH	*pH Units*	5.42	6.42	6.65	6.59	6.80	7.28	0.32

5.2.2 Covariates

For this experiment, all the covariates described in section 4.2.2 were individually tested using 2D universal kriging.

5.2.3 Validation

In order to determine the most accurate set of covariates for estimating the spatial and vertical variability of each observed soil property, a series of tests were carried out using a common 1-out cross-validation approach.
This method of validation is the most commonly used approach in geostatistics. It consists of excluding randomly each point of the dataset and re-predicting their value, with the remaining data. When all the points have been excluded the observations and the estimations are compared with goodness of fit indexes, in this case RMSD.

5.3 Results and discussion

In general, gamma-ray data are considered as topsoil measures. The majority (90%) of the gamma radiation signal is derived from the first 30 cm of soil (Taylor et al., 2002) and the entire spectrum cover the first 30-45 cm of ground

(Bierwirth and Brodie, 2008). For electromagnetic measures, even if the depth of investigation is in the order of less than a metre to several metres, the final ECa value is a depth average and most of it is affected by the first 50 cm of soil (McNeill, 1980).

From this information a trend was expected, where gamma ray covariates can accurately predict topsoil but fail to predict subsoil, while the contrary is true for EM data which have a higher depth of investigation and can probably provide more accurate subsoil estimates.

The results of this analysis are shown in Tables 5.3, 5.4 and 5.5. Each table represents the results, in term of RMSD values, from each of the depth layers investigated. From these results is possible to draw some general conclusions regarding the use of covariates for 3D soil mapping.

First of all, the prediction accuracy is higher in topsoil, which is characterized by a general loam to silty loam texture, with an average value of RMSD in the first horizon of 1.67, which increases at 1.74 in the second horizon and settles at 3.78 in the subsoil, in which there is an increase in clay content, an overall increase of 44%. These results identify a potential vertical decrement of the prediction accuracy which was also observed by other authors (Malone et al., 2009; Kempen et al., 2011). These authors, however, do not explain the causes of this vertical decrement.

The average RMSD value for each method, used independently (Table 5.2), indicate that gamma ray covariates predict better than others in the 1st horizon with an average RMSD of 1.58, which is in line with the low investigation depth of the method. By contrast, in the second horizon EM covariates, in particular the data collected by the EM38, are the best predictor, with an average RMSD value of 1.61, in line with the fact that EM38 data have a depth of investigation up to 0.5 m.

Gamma ray data are the best predictors in the third horizons, where these can obtain an average RMSD value of 3.52 compared with an EM average of 3.63. This is unexpected because surface gamma ray measurements should be constrained by a maximum depth of investigation of 30-45 cm and not be able to accurately predict deeper. From the details of the 3rd horizon predictions

(Table 5.5), it is clear that gamma ray covariates improve the universal kriging accuracy for almost all the variables, except clay content. This is probably due to the fact that clay is well correlated with EM data (Triantafilis and Lesch, 2005). All the other soil properties can be predicted in the subsoil more accurately in conjunction with gamma ray covariates.

Table 5.2: Average validation (RMSD values) results for each covariate type.

	1st Horizon	**2nd Horizon**	**3rd Horizon**
EM average	1.61	1.61	3.63
Gamma average	1.58	1.66	3.52
DEM average	1.69	1.69	3.75

The results indicate that if soil properties present a low standard deviation, they can be predicted with a very high level of accuracy, regardless of depth or covariates. For example, soil S and N content, which have standard deviations of 0.01 and 0.05, present RMSD averages between 0.01 and 0.03. The carbon content and the pH are also very easy to predict, resulting in average accuracy level always below 0.4.

By contrast, predicting soil texture is very challenging especially in the subsoil. Soil texture presents a generally high standard deviation and this decreases the accuracy of the prediction algorithm. However, this is the case only when estimating sand and silt, where the lowest possible RMSD value is around 7-8. On the other hand, clay is much easier to predict, as it very much correlated with EM data. For this reason clay prediction can reach an RMSD as low as 5.34 in conjunction with EM38 covariates.

Table 5.3: Validation (RMSD values) results for the 1st horizon, 0-10 cm

Covariates	1st Horizon							
	Sand	**Silt**	**Clay**	**SOC**	**S**	**N**	**pH**	*Covariate average*
EM38 h	3.29	4.13	2.74	0.26	0.01	0.02	0.24	*1.53*
EM38 v	3.40	4.17	3.15	0.26	0.01	0.02	0.25	*1.61*
EM31 h	3.34	4.26	3.36	0.25	0.01	0.02	0.25	*1.64*
EM31 v	3.32	4.23	3.52	0.24	0.01	0.02	0.25	*1.66*
Th	3.99	4.88	3.51	0.26	0.01	0.02	0.26	*1.85*
Cs	2.96	3.71	3.43	0.24	0.01	0.02	0.26	*1.52*
U	3.59	4.39	3.38	0.26	0.01	0.02	0.26	*1.70*
K	2.50	3.72	3.45	0.26	0.01	0.02	0.26	*1.46*
Total Count	2.56	3.39	3.38	0.24	0.01	0.02	0.26	*1.41*
Slope	3.52	4.36	3.42	0.26	0.01	0.02	0.26	*1.70*
Aspect	3.62	4.43	3.37	0.26	0.01	0.02	0.26	*1.71*
Curvature	3.49	4.43	3.47	0.26	0.01	0.02	0.26	*1.71*
Altitude	3.33	4.23	3.47	0.23	0.01	0.02	0.25	*1.65*
EM38 h + v	3.25	4.19	2.43	0.21	0.01	0.02	0.25	*1.48*
EM31 h + v	3.78	4.46	3.28	0.22	0.01	0.02	0.25	*1.72*
Gamma	2.06	3.93	4.07	0.28	0.01	0.02	0.29	*1.53*
Gamma+EM38	2.16	3.35	2.65	0.26	0.01	0.02	0.29	*1.25*
Gamma+EM31	2.18	3.90	3.75	0.29	0.01	0.02	0.29	*1.49*
Gamma+Total Count	2.15	3.90	4.10	0.28	0.01	0.02	0.30	*1.54*
DEM	3.98	5.51	3.97	0.27	0.02	0.02	0.29	*2.01*
DEM+altitude	4.20	5.60	4.16	0.27	0.01	0.02	0.28	*2.08*
Gamma+DEM	2.20	3.89	4.19	0.30	0.01	0.03	0.33	*1.57*
Gamma+DEM+altitude	2.30	3.83	4.23	0.31	0.01	0.03	0.34	*1.58*
DEM+EM38	4.10	6.00	2.85	0.28	0.02	0.02	0.30	*1.94*
DEM+altitude+EM38	4.43	5.97	3.01	0.29	0.02	0.02	0.29	*2.00*
DEM+EM31	4.52	5.15	3.29	0.23	0.01	0.02	0.29	*1.93*
DEM+altitude+EM31	4.33	5.33	3.47	0.23	0.01	0.02	0.30	*1.96*
Property Average	*3.28*	*4.42*	*3.45*	*0.26*	*0.01*	*0.02*	*0.28*	*1.67*

Table 5.4: Validation (RMSD values) results for the 2nd horizon, 10-30 cm

	2nd Horizon							
Covariates	**Sand**	**Silt**	**Clay**	**SOC**	**S**	**N**	**pH**	*Covariate average*
EM38 h	3.21	4.43	2.53	0.22	0.02	0.01	0.28	*1.53*
EM38 v	3.20	4.47	2.93	0.22	0.02	0.01	0.30	*1.59*
EM31 h	3.23	4.48	3.13	0.21	0.02	0.01	0.30	*1.63*
EM31 v	3.24	4.44	3.25	0.20	0.02	0.01	0.31	*1.64*
Th	3.99	5.00	3.37	0.21	0.02	0.01	0.32	*1.85*
Cs	3.31	4.28	3.34	0.19	0.02	0.01	0.31	*1.64*
U	3.49	4.63	3.24	0.20	0.02	0.01	0.32	*1.70*
K	2.97	4.21	3.30	0.21	0.02	0.01	0.31	*1.57*
Total Count	2.65	3.78	3.22	0.19	0.02	0.01	0.30	*1.45*
Slope	3.41	4.59	3.42	0.20	0.02	0.01	0.32	*1.71*
Aspect	3.50	4.54	3.27	0.22	0.02	0.01	0.32	*1.70*
Curvature	3.45	4.63	3.28	0.20	0.02	0.01	0.32	*1.70*
Altitude	3.24	4.41	3.33	0.18	0.02	0.01	0.31	*1.64*
EM38 h + v	3.31	4.49	2.45	0.17	0.02	0.01	0.28	*1.53*
EM31 h + v	3.68	4.90	3.11	0.19	0.02	0.01	0.31	*1.75*
Gamma	2.88	4.53	4.13	0.24	0.02	0.01	0.33	*1.73*
Gamma+EM38	3.48	4.29	2.73	0.24	0.02	0.01	0.33	*1.59*
Gamma+EM31	3.32	4.81	3.97	0.26	0.02	0.01	0.35	*1.82*
Gamma+Total	2.98	4.57	4.32	0.25	0.02	0.01	0.33	*1.78*
DEM	3.77	5.63	3.86	0.21	0.02	0.01	0.33	*1.98*
DEM+altitude	3.96	5.73	4.11	0.20	0.02	0.01	0.33	*2.05*
Gamma+DEM	3.07	4.13	4.41	0.22	0.02	0.01	0.38	*1.75*
Gamma+DEM+altitude	3.19	4.21	4.28	0.23	0.02	0.01	0.39	*1.76*
DEM+EM38	3.86	6.31	2.96	0.22	0.02	0.01	0.34	*1.96*
DEM+altitude+EM38	3.72	6.13	3.25	0.23	0.02	0.01	0.33	*1.95*
DEM+EM31	4.74	5.88	3.08	0.20	0.02	0.01	0.35	*2.04*
DEM+altitude+EM31	4.16	5.98	3.25	0.20	0.02	0.01	0.36	*2.00*
Property Average	*3.45*	*4.80*	*3.39*	*0.21*	*0.02*	*0.01*	*0.32*	*1.74*

Table 5.5: Validation (RMSD values) results for the 3rd horizon, 30-70 cm.

	3rd Horizon							
Covariates	**Sand**	**Silt**	**Clay**	**SOC**	**S**	**N**	**pH**	*Covariate average*
EM38 h	9.42	9.82	5.34	0.19	0.01	0.01	0.33	*3.59*
EM38 v	9.24	9.79	5.61	0.19	0.01	0.01	0.33	*3.60*
EM31 h	9.26	9.80	5.92	0.18	0.01	0.01	0.34	*3.65*
EM31 v	9.24	9.77	6.13	0.18	0.01	0.01	0.34	*3.67*
Th	9.30	10.02	6.38	0.16	0.01	0.01	0.33	*3.74*
Cs	8.01	8.35	6.47	0.19	0.01	0.01	0.32	*3.34*
U	8.83	9.55	6.50	0.17	0.01	0.01	0.32	*3.63*
K	7.94	8.85	6.48	0.18	0.01	0.01	0.32	*3.40*
Total count	7.94	8.50	6.53	0.18	0.01	0.01	0.32	*3.36*
Slope	9.75	9.94	6.36	0.19	0.01	0.02	0.35	*3.80*
Aspect	10.18	9.74	6.44	0.19	0.01	0.01	0.35	*3.85*
Curvature	9.03	9.99	5.75	0.17	0.01	0.01	0.35	*3.62*
Altitude	9.34	9.86	6.44	0.17	0.01	0.01	0.34	*3.74*
EM38 h + v	9.37	9.87	5.60	0.19	0.01	0.02	0.36	*3.63*
EM31 h + v	9.37	9.98	5.46	0.18	0.01	0.01	0.33	*3.62*
Gamma	8.80	8.88	7.34	0.18	0.01	0.01	0.35	*3.65*
Gamma+EM38	8.47	8.50	6.79	0.19	0.01	0.02	0.38	*3.48*
Gamma+EM31	8.23	9.28	6.36	0.19	0.01	0.02	0.36	*3.49*
Gamma+Total	9.34	8.59	7.67	0.18	0.01	0.01	0.37	*3.74*
DEM	10.84	10.41	5.74	0.18	0.01	0.01	0.38	*3.94*
DEM+altitude	11.49	10.85	6.09	0.18	0.01	0.01	0.36	*4.14*
Gamma+DEM	10.39	8.40	6.98	0.19	0.01	0.02	0.51	*3.79*
Gamma+DEM+altitude	10.54	8.75	7.29	0.20	0.01	0.02	0.53	*3.90*
DEM+EM38	12.39	12.06	6.07	0.19	0.01	0.02	0.40	*4.45*
DEM+altitude+EM38	12.53	12.02	6.25	0.20	0.01	0.02	0.42	*4.49*
DEM+EM31	12.42	10.54	6.26	0.18	0.01	0.01	0.40	*4.26*
DEM+altitude+EM31	12.84	11.20	6.44	0.18	0.01	0.02	0.41	*4.44*
Property Average	*9.80*	*9.75*	*6.32*	*0.18*	*0.01*	*0.01*	*0.37*	*3.78*

5.4 Conclusions

From this analysis is possible to draw some general conclusion about the use of covariates, and in particular geophysical data, in 3D DSM. First of all, their accuracy is highly influenced by depth, meaning that is easier to obtain accurate topsoil estimates.

In general soil properties that present a very high correlation with geophysical covariates, such as organic carbon and clay content, can be better predicted even in the subsoil. Furthermore, a good estimation can also be achieved with soil properties that vary very little with depth (St.Dev < 1), such as pH, sulphur and nitrogen.

For estimating sand and silt content soil scientists need to be careful because their high variance, and relatively low correlation with geophysical covariates, means they can be difficult to predict.

Regarding the covariates, it appears that for predicting organic carbon and clay content the best choice is using electromagnetic covariates, because of their high correlation. For sand and silt, the results indicate that the best prediction can be achieved using uniquely gamma ray covariates, even in the subsoil. For the others (pH, S and N), their variance is so low the choice of covariate is not as important as with the other soil properties.

CHAPTER 6 - Landscape scale estimation of soil carbon stock in three-dimensions for creating a carbon loss risk map

Abstract

Soil organic matter (OM) is extremely important for nutrient cycle, water dynamics and soil structure. It contains approximately 50% carbon (C), and consequently mapping soil C is a good way to determine the amount of available OM, and therefore assess one of the parameters from which soil fertility and productivity depend.

In this study, data from the soil survey of England and Wales were used to create a 3D soil C stock map for an area of approximately 13,948 km^2 in the West Midlands region. For this study, the method developed in Chapter 3 was applied using simple depth functions to describe the vertical variations of organic C and bulk density along the depth profile.

The results indicate that the top-down mapping method can well replicate the variance observed in the soil samples, even at a landscape scale. An independent validation was performed comparing the predictions with the National Soil Inventory (NSI) dataset. The results indicate that the top-down mapping method can achieve a high level of accuracy in predicting topsoil C. Moreover, from the uncertainty estimation it is possible to say that this method is able to achieve more than acceptable of accuracy even in the subsoil.

In summary, this study confirms the results from the previous chapters that the top-down mapping method can also be used with good results in mapping large areas.

6.1 Introduction

In 2006, the European Commission adopted a Thematic Strategy on the protection of soil (Commission of European Communities, 2006). This has identified a series of degradation processes that member states should consider when evaluating the optimum ways to protect their soils. Loss in organic matter is one of the phenomena to consider.

Organic matter (OM) is the organic fraction of soil. It comprises plant and animal residue in various degrees of decomposition. It is extremely important to soil fertility but also to secure the nutrient cycle, water dynamics and soil structure. OM contains approximately 50% of C (C; Schils et al., 2008), meaning that a loss of OM causes a direct loss of C stock in soil.

In the global cycle, C moves between several pools. In soil, C enters from plants and animal residues that are modified by physical, chemical and biological processes, and then released through microbial respiration or leaching. In this cycle, soil is the largest pool of organic carbon in the terrestrial biosphere (Schlesinger, 1997), accounting for three times as much carbon as that stored in vegetation and twice that of the atmosphere (Schils et al., 2008).

The capacity to predict the consequences of climate change on the soil C pool, and act accordingly, depends upon our understanding of C distribution in the soil volume (Jobbagy and Jackson, 2000) and how this affects the way in which soil exchanges C with the atmosphere.

In general, major soil C losses are related to land use and land use changes, especially when soil with high organic C content (e.g. peat soil) is converted into cropland (Schils et al., 2008). However, the majority of European topsoils are relatively poor in peat (Hiederer, 2006) but their exchanges of C with the atmosphere are still an important aspect to consider when modelling C cycling in soils.

Soil C present a complex vertical distribution, which is dependent on the climate, the type of vegetation and soil characteristics such as texture (Jobbagy and Jackson, 2000). Soil C profiles are characterized by a vertical pattern where the very top part has a relatively high C content that quickly decreases with depth (Batjes, 1996). This suggests that being able to estimate the amount

of C available in the very top part of the profile should be a priority, as this is the most at risk of being lost (by erosion, land use changes etc.).

Most of the available soil C stock maps, including the UK map (Bradley et al., 2005), provide only average estimates of C available in topsoil (from 0 to 30 cm) and subsoil (from 30 to 100 cm). However, because the decrease in C content with depth is rapid, estimating averages can underestimate the amount of C most at risk of being lost. This can potentially decrease the ability of environmental models to predict future changes in soil C stocks.

For this reason, the objective of this Chapter is to test the top-down mapping method in mapping soil organic C in 3D. With this method, an estimate of the amount of C stocked in the upper part of the profile, which is at much higher risk of being lost to the atmosphere, should be possible. A method is also introduced for computing the uncertainty associated with the predictions that can be implemented in other methods for 3D mapping involving depth functions.

6.2 Materials and methods

6.2.1 Study area

The area under study is situated in the West Midlands region, covering approximately 13,948 km^2 (Fig. 6.1).

The soil map of this area indicates that there are 118 soil associations. The most extended, with an area of 1285.18 km^2, is the Bromyard association which are reddish loamy to silty soils. While most of the area has loamy soils, there is an increase in silt towards the east and north, and an increase in clayey soils in the south (Fig. 6.1).

According to the CEH Land Cover Map 2000 (Fuller et al., 2002), around one third of the area is covered by arable land, generally considered a source of C emission (Schils et al., 2008); 50% is covered by natural, semi-natural or improved grassland and 11% is urban or suburban areas. The remaining land is classified as woodland, inland water or heath.

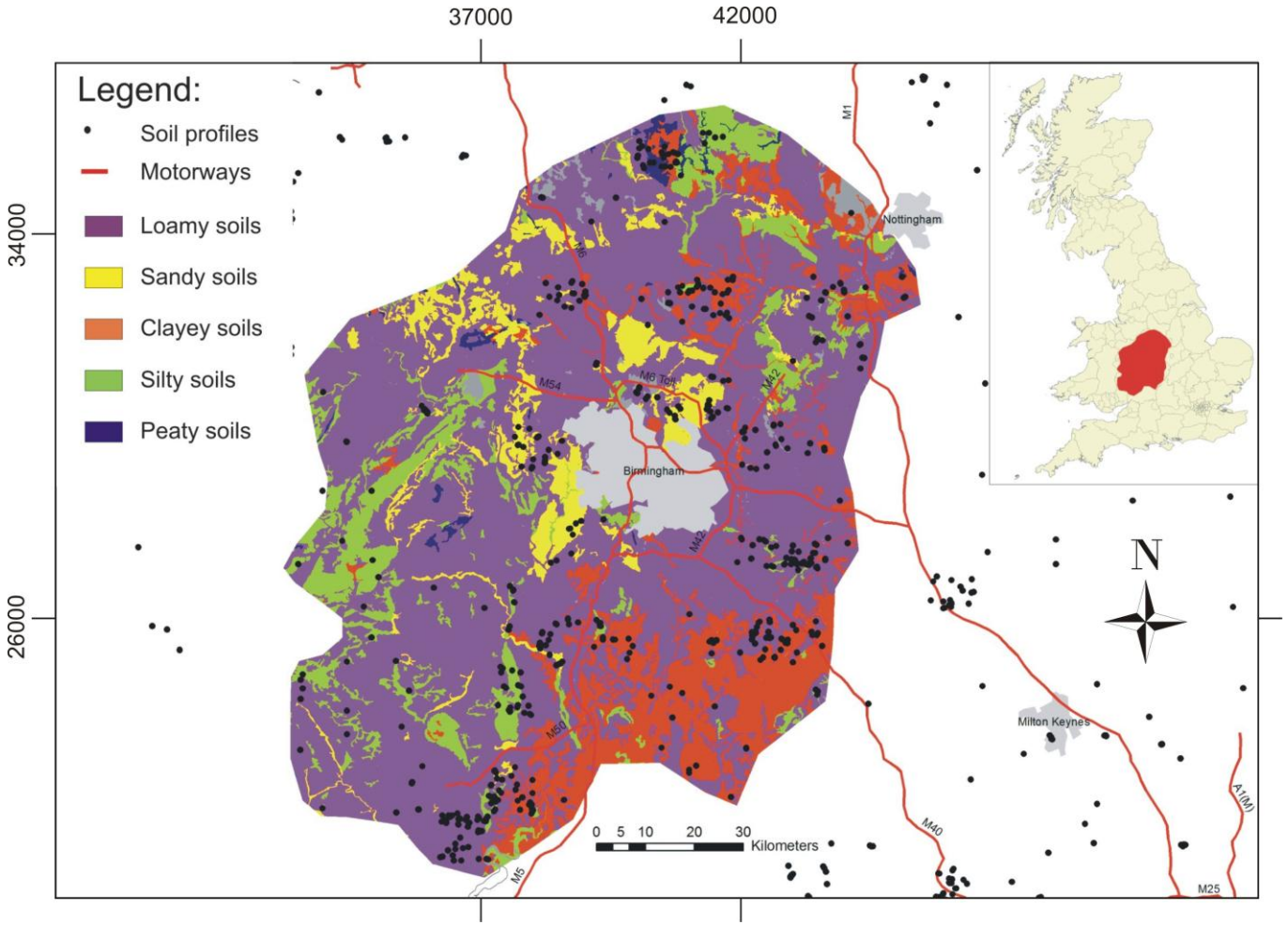

Fig. 6.1: Map of the area under study, with details of the general soil texture pattern.

6.2.2 Dataset description

6.2.2.1 Soil profiles dataset

The soil samples selected for the study are a subset of the data from the England and Wales soil survey, available from the National Soil Resources Institute (NSRI), Cranfield University. This dataset (n = 435) contains information about soils of England and Wales, collected from 1939 to 2006. Because the dataset has been sampled over an extended period of time and for different studies, the observation points are not very well distributed. There are clusters of high density sampling while a large area in the west, close to the Welsh border, has few profiles (see Fig. 6.1). This is a characteristic to take into account when working on legacy data, which were not sampled with digital soil mapping requirements.

6.2.2.2 Environmental covariates

In order to improve the accuracy of the soil C and Bulk Density (BD) predictions, four grids of environmental covariates were utilised, namely:

- Digital elevation model (DEM). A 50 m resolution DEM, created by the Ordnance Survey and constructed from the 1:50,000 topographic map., Five derivatives were obtained from these data: slope, aspect, curvature, profile curvature and plan curvature.
- Soil association map. A 1 km grid map with information about the predominant soil association in each grid cell. This map was available from the NSRI.
- Land Cover Map 2000. Available from the CEH, it has a resolution of 1 km with information about the predominant coverage of the land.
- Geological map. Available from the British Geological Survey (BGS) at the scale of 1:250,000.

6.2.3 Methodology

In this experiment the top-down mapping method, described in Chapter 3, was applied to the soil C and BD data.

A preliminary analysis of the two datasets concluded that the soil C general depth pattern can be described by an exponential equation, as suggested in literature (Hilinski, 2001; Hiederer, 2009), and this group was the focus of the framework. By contrast, for soil BD there were no indication in literature and the framework was applied in its entirety.

The following two depth functions were selected:

- A Power function for describing the vertical distribution of soil C:

$$\mathbf{C_i} = \beta_1 \cdot \mathbf{d_i^{\beta_2}} \tag{6.1}$$

  where C_i is the value of C at the i^{th} depth interval and d_i is the depth.

- An inverse power function for describing the vertical distribution of soil BD:

$$\mathbf{BD_i} = \frac{\mathbf{1}}{\beta_1 \cdot \mathbf{d_i^{\beta_2}}} \tag{6.2}$$

  where BD_i is the value of BD at the i^{th} depth interval and d_i is the depth.

6.2.4 Goodness of fit maps

Eq. 6.1 and 6.2 were fitted to each available soil profile and the local R^2 value was computed. These two equations are effective for describing the general pattern of the soil profiles, but because of their simplicity they can also be used as diagnostic tools, as described in section 3.3.2. From this goodness of fit analysis, two R^2 maps were produced.

6.2.5 Validation

The validation was undertaken using two methods: cross-validation and an independent validation against the NSI data.

The *cross-validation* approach relies on excluding a set percentage of soil profiles (5, 10, 20, 30%) and re-predicting their values. The observed and predicted values are then compared, calculating the R^2.

The second method is an *independent validation* accomplished by comparing the soil C percentage available in the NSI dataset, with the estimated soil C percentage. To assess the goodness of fit, the residuals between the NSI values and the estimations with the top-down mapping method were calculated.

6.2.6 Soil C stock estimation

The soil C density was calculated using the following equation, suggested by (Xu et al., 2011):

$$\mathbf{C\ Density} = \mathbf{C}_i \cdot \mathbf{BD}_i \cdot d_i \qquad (6.3)$$

where 'C Density' (t/ha) is the soil carbon density; C_i is the C (%) content of the soil layer *i*, BD_i is the BD (g/cm3) value of the soil layer *i* and d_i is the width in cm of the soil layer *i*.

The resulting density estimations were then overlaid with the Land Cover Map 2000 from CEH (Fuller et al., 2002) and the following corrections were made, as suggested in Bradley et al. (2005), Xu et al. (2011):

- For urban areas and water bodies the density value was set to 0.
- For semi urban areas the value was set to one half of the estimated value.

Subsequently, the C stock was computed with Eq. 6.4 (Xu et al., 2011):

$$\text{C Stock} = \sum \frac{\text{C Density} \cdot \text{Area}}{10^{10}} \quad (6.4)$$

where 'C Stock' (Tg) is the carbon stock value estimated after the corrections cited above and 'Area' is the area of a single prediction grid cell in m^2.
The C stock value was calculated for each depth interval estimated during the mapping process, namely: 0-10; 10-20; 20-30; 30-40; 40-50; 50-60; 60-70; 70-80; 80-90; 90-100 cm. Average values for topsoil (0-30 cm) and subsoil (30-100 cm) were also computed.

6.2.7 C Stock variation estimation

The uncertainty related to each point on the prediction grid was estimated, adapting a method proposed by Goidts (2009) and Schrumpf (2011), for assessing the error propagation of each variable in the C stock estimation. The variance of the C stock assessment is based on the following equation:

$$\text{Var}(\text{C Stock}) = (\text{C Stock})^2 \cdot \left(\frac{\sigma_C^2}{C^2} + \frac{\sigma_{BD}^2}{BD^2} + 2\frac{\sigma_{C-BD}}{C \cdot BD}\right) \quad (6.5)$$

where Var(C Stock) is the error associated with the prediction, in t/ha; σ_C and σ_{BD} denote the standard deviation of carbon content and bulk density; and $\sigma_{C\text{-}BD}$ is the covariance of C and BD. This equation was applied to two depth intervals, namely the 0-30 cm layer (topsoil) and the 0-100 cm layer (subsoil).

6.3 Results and discussions

6.3.1 Mapping results

From the framework, described in section 3.2.3, two depth functions were selected as best soil specific depth functions for C and BD, in this area. The accuracy of the two depth functions in describing the average pattern of the two

soil properties is visually demonstrated in Fig. 6.2, where the red crosses represent the average value at each depth layer and the function curves fit these points well.

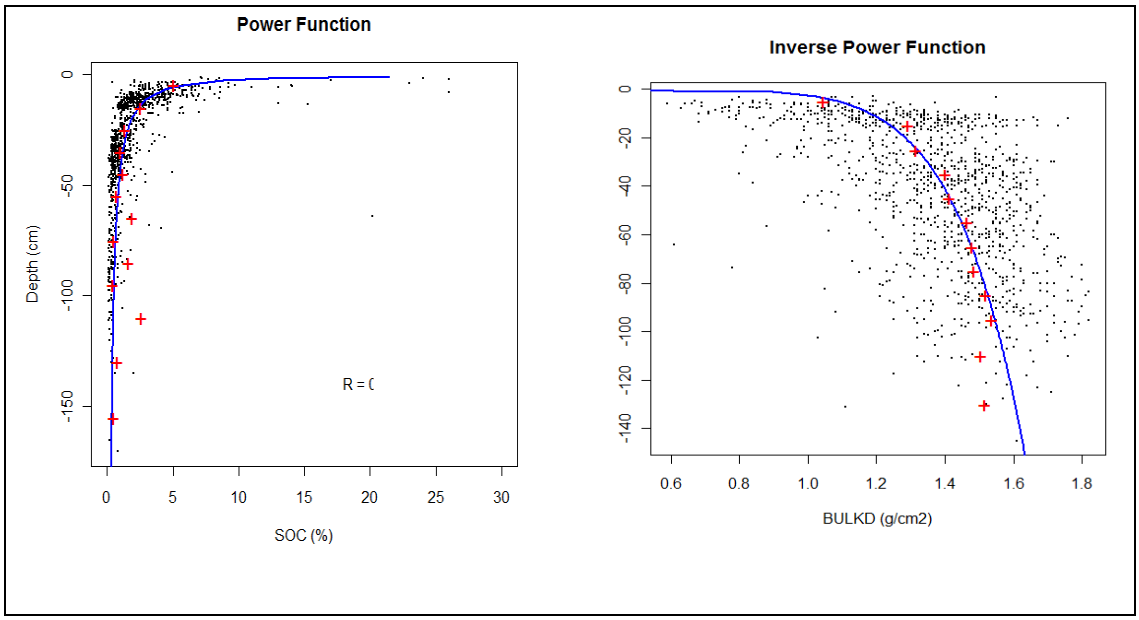

Fig. 6.2: General profiles of the two soil properties and depth functions fitting. In red crosses the mean value of the soil property in each depth layer.

In order to numerically demonstrate the accuracy of these two equations in describing the depth pattern of soil C and BD, they were fitted to each sampled profiles. The results of goodness of fit are presented in two R^2 interpolated maps presented in Fig. 6.3, below.

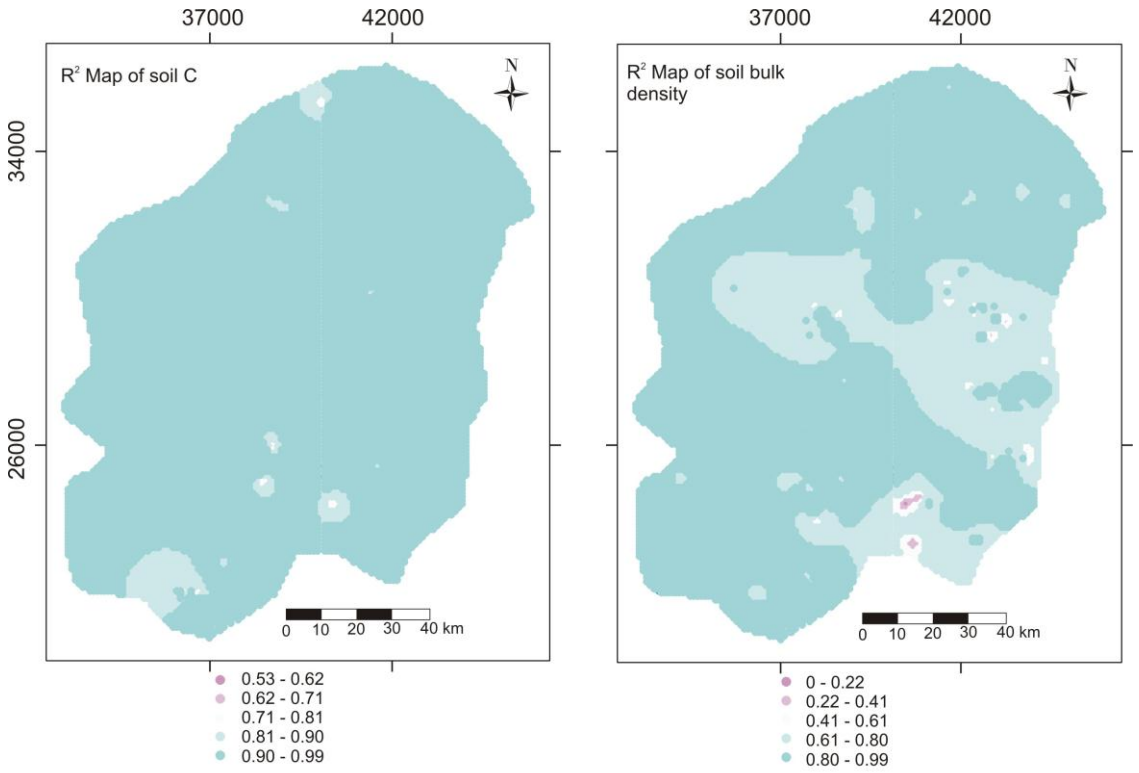

Fig. 6.3: R^2 values for soil C and bulk density within the study area.

Fig. 6.3 shows the two R^2 maps, created on the same prediction grid used for the 3D soil map, where the majority of the samples present high values of goodness of fit (R^2>0.5). Soil C profiles do not present any R^2 values below 0.5, meaning that the depth function is able to describe every soil profile with a good level of accuracy.

For BD the results are similar and the majority of the profiles present an acceptable goodness of fit. There are only two areas in the southern part (coloured in pink in Fig. 6.3 right), which present R^2 values below 0.5. This is due to the fact that three profiles in that area have a linear depth pattern that the inverse power function struggles to describe. Normally, bulk density increases with depth but in these three cases it remains almost constant. These differences are present in only three samples, and therefore they were considered as outliers and Eq. 6.2 was considered valid for the entire area.

In summary, even at landscape scale this method provides the same diagnostic power as at field scale. From these two maps is in fact already possible to

extrapolate crucial information about the spatial variation of the two soil properties, which with other method are very difficult to assess, at this stage.

After this step, and because the goodness of fit results were generally good, the value of soil C and BD was estimated with a universal co-kriging algorithm. Universal kriging was adopted because at this extent the assumption of intrinsic stationarity cannot hold and the soil process needs to be considered as non-stationary. This interpolation method is able to work under these circumstances, as described in section 2.6.

The final 3D grid of predictions has horizontal resolution of 1 km and vertical resolution of 10 cm. The total number of points in the prediction grid was 220,928. The computational time for the entire mapping process was around 5 min, a fraction of the time needed to estimate the same number of points using 3D geostatistics alone (Kerry and Hawick, 1998).

To investigate the results of the mapping, the summary statistics of the original dataset were compared with the predicted datasets (Table 6.1). This analysis was done as one of the advantages of the depth function mapping is that it can replicate the variance of the estimated dataset to a level that is very close to the observations. This concept is better explained in Chapter 2 and 3. It was important to verify this aspect also at this extent.

Table 6.1: Descriptive statistics of the observed and predicted datasets.

		Min	*Max*	*Mean*	*Median*	*St.Dev.*
Observed Dataset						
SOC	*Topsoil*	0.30	43.00	3.06	2.30	3.23
	Subsoil 100	0.10	39.10	1.01	0.60	2.73
BD	*Topsoil*	0.59	1.76	1.23	1.25	0.23
	Subsoil 100	0.61	1.82	1.45	1.47	0.16
Predicted with Top-down mapping						
SOC	*Topsoil*	0.00	45.75	4.36	2.95	4.24
	Subsoil 100	0.00	68.08	0.45	0.24	0.89
BD	*Topsoil*	0.27	2.82	1.07	1.14	0.26
	Subsoil 100	0.74	2.49	1.35	1.35	0.11

The estimated dataset maintains very similar mean values of both C and BD, especially in the topsoil. In fact, the mean C value in the observed data for the topsoil is 3.06 with a standard deviation of 3.23, compared to a predicted mean of 4.36, with a standard deviation of 4.24. The higher mean values in the estimated dataset was expected as the majority of soil data were sampled in the lowlands around Birmingham, where the soil C is relatively low, compared to the area on the Welsh border that is under-sampled. Regarding the BD values, the observed mean for the topsoil is 1.23, with a standard deviation of 0.23, while the predicted mean is 1.07, with a standard deviation of 0.26.

Conversely, the results for the subsoil are less accurate. The C observed mean is 1.01, with a standard deviation of 2.73, while the estimated mean is 0.24, with a standard deviation of 0.89. For BD, the subsoil results are much better. The observed mean is 1.45, with a standard deviation of 0.16, while the estimated

mean is 1.35, with a standard deviation of 0.11. This demonstrates the correctness of using an inverse power function for describing soil BD.

The topsoil estimates are more accurate than subsoil predictions. This means that the two depth functions are very accurate in describing the topsoil spatial variability and less accurate in lower horizons. This is probably caused by a general decrement in the data density below 50 cm, as shown in Fig. 6.2. This certainly decreases the fitting accuracy in lower horizons, where the sample support is lower.

6.3.1.1 Validation

The accuracy of the mapping method was tested with two methods: cross-validation and independent validation.

The *cross-validation* results indicate an average value of R^2 for the lowest exclusion percentage of 36% for C, with a standard deviation of 0.20; and 44% for BD, with a standard deviation of 0.15. These results are relatively low, but they are in line with previous validated research of 3D mapping at the catchment or landscape scale (Malone et al., 2009; Kempen et al., 2011).

The problem with mapping large areas using legacy soil observations is that the dataset was not sampled with probabilistic designs, making it less suitable for DSM. In this study, the majority of the area around Birmingham is well covered by clusters of high-density data, while the remaining area was only sparsely sampled. It is therefore difficult to consider cross-validation a sound method for validation under these circumstances, simply because when an excluded sample is re-predicted using other observations tens of kilometres apart, it is clear the estimation may substantially differ from the observation. Cross-validation is perfect where the sampling was executed with the DSM requirements, but in this case is not the best method for assessing the accuracy of the map.

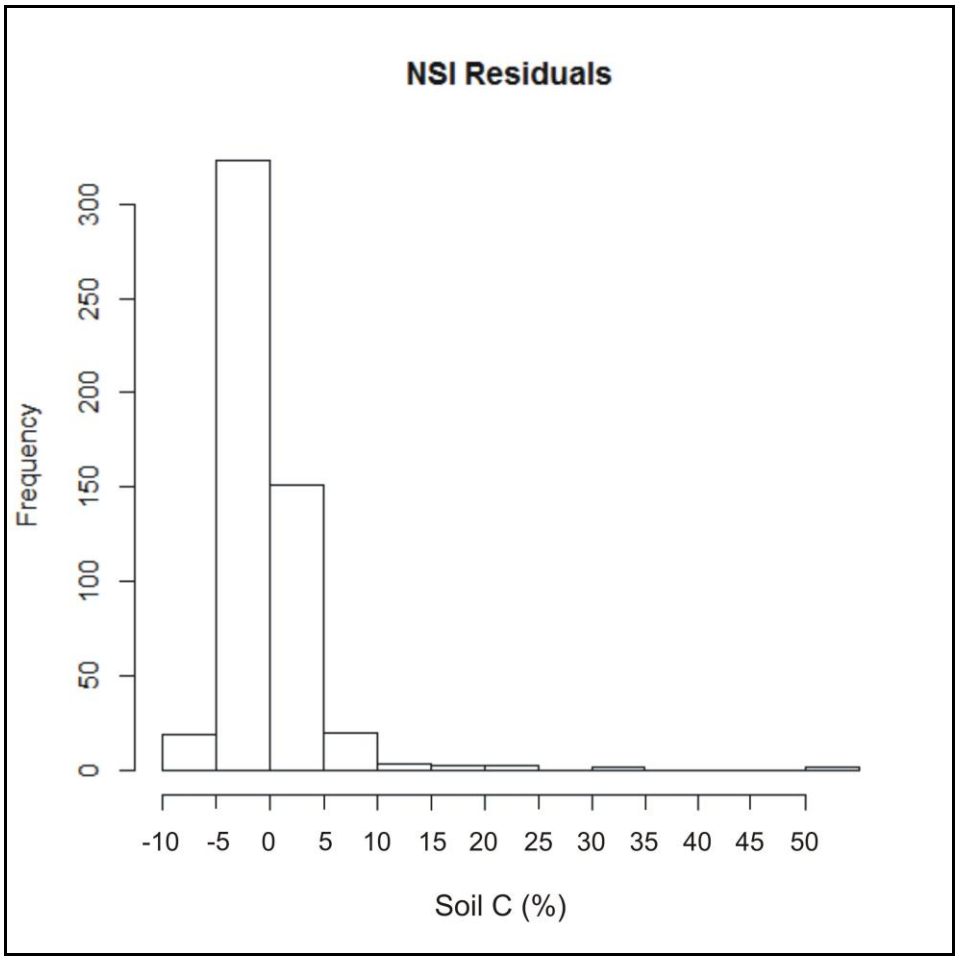

Fig. 6.4: Distribution of the residuals between the soil values observed in the NSI dataset and the values predicted in this study.

For this reason an *independent validation* was also performed, comparing the topsoil C prediction against the data in the NSI dataset. To assess the accuracy of the prediction, the residuals between the observed and the predicted values were calculated. Fig. 6.4 depicts the distribution of the residuals, while in Fig. 6.5, they are located on a map where the colour varies according to the value of the residuals.

The results indicate that the residuals are generally very low, with a mean C percentage of -0.59% and a standard deviation of 4.46. In Fig. 6.4, it is possible to appreciate that the majority of the residuals are in the interval between -5 and +5%, even though there is a small number of large percentage values. A plausible explanation for this is that there are areas of probable marshes where

the topsoil C content is particularly high, but these are almost impossible to predict as those areas were not originally sampled.

In order to study the spatial distribution of these residuals the map, showed in Fig. 6.5, was also created. As mentioned, the majority of the residuals have values between ±5%, and higher values are in areas poorly sampled in the representative profiles data.

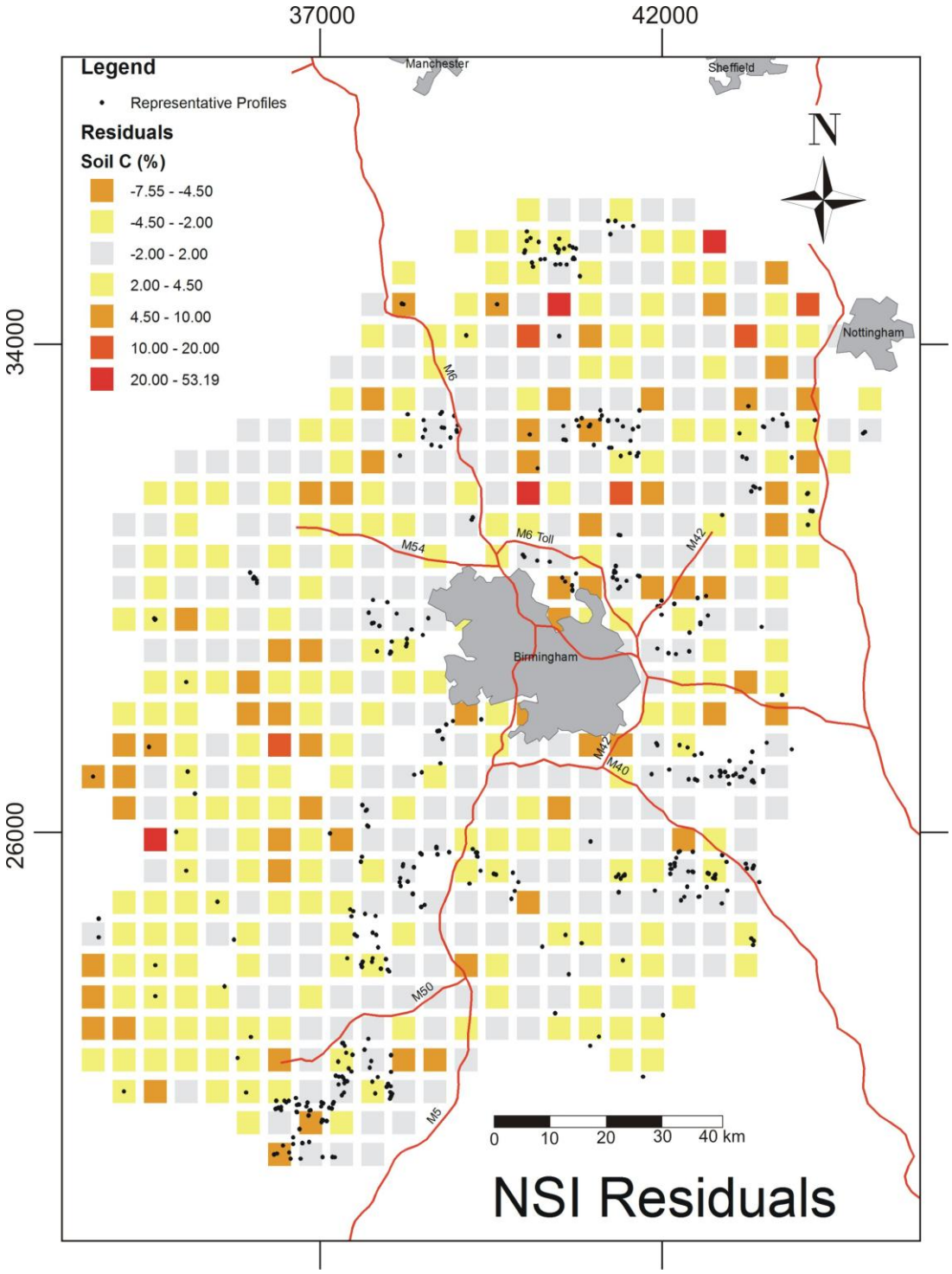

Fig. 6.5: Residuals of the validation with the NSI data.

6.3.2 Stock estimation results

The soil C stock was calculated and corrected using the procedure described in section 6.2.5. The results indicate that C stock in the topsoil is $162.91 \pm 3.63 \times 10^{-5}$ Tg, and C stock in the subsoil is $66.71 \pm 3.52 \times 10^{-5}$ Tg. The C stock estimates are presented in the maps in Fig. 6.6. It appears that on the higher ground on the Welsh border, the topsoil has a relatively higher C content, due the fact that the majority of this area is grassland. By contrast, the subsoil map presents a picture where the higher C content is in the arable lands around Birmingham, and this can probably be a result of C losses from the arable topsoil, as suggested by Bellamy et al. (2005). The C stock was also calculated for land use categories and the results are shown in Table 6.2.

The uncertainties of the point estimations were computed with the approach described in section 6.2.6 and the results are presented in Fig. 6.7. From this figure, it is possible to appreciate the relatively low level of uncertainty for the soil C predictions. In particular the majority of the topsoil predictions have an associated variance between 0 and 0.19 t/ha with peaks of 0.95 t/ha in the Welsh border area, where the sample density is very low. Moreover, the subsoil uncertainty estimations are also low, with the majority of the point uncertainties between 0 and 0.87 t/ha, and a peak on the Welsh border of 5.07 t/ha.

These results corroborate the data presented in the previous sections. In the topsoil, the top-down mapping method can achieve a generally high level of accuracy. On the other hand, from the data described in the previous sections it is impossible to validate the accuracy of the method in the subsoil. However, this uncertainty estimation gives a clear indication of the overall accuracy of the mapping process, which can achieve good results also in the subsoil.

These estimates were then compared with and resulted in higher stocks than the currently used map of the C stock for the United Kingdom created by Bradley et al. (2005). The latter calculated a topsoil stock of 91.33 Tg and subsoil stock of 48.66 Tg.

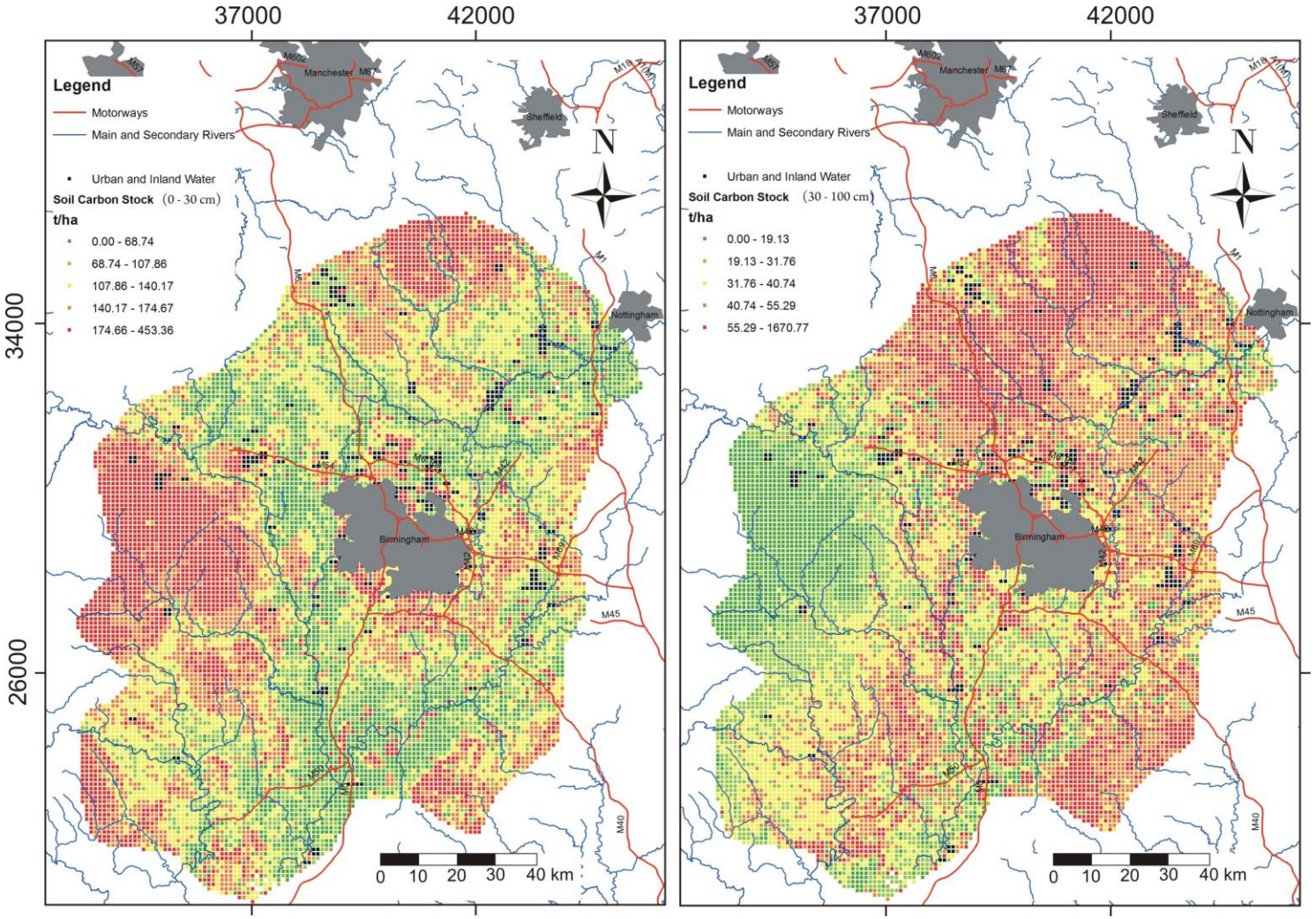

Fig. 6.6: Soil C stock maps.

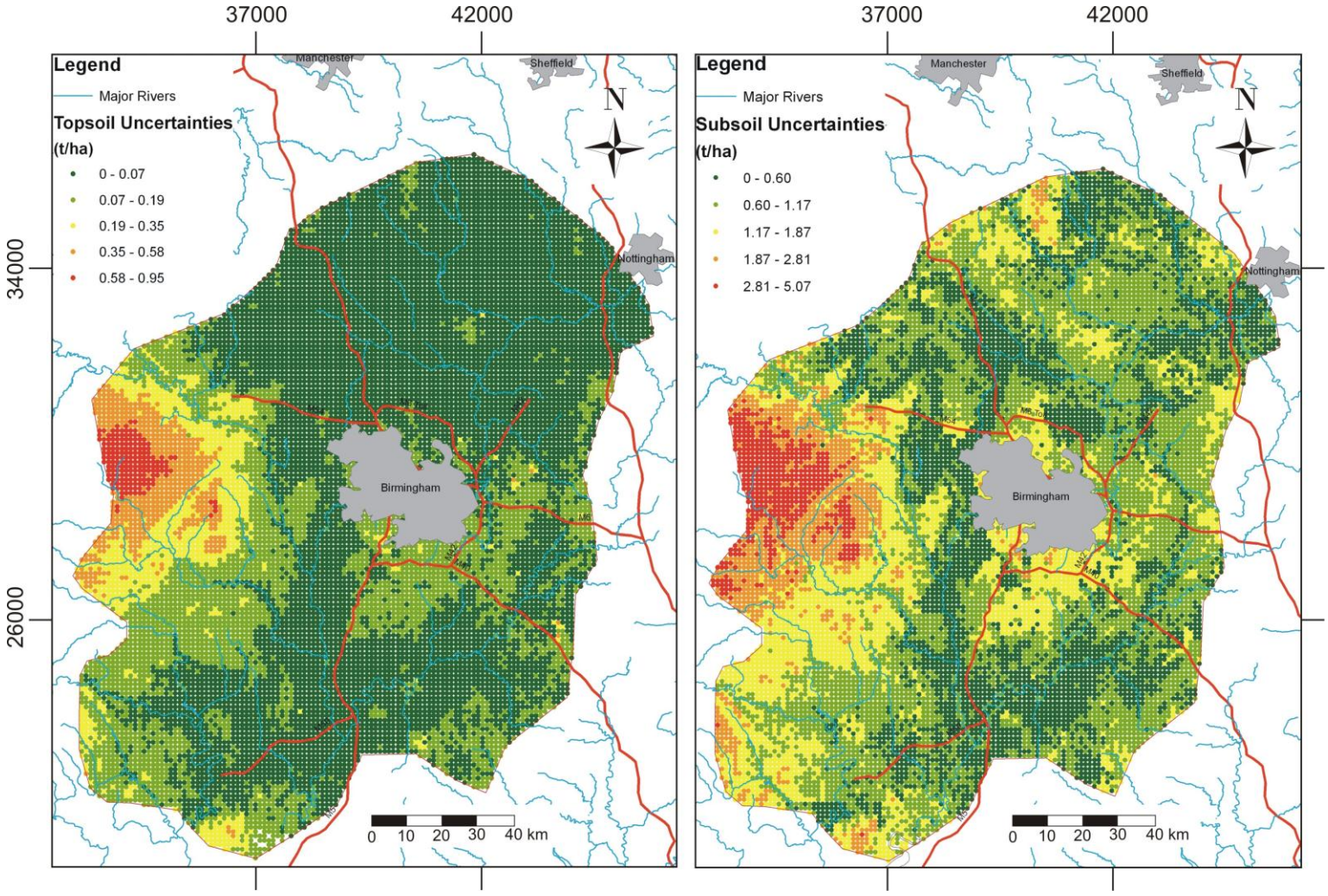

Fig. 6.7: Soil C stocks uncertainty maps.

Table 6.2: Carbon stock estimates divided by land use.

	Topsoil C Stock (Tg)	Subsoil C Stock (Tg)
Agricultural Land	20.68±0.17	54.42±0.22
Grassland (natural, semi-natural and improved)	88.9±0.38	33.23±0.25
Woodland	8.02±0.31	2.84±0.16

It is difficult however to draw any conclusion on this comparison since Bradley et al. (2005) used a completely different approach, based on pedo-transfer functions. Moreover, they used different soil datasets: the NSI data for the topsoil, and the soil series map for the subsoil. The NSI dataset has soil information only up to 15 cm depth, and therefore they had to extrapolate the soil C value from 15 to 30 cm from the soil series map. In addition, they do not provide any validation or uncertainty estimation and therefore it is impossible to properly compare the two maps.

6.3.3 Soil interpretation

Mapping C stock is extremely important to identify areas of higher concentration that are more at risk of C losses, as suggested by Bellamy et al. (2005). In general the study area can be divided into two distinct zones: the lowlands around Birmingham, where most of the arable and urban areas are concentrated, and the higher ground in the northern and eastern parts. These two zones are characterized by almost opposite soil profile patterns, where the lowlands present low C stocks in the topsoil and relatively high stocks in the subsoil, and the higher ground presents relatively high C stocks in the topsoil with a general decrease with depth.

The cause of this pattern in the lowland areas is land use. These areas are predominantly used for agriculture and this may have depleted the topsoil of OM, while leaving the subsoil C either ‘untouched’ or enriched it from leaching.

On the higher ground, the density of arable and urban land is much lower and this has left these areas in an almost natural state, with the higher concentration of C in the topsoil. This is a possible risk factor particularly for the Welsh border, because the soils there have a high silt percentage and this makes them vulnerable to erosion, as mentioned in the report of the PESERA pan–European erosion model (Kirkby et al., 2004). The fact that in these areas the value of C stock is higher indicates a high risk of C losses by erosion which should be addressed with appropriate erosion prevention practices. The majority of this area is grassland which reduces the overall erosion risk. However, a small percentage is in arable use and if more areas are changed, the risk may increase.

6.3.4 Soil fertility assessment

The overall objective of the EU Soil Thematic Strategy (Commission of European Communities, 2006) is the protection and the sustainable use of soil. To achieve this, the first guideline is the prevention of further soil degradation and the preservation of the soil functions. One approach is to understand the pressures on soil such as declining levels of soil organic matter.

To illustrate this issues, a map was created showing the percentage, by volume, of soil C in the topsoil of arable land, which is defined as the most vulnerable due to agricultural practices and/or erosion.

The loss of soil fertility is a major problem for arable soil, which can result in an increase in the amount of required fertiliser, and can potentially decrease crop productivity over time. Soil fertility is affected by the amount of OM present in soils and can be assessed by computing the percentage volume of soil C along the profile. In the study area, almost a third of the land was in arable use, according to the Land Cover Map 2000 from CEH (Fuller et al., 2002) and therefore it is important to assess the potential loss of soil fertility.

From the mapping results, the predicted points on the land defined as in arable use were extrapolated and then the percentage of C stock by volume was computed; the resulting map is presented in Fig. 6.8. Some studies have

proposed soil C percentage by volume below 2% can lead to a significant decline in soil structural stability and fertility (Loveland and Webb, 2003). For the purpose of this study, the 2% value was chosen as minimum colour threshold for the map.

Fig 6.8 shows a scenario where the majority of the arable land has values of C below or slightly above the 2% threshold. This means that if not acted upon, this low C level, could lead to increased probability of erosion and/or decrease in fertility. Since these areas are in the valleys around Birmingham, the most probable cause of these low C values is the intensive arable practice, because the flat terrain does not suggest any influence from soil erosion.

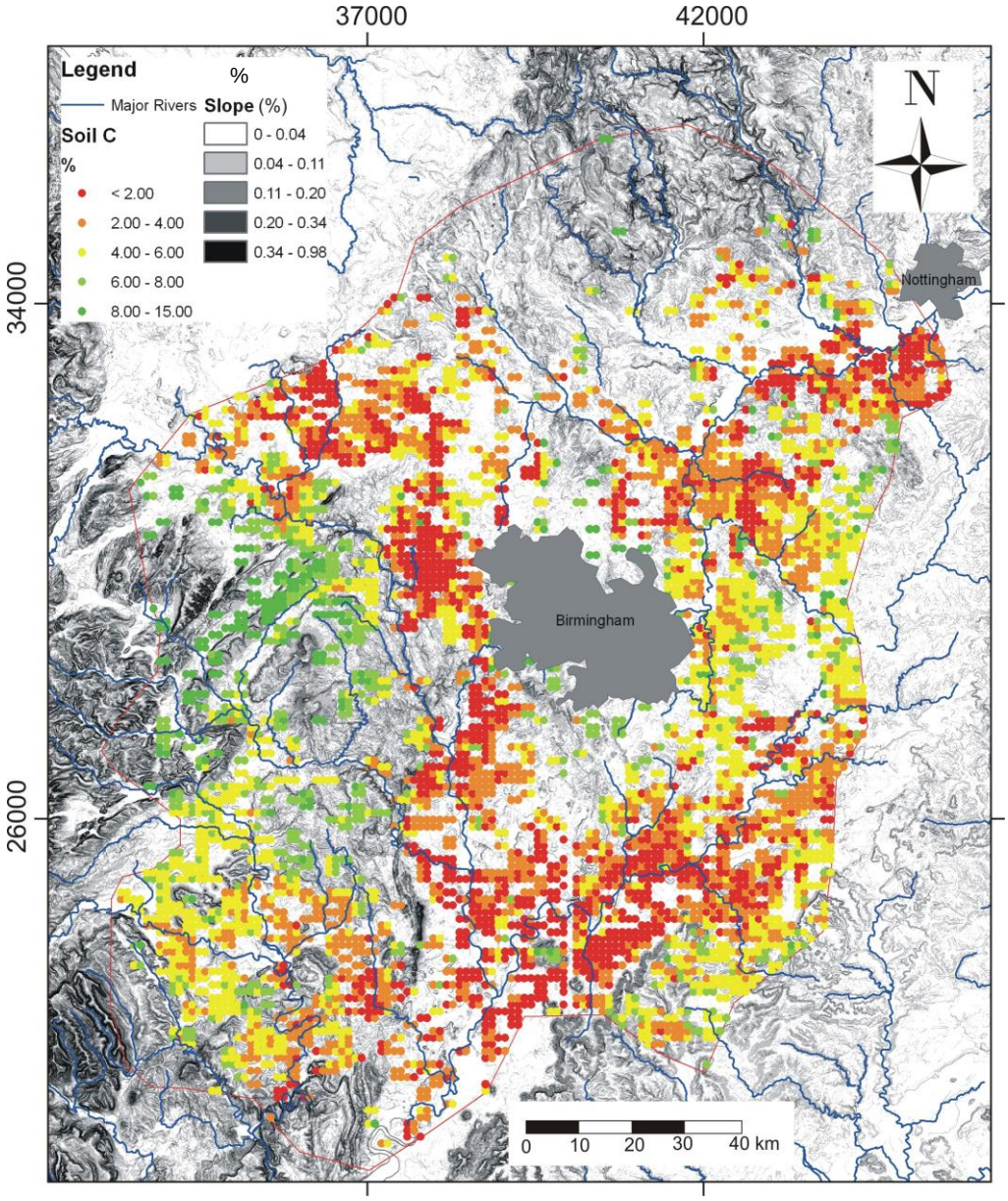

Fig. 6.8: Soil C percentage by volume on agricultural land.

6.4 Conclusions

In this chapter the top-down mapping method was tested at a landscape scale. The results indicate that the method can obtain good results especially when replicating the full amount of variability of the soil properties in the predicted dataset.

This method can achieve a high level of accuracy, in particular for estimating properties for the first 30 cm of soil. This indicates that this map can be readily implemented in a soil erosion model, for example, by increasing the amount of information in the very top part of the profile.
Regarding the subsoil, the uncertainty estimation indicates a good level of accuracy, with the majority of the soil C stock values, presenting a variance between 0 and 0.87 t/ha.

By analysing the soil patterns and comparing them with the land use and the soil erosion model, it is possible to conclude that the study area has very low level of OM. This can potentially lead to an increase in the probability of erosion, soil structure decrement and fertility losses.
In the higher ground on the Welsh border, the soils have a high concentration of C and were soils have a relatively higher silt content, are potentially prone to erosion if their land use is converted into arable.

CHAPTER 7 - Discussion

The literature review has identified a clear need for a new method that can be used to produce high resolution and accurate soil properties estimates in 3D by solving the issues identified in existing algorithms (e.g. smoothing effects, lack of connection between vertical and horizontal variation, and need for detailed soil datasets). Moreover, because soil maps nowadays are tools for obtaining continuous soil property estimates to use for environmental modelling, there is also a need for a method able to be used as a diagnostic instrument so that if the model is unable to obtain reliable outputs for a particular area, the soil map can give indications about the possible causes. The research presented in this thesis has therefore the main objective of developing and testing a new method for 3D digital soil mapping with the aforementioned characteristics. The secondary objective is to critically review existing methods for 3D mapping with and without the use of covariates.

The concept underpinning the development of a new method for mapping soil properties in 3D was that a simple mathematical function can effectively be used to describe soil property variation along the depth profile. This contrasts with views proposed in the majority of literature, in which the depth function is chosen in such a way that it fits as closely as possible to the soil observations. However, this view has two disadvantages: 1) it assumes that the soil observations along the profiles are correct; 2) it only has the objective of producing 3D lattices of soil estimations without considering the interpretability of the resulting maps.

The *first* issue is generally applicable to every soil dataset, where sources of errors vary from the technician operating the instrument to the laboratory handling the soil samples. In most cases, the impact of these errors on the results of a modelling exercise is minimal and can be ignored. However, there are datasets where ignoring the point uncertainties would be a mistake. An example is the soil cone-index measurements described in Chapter 3. For this reason relying on depth functions only for their accuracy in fitting the data can in some cases be erroneous.

The *second* issue is a direct result of mapping techniques developed for a bi-dimensional approach but adapted for 3D soil mapping. The main difference between mapping a surface and a volume is that in the first case it is easier to interpret the final output. In the case of a 2D soil map, it is very straightforward to understand that an area coloured in red has different characteristics compared with a blue area. However, when there is a need to visualise a volume, it is much more difficult to find a technique that communicates the same amount of information with the same simplicity. This problem is not solved by adapting a geostatistical interpolation on 3D soil modelling nor by using complex depth functions, because the only result is a 3D lattice of points, without any other supplementary information.

These two problems can be overcome by using a different approach that takes into account the accuracy of the final 3D model, but also gives additional information that can improve the accessibility to important aspects of the model. The top-down mapping method that was developed in the first stage of this work is based on simple depth functions which are chosen on the basis of how well they describe the average depth pattern observed in the soil data. These simple depth functions are, in general, able to describe a limited set of shapes and they fit badly as soon as the soil profile changes from the average. This gives an opportunity to rely on the goodness of fit of the depth functions, applied to each soil profile, to obtain information about the nature of the soils under investigation.

For example, the general pattern of soil carbon with depth is exponential; if a function of this type is not able to describe the soil pattern it means the soil has some characteristics that differ from this depth pattern (e.g. the presence of a buried peat horizon). By looking at a map of R^2 values, such information can be quickly obtained; from a 3D lattice the only way to have the same results would be to check several horizontal slices, which can be very time-consuming.

The use of pedological knowledge in creating soil specific depth function was already explored by Kempen et al. (2011). In this article, the authors argue that in certain areas, where there has been strong human impact on soils or in areas with highly contrasting parent material, the assumption that soil properties

varies continuously along the profile, which is the basis for the application of the equal area spline and other depth functions, is not valid and soils can display sharp discontinuities in the profile. Moreover, they suggest that using soil specific depth functions can guarantee “a more realistic representation of the depth distribution of soil properties”.

With the depth functions used in this research, the assumption of continuum variation along the profile has to be considered as true, but the pedological knowledge is still contemplated by defining a mathematical model that describes the general profile, thus including in the modelling precious information about soil formation. This method can then be used with legacy data and in areas where the sample coverage is relatively low.

For these reasons, the top-down mapping can be considered as an intermediate method among depth functions techniques. It fits between the equal area spline approach, which uses complex functions that fit each point without considering the general pattern, thus losing sight of the information that soil profiles can provide, and the Kempen et al. (2011) method, which relies on soil specific depth functions, but can work properly only in areas where the data coverage is extensive.

7.1 First stage

The idea that pedological knowledge can be used in developing simple soil specific depth functions was tested in the first stage, described in Chapter 3. Here the new method was developed using a dataset at the field scale, with cone resistance measurements taken at a constant depth interval of 4 cm. This dataset, having twelve observations for each profile, was ideal for testing depth functions of various complexity and accuracy.

From the box-plot of cone resistance versus depth (Fig. 3.4) a vertical pattern was observed where in the upper 30 cm of the soil, the average value was around 1.2 MPa and below that it rapidly increased to 2.5 MPa. These two well-defined layers can be described by numerous mathematical functions of various types and complexity. However, a preliminary analysis of the soil dataset

suggested that for this soil property in this area a simple depth function was selected in order to minimise the errors associated to the point uncertainty of penetrometer readings.

For this reason, a framework was set up for selecting the optimum depth function, by weighing its accuracy and its number of coefficients. With the help of this framework, the best soil specific depth function was a three-coefficient polynomial (Eq. 3.1). This function accurately describes the average pattern identified in the dataset relying only on three coefficients, meaning that it can describe a limited set of geometries. This is crucial to maximise the diagnostic ability of the function.

After this first step, the mapping process proceeded by assessing the spatial auto-correlation of the polynomial coefficients and then predicting them across the field, on a regular grid. Subsequently, for each interpolated point, the polynomial was solved, estimating the cone resistance in the vertical space and creating a 3D lattice. This method is referred to as top-down mapping for its ability to interpolate on the surface for creating a 3D lattice. With this approach it is possible to correctly account for the vertical variability of the soil property, as it is embedded in the function coefficients. Ordinary kriging was used for interpolating the coefficients because the objective was to test the method without any external influence from environmental covariates. Finally, the top-down mapping was compared to a benchmark method that was already used in literature for 3D cone resistance mapping, i.e. 3D ordinary kriging (Castrignanò et al., 2002), in order to test its accuracy.

The results indicate that a simple soil specific depth function can effectively be used to describe the variation of soil properties along the depth profile, scoring an overall value of R^2 of 0.84. A spatial analysis of the goodness of fit was also performed in order to find areas of the field where the depth function performed less accurately. Even though more than 70% of the samples present high values of R^2, there are points where the fit is relatively poor. In these samples the vertical pattern differs from the average described by the depth function. The reasons for this are: a higher than average compaction in the plough pan or an increase in point uncertainties in some samples, especially in the subsoil.

The top-down mapping method can compensate for the presence of these uncertainties by using a simple depth function that describes only the average profile pattern, excluding random fluctuations. This is probably one of the factors that increased the accuracy of this method, in comparison with 3D kriging. The other is that it can better describe the variance of the soil data in the estimates, reducing the smoothing effect.

Another advantage of this method is that with the spatial analysis of the goodness of fit it is possible to identify areas of higher or lower compaction, prior to the geostatistical interpolation. This allows the end user to have a general idea of the spatial compaction pattern in the field and this is useful for visualising the final 3D geostatistical map, as the visualisation can focus the attention of the reader on areas of the field where a more complex pattern is observed.

This concept is demonstrated by looking at previous 3D mapping attempts. In literature, when the objective was the creation of a 3D compaction map, such as in the case of Castrignanò et al. (2002) or Carrara et al. (2007), the visualisation was always undertaken with volumetric rendering, such in Fig. 7.1.

With this technique is easy to follow the compaction pattern in the first 5-10 cm, (for example, the blue track on the Fig. 7.1). However, understanding the changes below that level is extremely difficult.

The top-down mapping method can provide much more information than this type of visualization, just by looking at the goodness of fit maps (Fig. 3.4). In these three images the compaction pattern is much more clearly identifiable.

7.1.1 Case study limitations

This case study was characterised by an uncommon dataset, sampled at very high vertical resolution. Even though it was perfect for developing and testing the new method, it is not a typical soil dataset. Usually, a soil survey is undertaken by identifying the horizons and then measuring the average soil property value for each of these. Moreover, the cone resistance dataset

presented a very clear vertical pattern, which probably helped in obtaining good results.

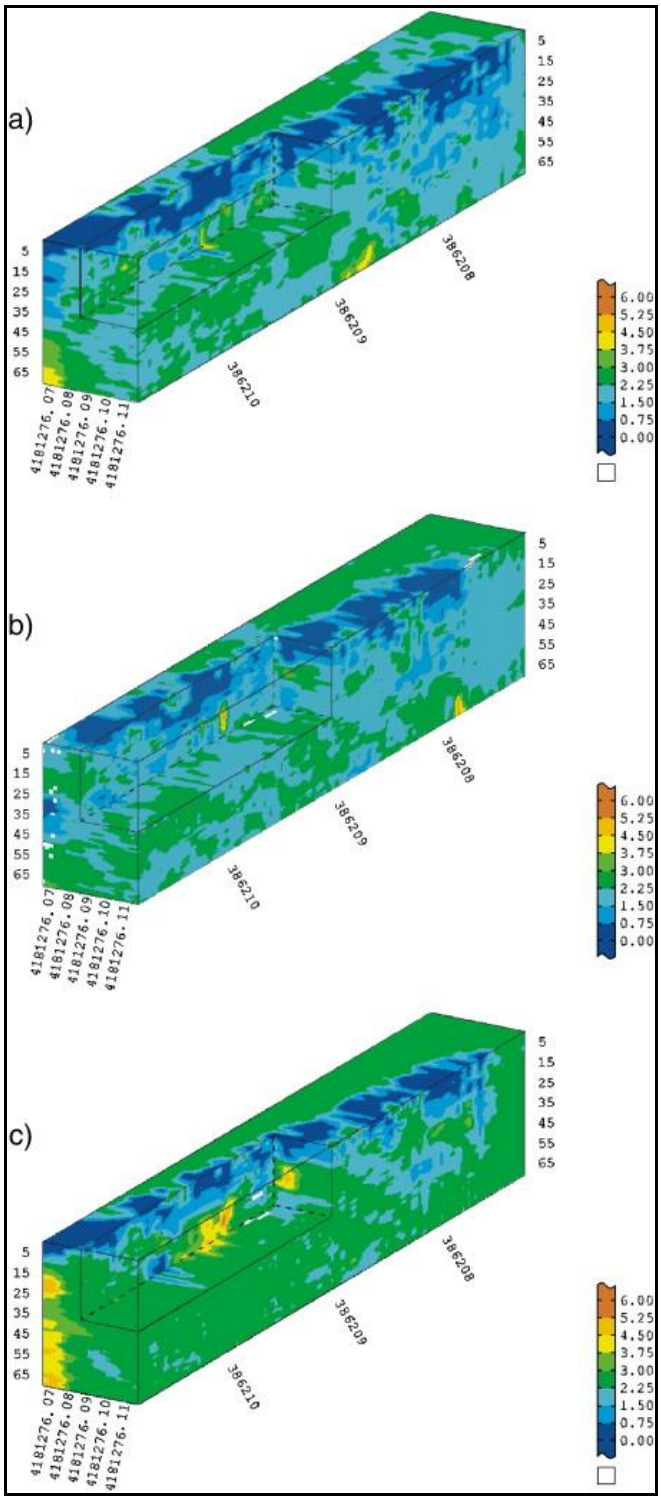

Fig. 7.1: Examples of volumetric rendering used for showing the soil compaction pattern. The three images, from Carrara et al. (2007), represent the soil compaction after zero (a), one (b) and five (c) tractor passages.

7.2 Second stage

Because of the limitations in the case study described in section 7.1.1, the second stage of the project, described in Chapter 4, focused on the design of another mapping experiment in which the top-down mapping method was compared with other common methods for soil mapping. This study aimed to test the method in a more common scenario where soil datasets are sampled by horizons, and environmental covariates are implemented in the modelling to increase the estimation accuracy, as suggested in the iSoil project. In this second experiment, a field scale dataset was used comprising 30 samples with texture percentages from three depth layers, and continuous covariates.

From the original dataset, a new set of soil observations was simulated on a regular 40 m horizontal resolution grid and at 10 cm vertical resolution. By averaging, the profile values were subsequently used to create another dataset with pseudo-horizons which was then used as the starting point for the mapping experiment. From this dataset, a series of validations were performed in order to compare the three methods in both describing the variation of soil texture along the profile and estimating it across the 3D space.

The results indicate that even though each method can assess the vertical variation with a good level of accuracy, the 3D universal kriging was the best predictor. A smoothing effect is present because the predicted dataset from 3D kriging underestimated the observed variance by 20%, but it is limited and it does not affect the overall prediction accuracy.

The depth function methods can better describe the variance of the dataset, and in the case of the equal area spline can also predict soil texture with results that are very close to those derived from 3D kriging. However, it cannot reach the same accuracy as 3D kriging. The reason is probably associated to the complexity of the soil profiles vertical pattern. Bishop et al. (1999) tried the equal area spline with soil texture profiles. They created spline profiles of clay and sand, alongside organic carbon, pH and other. Their results indicate that the spline approach is the best predictor for almost all the soil properties analysed. However, they also tested how different sampling schemes could help in generating more accurate profiles. For instance, they sampled the top

and bottom of each horizon and tested if these additional data could increase the accuracy of the spline. They concluded that for clay and sand the best predictor was the spline used in combination with bottom profile samples for clay and top profile samples for sand.

These additional data were not considered in this experiment because they are normally not available in soil datasets. This is probably the key for the lower accuracy of the equal area spline method compared with 3D kriging. The spline, if not bounded by top or bottom samples, is constrained only by the horizon average. This means that it can assume every possible soil value as long as the horizon average is constant. Probably, if the pattern is too complex this is not sufficient to produce reliable estimates, consequently reducing the overall mapping accuracy.

The top-down mapping also fails to accurately predict soil texture in the 3D space. This is due to the lack of a recognisable pattern in the texture profiles. The penetration resistance data presented a peculiar vertical pattern that could be readily recognised and described by a very simple three-coefficient polynomial. However, in the case of soil texture, the profiles presented a highly complex vertical pattern that could only be described by a four-coefficient polynomial and this was probably the key for the failing of the method. A high number of coefficients cause error propagation between the estimated coefficients and the predicted soil texture properties.

Although this error propagation is hard to fully demonstrate it was noticed in the first stage that in general the equation coefficients presented a poor spatial auto-correlation, with relatively high nugget values (Fig. 4.7). This has the consequence of modifying the kriging variance for the estimated points, causing error propagation between the coefficient predictions and the actual estimates of the soil properties. The higher the number of coefficients, the higher will be the error propagation. From this experiment it is possible to conclude that the top-down mapping method can work accurately only if the soil profile pattern can be described by a depth function with a maximum of three coefficients.

7.2.1 Use of covariates in 3D DSM

From the validation of the three methods for 3D soil mapping described in Chapter 4, it was noticed that every one of them presented a decrement of the mapping performances with depth (i.e. vertical decrease of accuracy). One of the reasons for this could be the use of geophysical covariates as a source of additional information during the geostatistical interpolation. These data are apparent values and are depth averages of the investigated volume. For instance, gamma-ray surveys measured a single datum that reflect the nuclei concentration of the first 30-45 cm of soil (Taylor et al., 2002; Bierwirth and Brodie, 2008); electromagnetic surveys that measure electrical conductivity values that are depth averages (McNeill, 1980), and depend on the instrument penetration, which ranges from 30 cm for the EM38 to 4-5 m for the EM31. Moreover, the geophysical value is affected by changes in several soil properties and it is difficult to relate it to a single soil feature. For example, clay content can highly affect electromagnetic surveys, even decreasing their penetration depth if the clay percentage is particularly high (King et al. 2001; 2003)

For these reasons it was hypothesised that probably the vertical decrement was caused by a general decrease in the correlation between the soil texture and the geophysical covariates. As a consequence, the use of geophysical covariates in 3D digital soil mapping was reviewed by setting up a simple experiment using the Lany dataset. In this study, the 30 original soil profiles were used with the following soil properties: soil texture, organic carbon, pH, S and N. The experiment was undertaken by simply validating, with a 1-out cross-validation, the predictions of all the available soil properties, at each depth layer. The available covariates were used singly or in combination with others, in order to find the most appropriate for each soil property.

The results indicate that on average there is a decrement in the subsoil prediction of 44%, in terms of RMSD value, compared to topsoil results. However, if the soil properties present a low variability (for example pH, S and N) they can be predicted with every combination of covariates, obtaining relatively high levels of accuracy. Soil organic carbon and clay content present

in general a high correlation with geophysical data, especially electromagnetic covariates, and this can effectively increase the accuracy of the prediction. Conversely, for textural properties, which present a high variability and a complex variation with depth, the estimation can be difficult and in general can be better predicted with gamma ray covariates.

These results are very interesting in the context of 3D DSM. In fact, several authors describe generally better prediction accuracy in the topsoil, compared to subsoil data (Minasny et al., 2006; Malone et al., 2009). In particular Malone et al. (2009) try to identify the possible cause of this behaviour, suggesting that the environmental covariates they used could only explain the soil variability at the surface level. However, they did not investigate this matter any further, after realising that they probably needed additional sources of data to describe the soil properties variability in the subsoil.

This experiment can explain this vertical decrement. As clearly demonstrated, the environmental covariates have a high correlation with topsoil data and therefore can be successfully used for topsoil predictions. However, the correlation decreases substantially in the subsoil and this causes a decrement in the prediction accuracy. For this reason as long as the only available data are surface covariates, digital soil mapping in 3D would continue to achieve relatively low level of subsoil accuracy. More research is needed to increase the use of covariates that are more suitable for 3D DSM, in particular, covariates that are more correlated with sub-surface layers (e.g. GPR and resistivity).

In summary, this experiment shifted the focus of the research from the development of a new method to a review of common techniques for modelling soils in 3D. In Chapter 4, attention was focused on the developments of algorithms to create a 3D map, how each method behaved and what were the advantages and disadvantages of each of the investigated techniques. In Chapter 5, attention was given to soil data and covariates in order to identify which properties are easier to predict and which require the use of specific covariates to be properly mapped.

7.3 Third stage

In the first two stages of the research, the analysis was done with a dataset at the field scale and under circumstances in which the number of observations and covariates were ideal for the use of geostatistics. Even though these studies have supplied important information about the applicability of the top-down method and its usage, it was important to test the new method over a larger area. The study of large areas, with spatial statistics and computer-assisted numerical analysis, has rapidly become common practice among soil scientists because of the advent of powerful and relatively cheap PCs. An example is the project of predicting key soil characteristics at global scale in the GlobalSoilMap project (GlobalSoilMap.net, 2011). For these reasons, the third stage of the thesis, the developed method was tested at a landscape scale using the soil survey data from England and Wales to predict soil organic carbon and bulk density levels in the West Midlands region, an area of approximately 13,948 km^2.

In the England and Wales survey dataset, the variation by depth of organic carbon can be described by a power equation (Eq. 6.1) with only two coefficients, which is optimal for applying the top-down mapping method. However, the objective of the mapping experiment was to model soil C stocks. For this reason the depth pattern of bulk density was also investigated. It was observed that this can be described by an inverse power function (Eq. 6.2), with two coefficients. As a consequence, the top-down mapping method could be tested, as both soil properties can be described by a two coefficients equation.

The results provide a very good insight into what this method can achieve and where its limitations lie.

First of all, with this method it is possible to map an area at the landscape scale, with a total number of 220,928 points, in less than five minutes, whereas using only geostatistical interpolation would have taken several hours. This demonstrates that the method can overcome one of the limitations of 3D interpolation (i.e. it is much quicker). This was one of the objectives of the first stage, when the method was developed. However, it was impossible to demonstrate until now because in mapping at the field scale, the number of grid

points was relatively low and the interpolation time of top-down mapping and 3D kriging were similar.

Kerry and Hawick (1998) investigated the time required for kriging interpolation, using a single core PC and a networked supercomputer consisting in 128-CPUs. Their results suggest that for estimating 4,000 points, a fraction of the points in this C stock estimation, their supercomputer needed 1,500 minutes. Of course, their experiment was carried out 14 years ago and certainly the processing power of modern computer can improve their results. However, it is difficult to believe that a supercomputer with 128 CPUs from 14 years ago can be less powerful than a modern 4-core CPU computer.

Another good result is the confirmation that even at this extent the top-down method can accurately reproduce the variability of the observed dataset, as reported in Table 6.1, avoiding the smoothing effect that can undermine the effectiveness of geostatistical interpolation for large scale mapping. This is particular evident in the topsoil, where the estimates standard deviation is very similar to the observed dataset. As a result, the method appears to be very accurate in mapping soil carbon values in the first 15 cm, as demonstrated by the very good results of the independent validation.

In the subsoil, it is much harder to verify the accuracy of the top-down mapping because of the lack of independent validation data. However, from the uncertainty estimation analysis it is possible to conclude that, even though there is an increase in the average error associated with the subsoil estimations, in general the soil C stock predictions in the subsoil are acceptably accurate.

The cross-validation results indicate an average R^2 value of, for the 5% exclusion, of 0.36 for C, with a standard deviation of 0.20; and 0.44 for BD, with a standard deviation of 0.15. These results may appear relatively low, but they are in line with previous validated research of 3D mapping at the catchment or landscape scale with a similar sample density (Malone et al., 2009; Kempen et al., 2011). In particular, Malone et al. (2009) estimated soil C in 3D at landscape scale, reaching an accuracy of 0.20-0.27 of R^2, with a sample density similar to this experiment. By contrast, Kempen et al. (2011) were able to reach a total R^2 of 0.46, divided 0.75 in the topsoil and around 0.10-0.20 in the subsoil.

However, in their experiment they studied an area of 125 km^2 having a sample support of 1211 profiles, of which 619 collected with a probabilistic sampling scheme adapted for digital soil mapping.

In digital soil mapping the samples support is the crucial aspect that drives the performance of the algorithm used in the prediction. This is evident in the 2D mapping experiment but it is much more important in 3D studies, where the number of points to predict is exponentially higher and therefore the error propagation is proportionally higher. In field scale experiments the error propagation can be kept to a minimum because the low extent of the area means a generally high sample density. On the other hand, for large areas the sample density can become a problem that greatly affects the prediction accuracy. This can be addressed by using sampling designed that keep into account the soil spatial variability and select the sampling location that best describe it, as in Kempen et al. (2011). In this case study, legacy soil data, collected without any specific sampling design, were used. Moreover, the general samples density was extremely low, with on average one sample every 32 Km^2, similar to the mapping experiment by Malone et al. (2009). For these two reasons, values of R^2 of 0.36 for C and 0.44 for BD can be considered an acceptable accuracy.

In summary, from this case study it was possible to verify that the top-down mapping method can also be used for mapping soil properties over large areas. The only problem is in the vertical pattern of these properties, which have to be describable by a simple equation. The results indicate that the top-down mapping is still able to closely replicate the variance of the observed dataset in the predictions, and obtain accurate estimates for both topsoil and subsoil. This study also confirms the use of soil specific depth functions as diagnostic tools. A simple depth function, selected for describing the general pattern of the soil property, can be used to spot areas of the landscape where there are changes in soil profiles. This can potentially be very useful when the 3D soil map is the major source of data for environmental models.

CHAPTER 8 - Conclusions

This research was inspired by the realisation that the methods available in literature for digital soil mapping in 3D were partially flawed. The aim was to develop a new method for 3D DSM that can solve these flaws, while maintaining an acceptable level of accuracy.

8.1 Hypothesis and objectives

This was the starting point of the research, and the hypothesis was written accordingly, as follow:
High resolution 3D mapping can be accurately achieved, with a method able to estimate soil properties even with relatively poor data support, thus minimising the cost of the survey, and which can reasonably be applied over large areas.

In order to test the validity of the hypothesis, the research aimed at developing and testing a new method for 3D DSM based on simple soil specific depth functions.
From this statement, a series of objectives were set and the study was divided into three stages, for establishing a clear path for testing the hypothesis.

8.1.1 First stage

In the first stage the primary objective was the development of a new method for accurately mapping soil properties in 3D; a method that was easier to use than 3D geostatistics and sufficiently flexible to be used with less dense datasets. The method was extensively tested, validated and compared to the established method of 3D ordinary kriging.
This stage of research concluded that a novel method had been developed, which can obtain high level of accuracy in mapping soil compaction, performing

much better than 3D ordinary kriging. This method is much easier to use compared to 3D geostatistics, because it relies on bi-dimensional interpolation; it is also flexible as it can be used with much less analytical data losing only a fraction of its accuracy.

8.1.2 Second stage

The second stage was concerned with the main objective of testing the developed method with a common dataset and in a scenario where soil profiles are not the only sources of information. In this research, and in the context of the iSoil projext, environmental covariates were introduced into the methodology because they can improve the accuracy of the prediction.

This study found that the developed method works well also with geostatistics algorithms that rely on environmental covariates. However, it was demonstrated that with soil properties that present a complex vertical pattern, the top-down mapping method cannot be used.

From the comparison of different mapping methods, the thesis demonstrated that 3D universal kriging was a better predictor of soil properties that the depth functions approach. Therefore, it was concluded that with complex patterns, all the methods that rely on depth functions tend to predict with a lower accuracy, compared to purely geostatistical methods.

The final part of the study was focused on testing the use of environmental covariates for 3D DSM. This experiment, confirmed that environmental covariates can effectively be used to increase the accuracy of the predictions in the topsoil, but their correlation with soil properties decreases greatly with depth.

When the property of interest is well correlated with the covariates, such as in the case of clay and EM, the accuracy of the prediction is relatively good both in the topsoil and in the subsoil. However, when the soil property presents a complex pattern and is not well correlated with the covariates, there is a drop in the accuracy from topsoil to subsoil.

8.1.3 Third stage

The final stage of the research was concerned with the testing of the top-down mapping method over a large extent, with all the changes that this implies (sparser data and low resolution covariates). The key points to test were similar to the field scale studies: estimation accuracy, impact of smoothing, computational time.

From the results it is possible to conclude that the top-down mapping method can effectively be used at landscape scale, as it is able to predict much quicker than geostatistics. It is also able to cope with sparser data and with the environmental covariates available at this scale: DEM derivatives, land use, soil associations and geology. Moreover, despite the fact that the area was 13,948 km^2, the top-down mapping was able to minimise the smoothing of the predictions, estimating soil C and BD with an acceptable level of accuracy.

8.1.4 Method applicability and limitations

During this research, the top-down mapping method was tested with several soil properties and different spatial extents. Some general conclusions can be drawn from these tests.

First of all, in order to use this method the condition that the soil properties vary continuously along the profile must be met. With datasets in which the soil properties present sharp discontinuities along the profile, this method cannot be used.

Another key component for the successful application of this method is the selection of the depth function. A framework is provided for testing various groups of equations, but if the results indicate that the best soil specific depth function has more than three coefficients, the top-down mapping method can become difficult to implement. This implies that there are soil properties for which this method is not appropriate, such as soil texture, as demonstrated in Chapter 4.

The tests were performed on relatively homogeneous areas, for which a single soil profile pattern was identified. This does not mean that the top-down mapping method cannot be used is spatially variable areas, where soil type changes substantially. In areas such as this, the method can be adapted by selecting different depth functions in relation to the vertical profile of the soil types. This way each soil type can be mapped separately.

8.1.5 Concluding remarks

This research demonstrated the successful creation of a new method for mapping soil properties in 3D. This method was shown to predict soil properties with an acceptable level of accuracy, when their soil vertical pattern can be describe by a simple depth function. It also demonstrated that if the previous condition is met, the method developed during this research can map large areas using sparse datasets and reaching a good level of accuracy.

The working hypothesis assumed that mapping soil properties in 3D was possible even with sparse datasets, reaching an acceptable level of accuracy, even for large areas. From the results it is possible to conclude that where the conditions for its applicability are met, as described in section 8.1.4, the top-down mapping method can effectively be used with sparse data obtaining good results, even for large extents. For this reason, under these circumstances the hypothesis can be considered valid.

8.2 Scientific advancements

This research increased the knowledge base in the field of digital soil mapping with a set of new findings. These include:

Novel method for 3D DSM

- Simple soil specific depth functions can be used as diagnostic tools for describing the general depth profile of important soil features (e.g. soil compaction and soil C stock).

- Their use was embedded in a new method for accurately describing and mapping soil properties in 3D.
- The combination of depth functions and geostatistics, makes this method much easier to use compared to 3D geostatistics alone.
- From a goodness of fit analysis, useful information can be obtained about the soil depth pattern from a simple 2D image. Information that us otherwise accessible only by looking at several horizontal slices.
- This method can be used at several spatial scales, and it works well both with and without environmental covariates.

Testing of literature mapping approach

- Geostatistics can be used in its 3D version for soil mapping, but scientists should consider that the smoothing effect can greatly decrease its prediction accuracy.
- Depth function method can reproduce much better the observed data distribution in the estimation, potentially increase the overall accuracy.
- Complex depth pattern is soil properties can cause a decrement in the prediction accuracy of depth function methods.

Geophysical covariates

- Despite the theoretical depth of investigation of geophysical covariates, they tend to lose prediction accuracy very rapidly with depth.
- Their use for 3D DSM needs to be carefully assessed by a correlation analysis, because if the soil property present a high variance, their use can be ineffective, especially for subsoil predictions.
- In general, gamma-ray data obtained better predictions for sand and silt, in both topsoil and subsoil.
- Electromagnetic data are more reliable for predicting clay, pH, soil C, N and S.

8.3 Future work

Several areas in which to continue the research have been identified, and are now briefly discussed.

8.3.1 Exploration of additional study area

The top-down mapping method was tested mapping soil C at landscape scale, with a relatively homogeneous dataset. However, in other areas or with higher resolution, buried peat can become a concern for the successful application of the method. In this scenario the most likely solution would involve the use of more than one depth function. In addition, the landscape would be clustered based on the depth function that better describe the soil profile in each area.
For testing this, the best area would be in North Yorkshire, where the soil survey dataset of England and Wales presents a sample density comparable to the West Midlands region. In North Yorkshire, peat is much more common and the soil C pattern should present less homogeneity.

8.3.2 Mapping at higher resolution

The use of depth function decreases greatly the smoothing effect typical of techniques such as kriging, as demonstrated in the thesis. They also greatly decrease the computational time required for the mapping. This means that method based on depth functions can be used to produce high resolution 3D digital soil map, at landscape or even continental scale, with spatial resolution that can reach 2-5 m and vertical resolution of up to 1 cm.
A 3D soil map of the whole country can be very useful for scientists, because it can provide the basis for increasing the accuracy of environmental models, such as JULES or erosion models.
A 3D soil map can also be very useful for field survey, when for example the effects of a particular erosion event need to be assessed. Having a detailed digital soil map can be extremely useful in these circumstances, because it could be accessed from a common smartphone with GPS in order to give a quick estimation of the soil properties values and the soil vertical pattern in the area.
In addition, the current soil map can be greatly simplified by using the prevalent depth function in addition to the soil association. Polygons that represent the

prevalent soil pattern, identified by a particular depth function, can be presented on the map, alongside soil series data.

8.3.3 Environmental covariates

In this research several types of covariates were used, non-geophysical and geophysical. The use of the covariates tested in this research is well documented for 2D soil mapping, but tests undertaken during the thesis appear to show that they cannot reach a high level of accuracy in subsoil prediction. However, in the experiment only covariates commonly used in soil science were explored (gamma-ray and EM).

It would be interesting to try other sources of covariates, at the field scale in order to explore their use as predictors in digital soil mapping. For instance, ground penetrating radar (GPR) data can be incorporated. With this instrument it is possible to obtain real 3D representations of the soil in form of electromagnetic reflectors. The aim would be trying to slice the GPR signal to assess if it is possible to have different GPR data as covariates for each soil layer.

The same idea can be applied with resistivity data from which can normally be created a resistivity model in 2D or 3D. The geophysical model can be sliced in order to obtain different covariates for different depth, and see how this changes the prediction.

REFERENCES

Batjes, N. H. (1996), "Total carbon and nitrogen in the soils of the world", *European Journal of Soil Science,* vol. 47, no. 2, pp. 151-163.

Bellamy, P. H., Loveland, P. J., Bradley, I., Lark, R. M. and Kirk, G. (2005), "Carbon losses from all soils across England and Wales 1978−2003", *Nature,* vol. 437, pp. 245-248.

Berry, W., Ketterings, Q., Antes, S., Page, S., Russell-Anelli, J., Rao, R. and DeGloria, S. (2007)*, Agronomy Fact Sheet Series - Soil Texture*, available at: http://water.rutgers.edu/Rain_Gardens/factsheet29.pdf (accessed 01/2012).

Bierwirth, P. N. and Brodie, R. S. (2008), "Gamma-ray remote sensing of aeolian salt sources in the Murray–Darling Basin, Australia", *Remote Sensing of Environment,* vol. 112, no. 2, pp. 550-559.

Bingham, I. J. and Wu, L. (2011), "Simulation of wheat growth using the 3D root architecture model SPACSYS: Validation and sensitivity analysis", *European Journal of Agronomy,* vol. 34, no. 3, pp. 181-189.

Bishop, T. F. A., McBratney, A. B. and Laslett, G. M. (1999), "Modelling soil attribute depth functions with equal-area quadratic smoothing splines", *Geoderma,* vol. 91, no. 1-2, pp. 27-45.

Bonomi, T., Canepa, P. and Del Rosso, F. (2007), "Three-dimensional textural models in heterogeneous aquifers", *Rendiconti della Societa Geologica Italiana,* vol. 4, pp. 19-22.

Bonomi, T., Cavallin, A., Stelluti, G. and Guerra, G. (2002), "3D subsoil parameterisation in a plain region of northern Italy", *Memorie Società Geologica Italiana,* vol. 57, pp. 543-550.

Bonomi, T. (2009), "Database development and 3D modeling of textural variations in heterogeneous, unconsolidated aquifer media: Application to the Milan plain", *Computers & Geosciences,* vol. 35, no. 1, pp. 134-145.

Bourke, P. (1993), "Computer based terrain visualization techniques", http://paulbourke.net/miscellaneous/terrainvis (accessed: 01/2013).

Bradley, R. I., Milne, R., Bell, J., Lilly, A., Jordan, C. and Higgins, A. (2005), "A soil carbon and land use database for the United Kingdom", *Soil Use and Management,* vol. 21, no. 4, pp. 363-369.

Brewer, R. (1968), "Clay illuviation as a factor in particle-size differentiation in soil profiles", *Transcript 9th International Congress Soil Scence.,* vol. 4, pp. 489-499.

Brown, R. B. (2003)*, Soil Texture*, available at: http://edis.ifas.ufl.edu/pdffiles/SS/SS16900.pdf (accessed 01/2012).

Brys, G., Hubert, M. and Struyf, A. (2004), "A robust measure of skewness", *Journal of Computational and Graphical Statistics,* vol. 13, no. 4, pp. 996-1017.

Busscher, W. J., Bauer, P. J., Camp, C. R. and Sojka, R. E. (1997), "Correction of cone index for soil water content differences in a coastal plain soil", *Soil and Tillage Research,* vol. 43, no. 3-4, pp. 205-217.

Butscher, C. and Huggenberger, P. (2007), "Implications for karst hydrology from 3D geological modeling using the aquifer base gradient approach", *Journal of Hydrology,* vol. 342, no. 1–2, pp. 184-198.

Campbell, N. A., Mulcahy, M. J. and McArthur, W. M. (1970), "Numerical classification of soil profiles on the basis of field morphological properties", *Australian Journal of Soil Research,* vol. 8, pp. 43-58.

Carrara, M., Castrignanó, A., Comparetti, A., Febo, P., Orlando, S. (2007), "Mapping of penetrometer resistance in relation to tractor traffic using multivariate geostatistics", Geoderma, vol. 142, no. 3–4, pp. 294–307

Carré, F., McBratney, A. B. and Minasny, B. (2007), "Estimation and potential improvement of the quality of legacy soil samples for digital soil mapping", *Geoderma,* vol. 141, no. 1–2, pp. 1-14.

Castrignanò, A., Maiorana, M., Fornaro, F. and Lopez, N. (2001), "Mapping spatial and temporal variability of cone resistance data in an Italian field cropped to durum wheat", *Proceedings of the 3rd European Conference on Precision Agriculture,* , pp. 355-360.

Castrignanò, A., Maiorana, M., Fornaro, F. and Lopez, N. (2002), "3D spatial variability of soil strength and its change over time in a durum wheat field in Southern Italy", *Soil and Tillage Research,* vol. 65, no. 1, pp. 95-108.

Cignoni, P., Puppo, E., Scopigno, R. (1997), "Representation and visualization of terrain surfaces at variable resolution". *The Visual Computer,* vol. 13, pp. 199-217.

Colwell, J. D. (1970), "A statistical-chemical characterization of four great soil groups in southern New South Wales based on orthogonal polynomials", *Australian Journal of Soil Research,* vol. 20, pp. 221-238.

Commission of European Communities (2006), *Thematic Strategy for Soil Protection,* COM(2006)231 final.

Corwin, D. L., Kaffka, S. R., Hopmans, J. W., Mori, Y., van Groenigen, J. W., van Kessel, C., Lesch, S. M., Lesch, J. D. (2003). "Assessment of field-scale mapping of soil quality properties of a saline-sodic soil". *Geoderma*, vol. 114, pp. 231-259.

Cox, P. M., Betts, R. A., Bunton, C. B., Essery, L. R. H., Rowntree, P. R. and Smith, J. (1999), "The impact of new land surface physics on the GCM simulation of climate and climate sensitivity", *Climate Dynamics,* vol. 15, pp. 183-203.

Cressie, N. A. C. (2008), "Statistics for Spatial Data", *New York: John Wiley & Sons,* vol. 900, pp. 1991.

Czech Geological Survey (2004), *Interactive Geological Map*, available at: http://mapy.geology.cz/website/geoinfo_an/ (accessed: 17/05/2012).

Dagallier, G., Laitinen, A. I., Malartre, F., Van Campenhout, I. P. A. M. and Veeken, P. C. H. (2000), "Ground penetrating radar application in a shallow marine Oxfordian limestone sequence located on the eastern flank of the Paris Basin, NE France", *Sedimentary Geology,* vol. 130, no. 3-4, pp. 149-165.

Darabi, H., Kavousi, A., Moraveji, M. and Masihi, M. (2010), "3D fracture modeling in Parsi oil field using artificial intelligence tools", *Journal of Petroleum Science and Engineering,* vol. 71, no. 1–2, pp. 67-76.

Davis, M., (1987), "Production of conditional simulations via the LU triangular decomposition of the covariance matrix", *Mathematical Geology*, vol. 19, no. 2, pp. 91-98.

Deutsch, C.V. and Journel, A.G., (1998), *GSLIB: geostatistical software library and user's guide. Second edition*. OUP USA.

Dollner, J., Baumann, K., Hinrichs, K. (2000), "Texturing techniques for terrain visualization", *Proceedings of the conference on Visualization '00*, Salt Lake City, Utah, USA.

Egmond, F.M., Loonstra, E.H. and Limburg, J., (2010), "Gamma Ray Sensor for Topsoil Mapping: The Mole", *Proximal Soil Sensing*, vol. 1, no. 5, pp. 323-332.

Erh, K. T. (1972), "Application of spline function to soil science", *Soil Science,* vol. 114, pp. 333-338.

Essery, R., Best, M. and Cox, P., (2001), *Moses 2.2 Technical documentation*, Hardley Centre, MET Office.

Fenster, A., Surry, K., Smith, W., Gill, J. and Downey, D. B. (2002), "3D ultrasound imaging: applications in image-guided therapy and biopsy", *Computers & Graphics,* vol. 26, no. 4, pp. 557-568.

Friedlinger, M., Schad, L. R., Blüml, S., Tritsch, B. and Lorenz, W. J. (1995), "Rapid automatic brain volumetry on the basis of multispectral 3D MR imaging data on personal computers", *Computerized Medical Imaging and Graphics,* vol. 19, no. 2, pp. 185-205.

Fuller, R. M., Smith, G. M., Sanderson, J. M., Hill, R. A., Thomson, A. G., Cox, R., Brown, N. J., Clarke, R. T. and Rothery P. & Gerard, F.F. (2002), *Land Cover Map 2000: A guide to the classification system,* CEH.

GlobalSoilMap.net (2011), *Specifications GlobalSoilMap.net products - version 2.0,* GlobalSoilMap.net.

Goidts, E., Van Wesemael, B. and Crucifix, M. (2009), "Magnitude and sources of uncertainties in soil organic carbon (SOC) stock assessments at various scales", *European Journal of Soil Science,* vol. 60, no. 5, pp. 723-739.

Golden Software, (2008), *Voxler - Software for 3D Data Visualization*, Golden Software.

Gomez-Hernandez, J. J. and Journel, A. G. (1993), "Joint sequential simulation of multigaussian fields", *In A. Soares, editor, Geostatistics Troia '92*, pp. 85-94.

Hamza, M. A. and Anderson, W. K. (2005), "Soil compaction in cropping systems: A review of the nature, causes and possible solutions", *Soil and Tillage Research,* vol. 82, no. 2, pp. 121-145.

Hiederer, R. (2009), *Distribution of Organic Carbon in Soil Profile Data.* EUR 23980 EN.

Hikishima, K., Yagi, K., Numano, T., Homma, K., Nitta, N., Nakatani, T. and Hyodo, K. (2008), "Volumetric q-space imaging by 3D diffusion-weighted MRI", *Magnetic resonance imaging,* vol. 26, no. 4, pp. 437-445.

Hilinski, T.E., (2001), *Implementation of Exponential Depth Distribution of organic carbon in the CENTURY model*, Department of Soil and Crop Sciences, Colorado State University.

Intergovernmental Panel on Climate Change - IPCC (2007), *Climate Change 2007: Synthesis Report.*

Israil, M. and Pachauri, A. K. (2003), "Geophysical characterization of a landslide site in the Himalayan foothill region", *Journal of Asian Earth Sciences,* vol. 22, no. 3, pp. 253-263.

IUSS Working group WRB (2006). "World reference base for soil resources 2006", *World soil resources report No. 103,* FAO, Rome.

Jenny B. (2001), " An interactive approach to analytical relief shading", *Cartographica,* vol. 31, issues 1-2, pp. 67-75.

Jenny B. and Patterson, T. (2007), " Introducing plan oblique relief", *Cartographic perspectives*, vol. 57, pp. 21-40 and 88-90.

Jenny, H. (1941), *Factors of soil formation*, McGraw-Hill, New York.

Jenny, H., Jenny, B., Cartwright, W. E. and Hurni, L. (2011), " Interactive local terrain deformation inspired by hand-painted panoramas", *The Cartographic Journal*, vol. 48, issue 1, pp. 11-20.

Jian, W. and Fanhua, L. (2009), "Prediction of oil-bearing single sandbody by 3D geological modeling combined with seismic inversion", *Petroleum Exploration and Development,* vol. 36, no. 5, pp. 623-627.

Jiang, D., Hu, Y., Yan, S., Zhang, L., Zhang, H. and Gao, W. (2005), "Efficient 3D reconstruction for face recognition", *Pattern Recognition,* vol. 38, no. 6, pp. 787-798.

Jobbagy, E. and Jackson, R. (2000), "The Vertical Distribution of Soil Organic Carbon and Its Relation to Climate and Vegetation", *Ecological Applications,* vol. 10, no. 2, pp. 423-436.

Jones, R.J.A. and Montanarella, L. (2001), "Soil compaction: a hidden form of soil sealing in Europe", *INCO-COPERNICUS 3rd workshop*, Busteni, Romania.

Kempen, B., Brus, D. J. and Stoorvogel, J. J. (2011), "Three-dimensional mapping of soil organic matter content using soil type–specific depth functions", *Geoderma,* vol. 162, no. 1-2, pp. 107-123.

Kerry, K. E. and Hawick, K. A. (1998), "Kriging interpolation on high-performance computers", *High-performance computing and networks,* Amsterdam.

Kerry, R. and Oliver, M. A. (2007), "Comparing sampling needs for variograms of soil properties computed by the method of moments and residual maximum likelihood", *Geoderma,* vol. 140, no. 4, pp. 383-396.

King, J.A., Dampney, P.M.R., Lark, M., Mayr, T.R., Bradley, R.I. (2001), "Sensing soil spatial variability by electro-magnetic induction (EMI): its potential in precision farming". *Proceedings of Third European Conference on Precision Agriculture*, Monpellier, vol. 1, pp. 419-424.

King, J.A., Dampney, P.M.R., Lark, M., Wheeler, H.C., Bradley, R.I., Mayr, T.R., Russill, N. (2003). "Evaluation of non-intrusive sensors for measuring soil physical properties". *HGCA Project Report No. 302*, HGCA, London

Kirkby, M. J., Jones, R. J. A., Irvine, B., Gobin, A., Govers, G., CerdainO., Van Rompaey, A. J. J., Le Bissonnais, Y., Daroussin, J., King, D., Montanarella, L., Grimm, M., Vieillefont, V., Puigdefabregas, J., Boer, M., Kosmas, C., Yassoglou, N., Tsara, M., Mantel, S., Van Lynden, G. J. and Huting, J. (2004), "Pan-European soil erosion risk assessment: the PESERA map", *Special Publication Ispra,* vol. 73, no. S.P.I.04.73.

Lark, R. M. and Bishop, T. F. A. (2007), "Cokriging particle size fractions of the soil", *European Journal of Soil Science,* vol. 58, no. 3, pp. 763-774.

Lark, R. M. and Cullis, B. R. (2004), "Model-based analysis using REML for inference from systematically sampled data on soil", *European Journal of Soil Science,* vol. 55, no. 4, pp. 799-813.

Lee, S. J., Park, K. R. and Kim, J. (2011), "A SfM-based 3D face reconstruction method robust to self-occlusion by using a shape conversion matrix", *Pattern Recognition,* vol. 44, no. 7, pp. 1470-1486.

Leonowicz, A.M., Jenny, B. and Hurni, L. (2010), " Terrain Sculptor: Generalizing terrain models for relief shading", *Cartographic Perspectives,* vol. 67, pp. 51-60.

Leonowicz, A.M., Jenny, B. and Hurni L. (2010b), " Automated reduction of visual complexity in small-scale relief shading", *Cartographica,* vol. 45, issue 1, pp. 64-74.

Liu, L., Zhao, Y. and Sun, T. (2012), "3D computational shape- and cooling process-modeling of magmatic intrusion and its implication for genesis and exploration of intrusion-related ore deposits: An example from the Yueshan intrusion in Anqing, China", *Tectonophysics,* vol. 526–529, no. 0, pp. 110-123.

Loveland, P. and Webb, J. (2003), "Is there a critical level of organic matter in the agricultural soils of temperate regions: a review", *Soil and Tillage Research,* vol. 70, no. 1, pp. 1-18.

Malone, B. P., McBratney, A. B. and Minasny, B. (2011), "Empirical estimates of uncertainty for mapping continuous depth functions of soil attributes", *Geoderma,* vol. 160, no. 3-4, pp. 614-626.

Malone, B. P., McBratney, A. B., Minasny, B. and Laslett, G. M. (2009), "Mapping continuous depth functions of soil carbon storage and available water capacity", *Geoderma,* vol. 154, no. 1-2, pp. 138-152.

Matheron, G. (1965), *Les variables régionalisées et leur estimation,* Masson et Cie Luisant-Chartres, impr. Durand, Paris.

Matheron, G. (1969), "Le Krigeage Universel: Recherche d'Estimateurs Optimaux en Présence d'une Dérive (Universal kriging)", *Fascicule 1, Les Cahiers du Centre de Morphologie Mathématique, Edité par l'Ecole Nationale Supérieure des Mines de Paris, Fontainebleau, France*, pp. 83 p.

McBratney, A. B., Bishop, T. F. A. and Teliatnikov, I. S. (2000), "Two soil profile reconstruction techniques", *Geoderma,* vol. 97, no. 3-4, pp. 209-221.

McNeill, J. D. (1980), *Electromagnetic terrain conductivity measurements al low induction numbers. Tech. Notes TN-6,* , Geonics, LTD.

Medvedev, V. V. and Cybulko, W. G. (1995), "Soil criteria for assessing the maximum permissible ground pressure of agricultural vehicles on Chernozem soils", *Soil and Tillage Research,* vol. 36, no. 3-4, pp. 153-164.

Meersmans, J., van Wesemael, B., De Ridder, F. and Van Molle, M. (2009), "Modelling the three-dimensional spatial distribution of soil organic carbon (SOC) at the regional scale (Flanders, Belgium)", *Geoderma,* vol. 152, no. 1-2, pp. 43-52.

Minasny, B., McBratney, A. B., MendonÃ§a-Santos, M. L., Odeh, I. O. A. and Guyon, B. (2006), "Prediction and digital mapping of soil carbon storage in the Lower Namoi Valley", *Australian Journal of Soil Research,* vol. 44, no. 3, pp. 233-244.

Mishra, U., Lal, R., Slater, B., Calhoun, F., Liu, D. and Van Meirvenne, M., (2009), "Predicting Soil Organic Carbon Stock Using Profile Depth Distribution Functions and Ordinary Kriging", *Soil Science Society of America Journal*, vol. 73, no. 2, pp. 614-621.

Moore, A. W., Russell, J. S. and Ward, W. T. (1972), "Numerical analysis of soils: A comparison of three soil profile models with field classification", *Journal of Soil Science,* vol. 23, pp. 193-209.

Myers, D. E. (1989), "Vector conditional simulation", *Geostatistics,* , pp. 283-293.

Oliver, M., Webster, R. and Gerrard, J. (1989), "Geostatistics in physical geography. Part I: theory", *Transactions of the Institute of British Geographers,* vol. 14, no. 3, pp. 259-269.

Pairaud, I. L., Gatti, J., Bensoussan, N., Verney, R. and Garreau, P. (2011), "Hydrology and circulation in a coastal area off Marseille: Validation of a nested 3D model with observations", *Journal of Marine Systems,* vol. 88, no. 1, pp. 20-33.

Parajola, R. (1998), "Large scale terrain visualization using the restricted quadtree triangulation", *Proceedings of the conference on Visualization '98*, Zurich, Switzerland.

Patterson, H. D. and Thomson, R. (1971), "Recovery of inter-block information when block sizes are unequal", *Biometrika,* vol. 58, no. 3, pp. 545-554.

Pebesma, E. J. (1992), *Gstat user's manual*, available at: http://www.biodiversity-lorenzomarini.eu/R_manuals/gstat.manual.pdf (accessed: 17/05/2012).

Pebesma, E. J. (2004), "Multivariable geostatistics in S: The gstat package", *Computers and Geosciences,* vol. 30, no. 7, pp. 683-691.

Ponce-Hernandez, R., Marriott, F. H. C. and Beckett, P. H. T. (1986), "An improved method for reconstructing a soil profile from analyses of a small number of samples.", *Journal of Soil Science,* vol. 37, no. 3, pp. 455-467.

R Development Core Team (2009), *R: A Language and Environment for Statistical Computing*, R Foundation for Statistical Computing, Vienna.

Rampant, P. and Abuzar, M. (2004), "Geophysical tools and Digital Elevation Models: Tools for understanding crop yield and soil variability. Supersoil 2004", *Proceedings of the 3rd Australian New Zealand Soils Conference,* vol. 9.

Rhoades, J. D., Raats, P. A. C., and Prather, R. J. (1976), "Effects of liquid-phase electrical conductivity, water content, and surface conductivity on bulk soil electrical conductivity". *Soil Science Society of America Journal*, vol. 40, pp. 651-655.

Russell, J. S. and Moore, A. W. (1968), "Comparison of different depth weightings in the numerical analysis of anisotropic soil profile data", *Proceedings of the 9th International Congress of Soil Science,* vol. 4, pp. 205-213.

Samouëlian, A., Cousin, I., Tabbagh, A., Bruand, A. and Richard, G. (2005), "Electrical resistivity survey in soil science: A review", *Soil and Tillage Research,* vol. 83, no. 2, pp. 173-193.

Schils, R., Kuikman, P., Liski, J., Van Oijen, M., Smith, P., Webb, J., Alm, J., Somogyi, Z., Van den Akker, J., Billett, M., Emmett, B., Evans, C., Lindner, M., Palosuo, T., Bellamy, P., Jandl, R. and Hiederer, (2008), *Review of existing information on the interrelations between soil and climate change. Final report,* Climsoil, European Commission.

Schlesinger, W. H. (1997), *Biogeochemistry, an analysis of global change*, Academic press, San Diego, California, USA.

Schnyder, J., Ruffell, A., Deconinck, J. and Baudin, F. (2006), "Conjunctive use of spectral gamma-ray logs and clay mineralogy in defining late Jurassic–early Cretaceous palaeoclimate change (Dorset, U.K.)", *Palaeogeography, Palaeoclimatology, Palaeoecology,* vol. 229, no. 4, pp. 303-320.

Schrumpf, M., Schulze, E. D., Kaiser, K. and and Schumacher, J. (2011), "How accurately can soil organic carbon stocks and stock changes be quantified by soil inventories?", *Biogeosciences,* vol. 8, pp. 1193-1212.

Schunn, C. D. and Wallach, D. (2005), "Evaluating goodness-of-fit in comparison of models to data", *Psychologie der Kognition: Reden and Vorträge anlässlich der Emeritierung von Werner Tack*, pp. 115-154.

Soane, B. D. and van Ouwerkerk, C. (1995), "Implications of soil compaction in crop production for the quality of the environment", *Soil and Tillage Research,* vol. 35, no. 1-2, pp. 5-22.

Student (1914), "The elimination of spurious correlation due to position in time or space", *Biometrika,* vol. 10, pp. 179-181.

Taylor, M. J., Smettem, K., Pracilio, G. and Verboom, W. (2002), "Relationships between soil properties and high-resolution radiometrics, central eastern Wheatbelt, Western Australia", *Exploration Geophysics,* vol. 33, no. 2, pp. 95-102.

Thierry, P., Prunier-Leparmentier, A., Lembezat, C., Vanoudheusden, E. and Vernoux, J. (2009), "3D geological modelling at urban scale and mapping of ground movement susceptibility from gypsum dissolution: The Paris example (France)", *Engineering Geology,* vol. 105, no. 1-2, pp. 51-64.

Triantafilis, J., Ahmed, M.F., Odeh, I.O.A. (2002), " Application of a mobile electromagnetic sensing system (MESS) to assess cause and management of soil salinization in an irrigated cotton-growing field", *Soil use and Management*, vol. 18, pp. 330-339.

Triantafilis, J. and Lesch, S. M. (2005), "Mapping clay content variation using electromagnetic induction techniques", *Computers and Electronics in Agriculture,* vol. 46, no. 1-3 SPEC. ISS., pp. 203-237.

van Wijngaarden, M., Venema, L.B., De Meijer, R.J., Zwolsman, J.J.G., Van Os, B. and Gieske, J.M.J. (2002), " Radiometric sand-mud characterisation in the Rhine-Meuse estuary Part A. Fingerprinting", *Geomorphology,* vol. 43, pp. 82-101.

Wagner, B., Gärtner, H., Santini, S. and Ingensand, H. (2011), "Cross-sectional interpolation of annual rings within a 3D root model", *Dendrochronologia,* vol. 29, no. 4, pp. 201-210.

Wang, G., Zhu, Y., Zhang, S., Yan, C., Song, Y., Ma, Z., Hong, D. and Chen, T. (2012), "3D geological modeling based on gravitational and magnetic data inversion in the Luanchuan ore region, Henan Province, China", *Journal of Applied Geophysics,* vol. 80, no. 0, pp. 1-11.

Webster, R. and Burgess, T. M. (1980), "Optimum interpolation and isarithmic mapping of soil properties. III. Changing drift and universal kriging. ", *Journal of Soil Science,* vol. 31, pp. 505-524.

Webster, R. and Oliver, M. A. (2007), *Geostatistics for environmental scientists*, Wiley.

Wu, L., McGechan, M. B., McRoberts, N., Baddeley, J. A. and Watson, C. A. (2007), "SPACSYS: Integration of a 3D root architecture component to carbon, nitrogen and water cycling—Model description", *Ecological Modelling,* vol. 200, no. 3–4, pp. 343-359.

Xu, X., Liu, W., Zhang, C. and Kiely, G. (2011), "Estimation of soil organic carbon stock and its spatial distribution in the Republic of Ireland", *Soil Use and Management,* vol. 27, no. 2, pp. 156-162.

Xue, Y., Sun, M. and Ma, A. (2004), "On the reconstruction of three-dimensional complex geological objects using Delaunay triangulation", *Future Generation Computer Systems,* vol. 20, no. 7, pp. 1227-1234.

Yang, Y., Li, Y., Liu, T., Zhan, Y. and Feng, J. (2011), "Interactive 3D forward modeling of total field surface and three-component borehole magnetic data for the Daye iron-ore deposit (Central China)", *Journal of Applied Geophysics,* vol. 75, no. 2, pp. 254-263.

You, K. and Lee, J. S. (2006), "Estimation of rock mass classes using the 3-dimensional multiple indicator kriging technique", *Tunnelling and Underground Space Technology,* vol. 21, no. 3-4, pp. 229-229.

Zhang, L. (2003), "Key algorithms study on global terrain visualization", *Proceedings of the Geoscience and Visualization Symposium*, Beijing, China.

APPENDIX 1 - Interactive GUI for using *R* in geostatistical analysis

Software Availability

Name of the software:	IntR
Developers:	Veronesi, F.
Contact address:	Cranfield University, Bld. 37 – College Road, Cranfield. MK43 0JX
E-mail:	f.veronesi@cranfield.ac.uk
Availability and online documentation:	free download with manual and sample dataset at: http://public.cranfield.ac.uk/s124437/
Year first available:	2011
Hardware requirements:	Windows operating system
Program language:	*Python*
Software required:	none, standalone software
Program size:	47.9 MB IntR 2D 60.7 MB IntR 3D

Abstract

In recent years, *R* is increasingly being used by environmental scientists, because it is free, open-source, and has a large number of packages for environmental and spatial statistics. On the other hand, the necessity to learn a new programming language, with a relatively steep learning curve, has limited its use in the scientific community. This software is designed to help solve this problem and speed up the learning process of both *R* itself and make

geostatistics more accessible in general. IntR is a graphical user interface, developed in *Python*, that eases the procedure of creation and execution of an *R* script for 2D and 3D geostatistical interpolation. This interface works by asking interactive questions to the user and compiling the *R* script following the user answers. Once the script is created, the software runs it in batch mode and shows the results.

Introduction

Since its first launch, *R* (R Development Core Team, 2010) has gained a lot of traction among environmental scientists, because it is free and open-source but also to the large number of packages dedicated to environmental and spatial statistics and geostatistical interpolation. However, the necessity to learn a brand new programming language, with a relatively steep learning curve, has undermined its spread in the scientific community. On the other hand, the multitude of packages and the large community of users make it a useful instrument for environmental and spatial statistics. Furthermore, the continual renewal of the software itself and of all the common packages has maintained *R* at a very high standard of quality compared with other, more common and widespread, statistical and geostatistical software.

This software is designed to decrease threshold and speed up the learning process of both *R* and geostatistics in general. IntR is a graphical user interface, wrote in *Python*, that eases the procedure of creation and execution of an *R* script for 2D and 3D geostatistical interpolation.

The user needs to have some background of spatial statistics, in order to fully understand the procedure for creating and executing the script. However, the *R* packages and scripts used to execute the geostatistical algorithms are designed to give a fair amount of confidence to the user on the result of his computations, even in the case that the user is new to geostatistics.

Feature and Capabilities

When the user starts IntR it shows a simple panel with a button for each algorithm implemented (see Fig. 1, below).

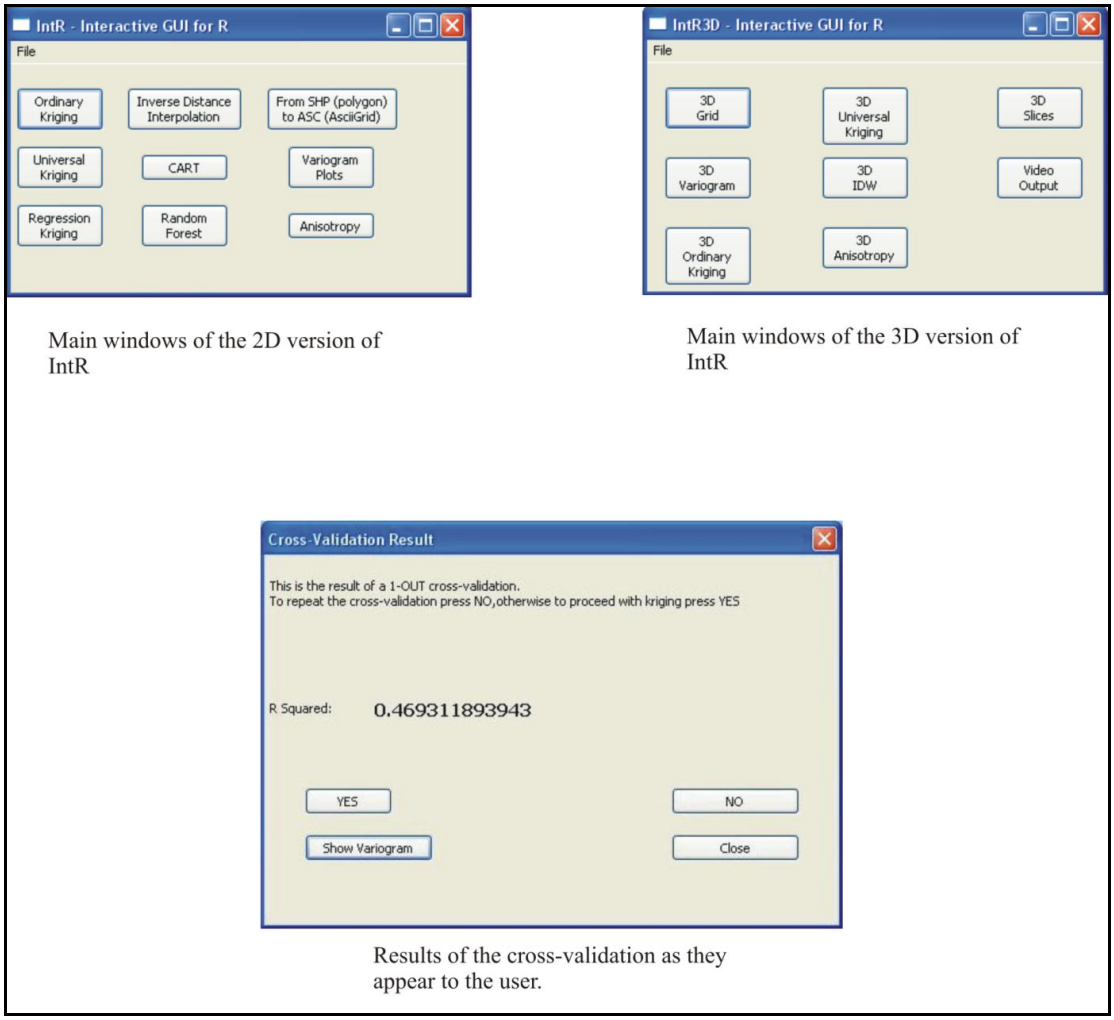

Fig. 1: Example of dialogs. The first two are the main windows of IntR and IntR3D, the user here can choose the algorithm. The last dialog is the result of a cross-validation in a kriging process; the user here can see the value of R^2 and the image of the variogram (by clicking on "Show Variogram") and decide to repeat the cross-validation with other covariates or complete the kriging interpolation.

The algorithms that can be used in IntR are: for the 2D version, inverse distance interpolation, ordinary kriging, universal kriging and regression kriging, random forest and CART, plus a module for obtaining a point grid from a shape file and a module for variogram and anisotropy analysis. For the 3D version, the user can choose between inverse distance, ordinary kriging and universal kriging, plus a module to create a 3D prediction grid, a module for variogram and anisotropy analysis, a module for creating a series of slice images of the 3D map and a module for sticking the slices in an animation video. The *R* packages used to perform all the analysis are: **gstat** (Pebesma, 2004), **sp** (Bivand et al., 2008; Pebesma and Bivand, 2005), **maptools** (Lewin-Koh & Bivand, 2005), **randomForest** (Liaw & Wiener, 2002), **tree** (Ripley, 1998), **rgdal** (Keitt et al., 2003), **lattice** (Sarkar, 2008), **akima** (Gebhardt, 1998). For the creation of the video we rely on the free software Mencoder (http://www.mplayerhq.hu). After the user has selected the algorithm the software works by asking "questions" to the user, using graphical dialogs: for instance to select the data file, the model of the variogram, and compiling the *R* script based on the "answers". The user is therefore in full control of every part of the process. At the end of each module the compiled script is submitted to *R* via a bat file and the results are saved as images, text files. The script is also saved for the user to control it and thus learn the language.

The software can be tried with two different datasets, both simulated, one in 2D and the other in 3D.

The bi-dimensional dataset is composed by 150 samples with sand percentages. The second dataset is composed by 1651 observations, from 0 to 50 cm of depth. In both cases are also available two covariates, slope and aspect, for universal kriging. Alongside the two datasets are also provided the shape file (ESRI, 1998) with the field border for trying the grid creation modules and a text file with a prediction grid for trying an interpolation.

References

Bivand, R.S., Pebesma, E.J., Gomez-Rubio, V. (2008). *Applied spatial data analysis with R*. Springer, NY.

ESRI (1998). *ESRI Shapefile Technical Description*. www.esri.com/library/whitepapers/pdfs/shapefile.pdf *[last accessed: 03/06/2011]*

Liaw, A., and Wiener, M. (2002). "Classification and Regression by randomForest". *R News*, vol. 2, no. 3, pp. 18-22.

Pebesma, E.J. (2004). "Multivariable geostatistics in S: the gstat package". *Computers & Geosciences*, vol. 30, pp. 683-691.

Pebesma, E.J., Bivand, R.S. (2005). "Classes and methods for spatial data in R". R News, vol. 5, no. 2, pp. 9-13.

Ripley, B. (1998). *Tree: Classification and regression trees*. http://cran.r-project.org/web/packages/tree/ [last accessed: 03/06/2011]

Sarkar, D. (2008). *Lattice: Multivariate Data Visualization with R*. Springer, New York.

Gebhardt, A. (1998). *Akima: Interpolation of irregularly spaced data*. http://cran.r-project.org/web/packages/akima/index.html [last accessed: 03/06/2011]

Lewin-Koh, N.J., and Bivand, R. (2005). *Maptools: Tools for reading and handling spatial objects*. http://cran.r-project.org/web/packages/maptools/index.html [last accessed: 03 June 2011]

Keitt, T.H., Bivand, R., Pebesma, E., Rowlingson, B. (2003). *Rgdal: Bindings for the Geospatial Data Abstraction Library*. http://cran.r-project.org/web/packages/rgdal/index.html [last accessed: 03/06/2011]

APPENDIX 2 – Publications

JOURNAL ARTICLE:

Veronesi, F.; Corstanje, R.; Mayr, T. (2012). "Mapping soil compaction in 3D with depth functions". *Soil and Tillage Research*. vol 124, p. 111-118, in press. http://dx.doi.org/10.1016/j.still.2012.05.009

CONFERENCE PAPERS:

Veronesi, F.; Corstanje, R.; Mayr, T. (2011). "3D soil compaction mapping with a three-coefficients polynomial". *Proceedings of the second global workshop of proximal soil sensing*, Montreal.

Veronesi, F.; Corstanje, R. (2011). "IntR - Interactive GUI for R". *The R Users Conference - UseR 2011*, Warwick.

Veronesi, F.; Corstanje, R.; Rickson, J. And Mayr, T. (2012). "Landscape scale estimation of soil carbon stock in three-dimensions for creating a carbon loss risk map". *EGU General Assembly 2012,* Vienna.

NOTE: In the pdf version of the thesis, by clicking on the first author it should opens an electronic version of the material.
Alternatively they are located in the folder "Articles_&_Conferences "

DIGITAL APPENDIX 1 – 3D animation of soil compaction pattern in Lany field

NOTE: by clicking on each of the following image, it should open the related video. Alternatively they are located in the folder “Digital_Appendix_1”.

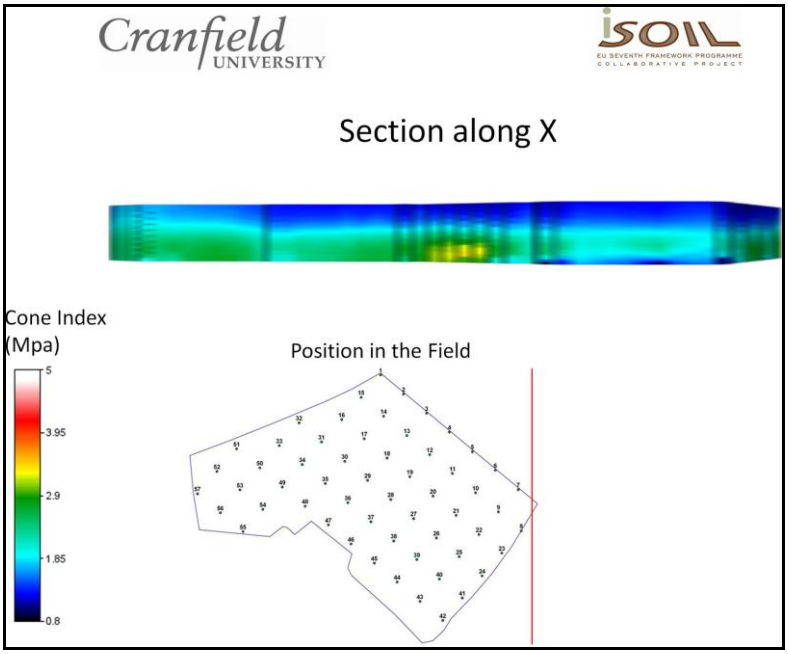

Animation 1: Sections along the X axis

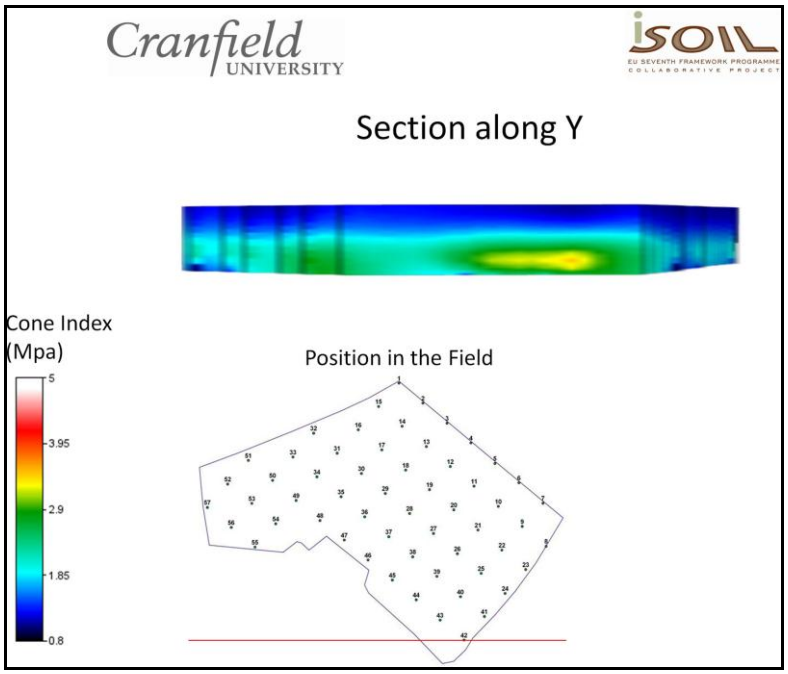

Animation 2: Sections along the Y axis

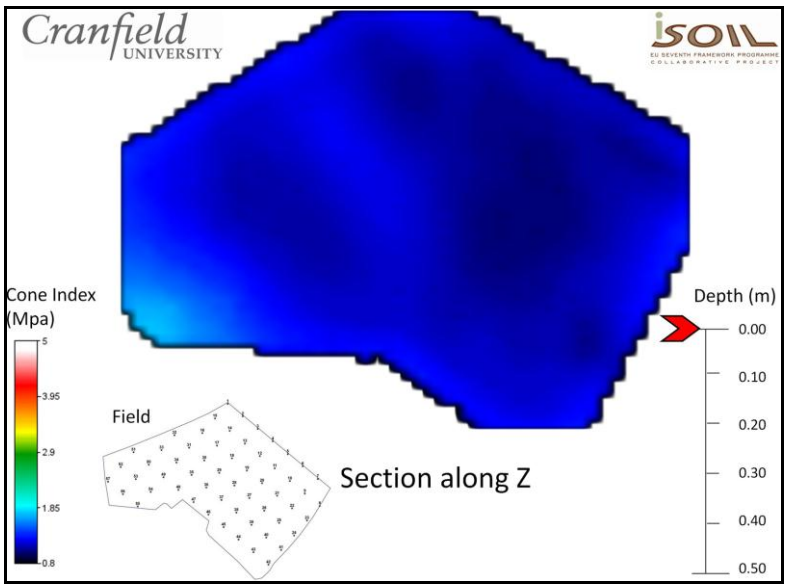

Animation 3: Sections parallel to the horizontal plane.